Durham E-Theses

Remote sensing of subglacial bedforms from the British Ice Sheet using an Unmanned Aerial System (UAS): Problems and Potential.

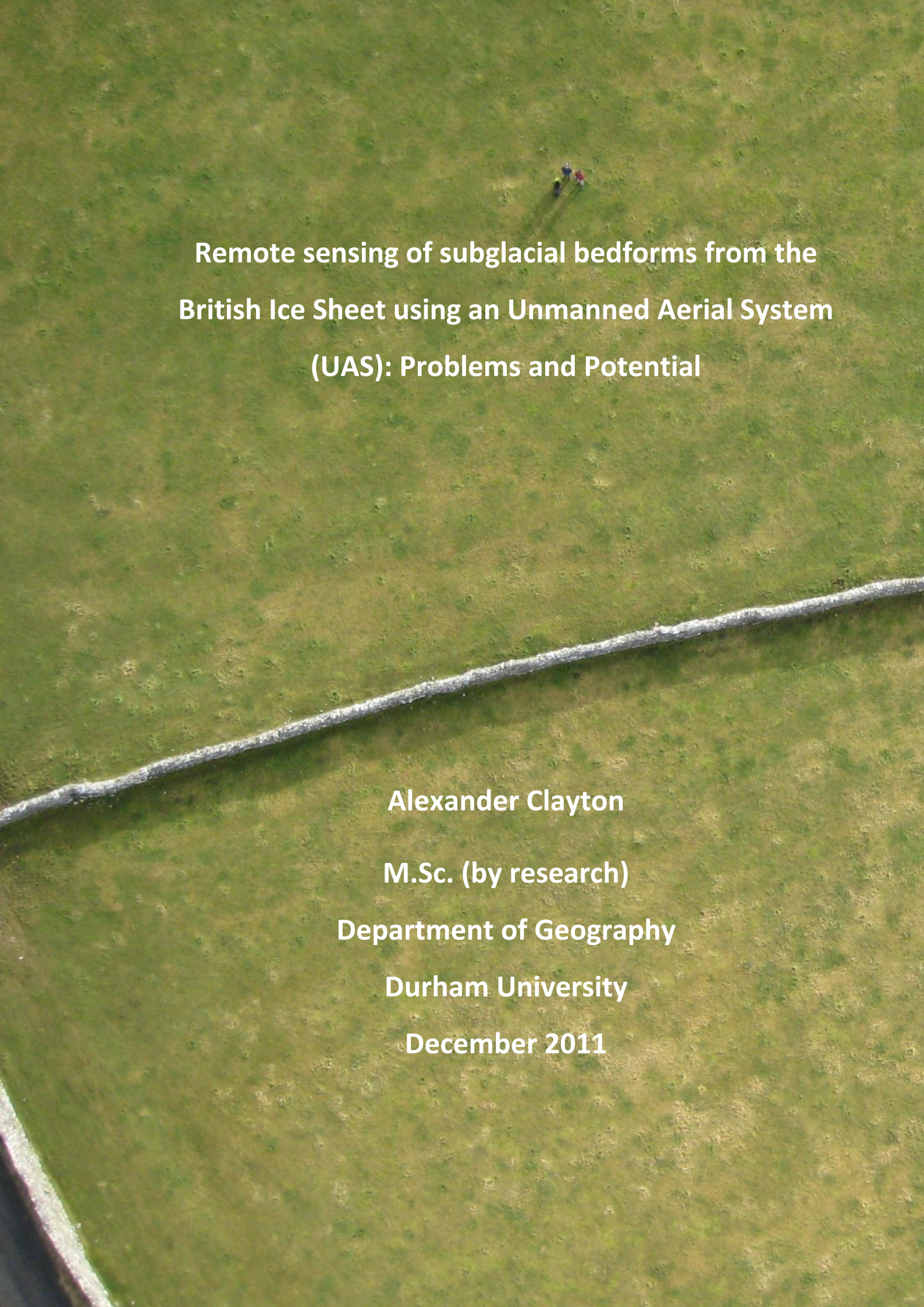CLAYTON, ALEXANDER,IAN

Remote sensing of subglacial bedforms from the British Ice Sheet using an Unmanned Aerial System (UAS): Problems and Potential

Alexander Clayton

M.Sc. (by research)

Department of Geography

Durham University

December 2011

Declaration of Copyright

Alexander Ian Clayton

Department of Geography

Durham University

December 2011

Abstract

Photogrammetry can be applied to the results of UAS (Unmanned Aerial Systems) based photographic surveys to produce high resolution DEMs (Digital Elevation Models) of small areas (c. 1 km^2). However, this method has not been widely used in academia due to photogrammetric programmes working poorly with the ill constrained intrinsic and extrinsic properties that often accompany UAS based photographs. In this study a PAMS (Personal Aerial Mapping System) SmartOne B UAS was used to provide image sets for testing a number of different photogrammetry packages; LPS, Bundler, PhotoSynth and PhotoScan, with the aim of producing sub-metric accuracy DEMs with a low complexity methodology and without significant financial investment.

To demonstrate the potential use of a UAS photogrammetric survey methodology it was applied here to an investigation into scale dependant remote sensing of glacial geomorphology. Subglacial bedforms, landforms produced by the flow of ice over land, are thought to 'seed' with a minimum horizontal dimension of 100 m. This hypothesis is based on surveys of bedforms across the UK and Ireland using NEXTMap DEMs with 1 m accuracy and 5 m resolution. Here we test that hypothesis using sub-metric accuracy DEMs produced via photogrammetry of an area in the Eden Valley drumlin field, NW England.

The UAS was found to be suitable for this type of survey, but only one of the four photogrammetry programmes provided an effective and low complexity methodology. This programme, PhotoScan, was shown to require minimal user training and could produce DEMs from the survey imagery on the day of flying with a standard high performance computer at a resolution of 0.12 m^2. The DEM produced was down sampled and validated against pre-existing 1 m LiDAR (Light Detection And Ranging) data of the same area. It showed poor absolute accuracy due to a systematic parabolic error introduced during processing that made quantification of the DEM error problematic. However, estimates of the error additional to this systematic error put it at around 0.5 m which makes the DEM suitable for mapping low amplitude bedforms.

Use of the DEM for mapping subglacial bedforms yielded ambiguous results. 17 additional linear ridges were identified that were not visible on the NEXTMap DEM.

Their dimensions were not remarkably shorter than the 100 m limit, with only 6 measuring <100 m, but their width was much narrower than those mapped previously. However, whilst these dimensions could suggest that bedforms do not 'seed' at a certain size and may fine into smaller features such as flutes, there was no way to demonstrate that they were in fact glacial in origin. This highlighted that whilst sub-metric resolution DEMs are undoubtedly highly useful tools in the survey of glacial bedforms, they may require additional data from field investigations in order for robust conclusions to be drawn due to the numerous processes capable of produce geomorphic features at a sub-metric vertical scale.

Contents

List of Figures

List of Tables

Acknowledgements

Chapter 1 Introduction and Rationale

1.1. Subglacial Bedforms

It could be argued that remote sensing has progressed glacial geomorphology from a collection of local studies on individual or small populations of landforms, to the observation and interpretation of glacial landscapes on a continental scale (Bingham *et al.*, 2010). The study of subglacial bedforms, landforms produced by the flow of ice over land (Boulton *et al.*, 1985; Boulton & Clark, 1990; Kleman *et al.*, 1997) that cover vast tracts of previously glaciated areas, has perhaps benefited the most from remote sensing. Subglacial bedforms are perhaps most striking in Canada where they cover 70% of the country, but with 50%, 40% and 15% coverage in Ireland, Scandinavia and Britain respectively they are ubiquitous. Subglacial bedforms range in scale from 10-10^5 m, but quantification of the upper end of this scale, e.g. mega-scale glacial lineations, was not possible before imagery from Earth observation satellites such as Landsat became available (Clark, 1993; Clark, 1994).   At smaller scales there is evidence to suggest that the resolution of our remote sensing techniques may still be a limitation to observation (Clark *et al.*, 2009). Consequently, previous mapping studies using remote sensing without field investigation may have omitted the smallest bedforms and this potentially raises questions about the conclusions that are drawn (e.g. Clark *et al.*, 2009).

Study of subglacial bedforms began nearly 200 years ago and evolved from initial field based studies (e.g. Bryce, 1833; Close, 1867; Goodchild, 1875) to those supplemented by aerial imagery (e.g. Piotrowski & Smalley, 1987; Hattestrand *et al.*, 1999), then satellite imagery (e.g. Clark, 1993, 1994, 1997; Stokes, 2002; Jansson & Glasser, 2005), and now digital elevation models (DEMs) of various origins (e.g. Jansson & Glasser, 2005; Smith & Clark, 2005; Greenwood & Clark, 2008; Hess & Briner *et al.*, 2009; Hughes *et al.*, 2010). The availability of high (metric) resolution digital elevation models (DEMs) for mapping subglacial bedform features has dramatically increased our ability to make empirical conclusions about the shape, size and morphology of

subglacial bedforms, and in particular, drumlins (Clark *et al*., 2009; Hughes *et al*., 2010; Spagnolo *et al*., 2010; Spagnolo *et al*., 2011).

1.2. Drumlins

Drumlins are the most common subglacial bedform (Clark, 2010), and are recorded in large numbers or 'swarms' with a similar long axis orientation (Benn & Evans, 2010). They have been described as having a multitude of different forms from lenticular (Hitchcock, 1876), elliptical (Chamberlin, 1883) and oval (Charlesworth, 1957) to a half torpedo (Alden, 1905), baguette (Rouk and Raukas, 1989) and cigar (Ebers, 1926). Current opinion has moved away from the more eccentric descriptions towards a comparison with a hemiellipsoid (Reed *et al*. 1962; Spagnolo *et al*. 2010) that conforms to the simple equation:

$$\frac{x^2}{a} + \frac{y^2}{b} + \frac{z^2}{c} = 1$$

Equation 1

Drumlins are one of the most enigmatic landforms in glacial geomorphology and there is a wealth of literature, perhaps prompted by their widespread presence in deglaciated landscapes and the puzzles over their formation. To date around 1400 articles have been produced on them and there are no signs of this interest abating with over 27 published in the first three quarters of 2011 alone (Clark, 2010). Despite the abundance of studies on drumlins, the variety in observation techniques and observer preconceptions are such that it is difficult to reach empirical conclusions about drumlin morphology and size from a review of previous work. Because of this, extensive mapping efforts from DEMs of previously glaciated areas (e.g. Greenwood & Clark, 2008; Hess & Briner *et al*., 2009; Hughes *et al*., 2010) provide new opportunities to reach quantitative definitions and statistically valid observations of drumlins.

1.3. A Scaling Law for Drumlins

After analysing a dataset of drumlins mapped by Hughes *et al*. (2010) on the British Isles and bedforms mapped by Greenwood & Clark (2008) in the Republic of Ireland and Northern Ireland, Clark *et al*. (2009) noted that there appeared to be a threshold of c.100 m for minimum drumlin size. If correct, this observation of a fundamental

threshold for drumlin form is a crucial piece of information in solving the drumlin problem, suggesting that they initiate at, or grow rapidly, to a relatively large size. However, this observation might also be an artefact of the resolution of the DEMs used in gathering the source data that may have meant they missed very small drumlins. The main aim of this study was to test the use of an unmanned aerial system for mapping subglacial bedforms but a further secondary aim was to examine whether this threshold is a feature of drumlins and their formation process or just a product of the resolution of the NEXTMap DEM (5 m contours, +/- 2.5 m horizontal accuracy, +/- 1.0 m RMSE) (Getmapping, 2011) used by Hughes *et al*. (2010). By remapping a small area from the Hughes *et al*. (2010) data set with higher resolution sub-metric DEMs, the aim is to investigate whether unmapped and possibly shorter bedforms are present. Such knowledge would be helpful for constraining current models of bedform evolution where the minimum size is a key factor (e.g. Fowler, 2010). In turn, these models help us understand how ice flows through developing our knowledge of the dynamic ice-bed relationship.

1.4. Photogrammetry

NEXTMap data was produced with IfSAR (Interferometric Synthetic Aperture Radar) over a series of flights across the UK in 2002-3 (Getmapping, 2011). Its high accuracy is a result of a relatively low flying altitude of 20,000-28,000 ft. Usually when a higher resolution DEM is required, LiDAR is used. This can produce centimetric resolution Digital Surface Models (DEMs) and provide additional information about the surface that allows creation of bare Earth DEMs. An alternative to these two methods is photogrammetry: "the art, science, and technology of obtaining reliable information about physical objects and the environment through processes of recording, measuring and interpreting photographic images and patterns of recorded radiant electromagnetic energy" (Wolf & Drewitt, 2000). In recent years, progress in high resolution image acquisition from airborne or satellite platforms has enabled the production of sub-metric accuracy DEMs through photogrammetry with some degree of automation (Chandler, 1999; Marzolff & Poesen, 2009; Verhoeven, 2011; Neithammer *et al*., in press).

To those with no prior knowledge of photogrammetry the instant appeal is the concept of producing DEMs from something as simple as a photograph. The flexibility and low cost nature of such an approach obviously appears to have the potential to make DEMs freely available without the constraints of cost and technology that are associated with anything with laser or radio in the title. But unfortunately photogrammetry is not without issues. It is, in essence, a complicated geometric calculation with three unknowns; the location of the ground, the location of the camera, and the distortion of light as it travels through the camera's lens (Wolf & Drewitt, 2000). Therefore, to produce accurate information from images the unknowns must be solved or constrained. This complicates matters as it can require the use of expensive calibrated cameras where focal length and lens distortion is known, fixed and ideally minimised, and it can require the use of survey grade differential GPS to monitor the location of images. In addition, when one comes to process the images it traditionally requires a great deal of supervision to identify the same point on several images and so provide tie points for image triangulation and DEM construction.

1.5. Potential for UASs

In this study, high resolution aerial imagery of areas of subglacial bedforms was used to produced sub-metric resolution DEMs via photogrammetry. The aerial surveys were conducted with a PAMS SmartOne B UAS (Unmanned Aerial System) (http://www.smartplanes.se/) using small format camera, a compact Canon Ixus10. This is a relatively novel technique, especially within glacial geomorphology. UASs provide an excellent opportunity to conduct structured centimetric resolution aerial surveys with minimal user training required due to the automation of flight (Hardin & Jensen, 2011). They provide a level of flexibility to a study, allowing repeat survey of an area, or a survey of a site too small to justify commissioning a standard flight.

Imagery collected with UASs can be problematic to use in photogrammetry. Small format UAS cameras are generally not calibrated which leads to poor constraints on lens distortion and focal length. Furthermore, the on board GPS, if available at all, is generally of low accuracy which in turn leads to low quality measurement of image acquisition locations. As a result, the photogrammetric processing can suffer from an

increase in the already high levels of supervision. This is unfortunate as to maintain the advantages of the UAS in terms spatial and temporal flexibility, the post processing ideally should be equally quick and simple.

Recent programmes based on Structure from Motion (SfM) computer vision techniques have provided an opportunity to circumnavigate these issues. They perform 'bundle adjustments' which is a least squares minimisation of the error of reprojection (Szelsiki, 2010) and so do not require anything more than a rough initial value for camera parameters. This is not a new technique (Aber, 2010), but use of a SIFT style algorithm (Szelsiki, 2010) dramatically increases the numbers of points used in the bundle adjustment and is more accurate than previous feature matching algorithms. This makes the least squares problem tractable despite the large number of unknowns and so initial GCPs and tie points are not required. With user supervision no longer necessary at the feature matching stage the process of creating a model in a Euclidean co-ordinate system is essentially automatic, limiting supervision to adding control points in order to georeference the model. This makes processing of large numbers of poorly parameterised images simple and fast.

In this study four different programmes were tested, three of them based on SfM. The aim was to establish whether it is possible to simply, effectively and cheaply, produce sub-metric accuracy DEMs of field sites on demand from UAS aerial survey imagery. The SfM based programmes used were Bundler, Microsoft PhotoSynth and AgiSoft PhotoScan. The other programme that does not rely on SfM was LPS. This programme is widely available to GIS users and has been used in several previous studies (e.g Smith *et al.*, 2008, Laliberte *et al.*, 2011) so was included as a comparison to the more novel programmes.

1.6. Aims and Objectives

1. To create high resolution sub-metric accuracy DEMs using aerial photography from UAS surveys.

2. To establish whether UAS based photogrammetry is a sufficiently low cost and low complexity methodology for producing DEMs for use in glacial geomorphology.

3. To identify whether drumlinised areas require mapping at a higher accuracy than provided by existing DEMs.

Chapter 2 Remote Sensing & UASs

2.1. Remote Sensing of Glacial Geomorphology

Early studies on glacial geomorphology were understandably dependant on field mapping (e.g. Davis, 1884). Thus the early literature is scattered with a variety of studies based on limited numbers of landforms. The pace of development in our understanding has accelerated rapidly since the mid-19th century due to the emergence of new remote sensing methodologies (see section 1.1). Remote sensing is well placed to aid geomorphology, and can help in four key areas (Smith & Pain, 2009): 1) identifying the location and distribution of landforms; 2) establishing surface elevations; 3) mapping land surface composition; and 4) enabling none destructive subsurface investigations. This investigation was principally concerned with the second point with a view to refining the first.

2.1.1. 2-D Sensing

Early photographers were quick to realise the value of taking their cameras aloft. Aerial photography from balloons was adopted as early as 1858 by Gaspard-Felix Tournachon (also known as Nadar) (Carbonneau & Piégay, in press) and the imagery used for mapping by Aimé Laussedat via the application of perspective methodologies (Lo, 1976). The major progressions in the subject came about through the two world wars where hundreds of aerial photography missions were flown and camera and analysis technology was understandably rapidly improved. In the post war period, the quantitative revolution of the mid-1960s combined with new levels of computing power resulted in the wide spread development of photogrammetry (Paine & Kiser, 2003). The use of stereoscopy that uses binocular vision to achieve 3-D vision had for some time been a major addition to the geomorphologists mapping arsenal, but photogrammetry allowed quantitative information to be extracted from the imagery.

Whilst aerial imagery had drastically changed the way we considered our landscape the advent of satellite imagery and movement towards full 'Earth observation' was also an important advance for glacial geomorphology. The scale of the coverage revealed new landforms (Clark, 1993, 1994; Greenwood *et al.* 2010) and provided a more synoptic view of the landscape (Smith & Pain, 2009). However, whilst early satellite imagery was ground breaking in terms of coverage, the early Landsat imagery was not entirely suitable for morphological investigations due to it's low spectral and spatial resolution (Millington & Townshend, 1987). Over the last 10 years the number of satellites available has expanded rapidly. Satellites such as ASTER, IKONOS, GeoEye and World-View provide far higher resolution imagery than Landsat does and increase the opportunity for satellite imagery based photogrammetry (Smith & Pain, 2009). But whilst this new imagery is extremely useful, the older satellites should not yet be discounted. They still play a significant role in investigations examining temporal change due to the archives of now free imagery that extend back to 1972 (http://landsat7.usgs.gov).

2.1.2. Towards 3-D Sensing

Stereoscopic vision is not a new technology and has been used extensively to improve mapping from aerial photography (e.g. Hattestrand *et al.*, 1999) but use of DEMs for quantitative analysis of morphometry and volumetric changes is a relatively recent and ongoing development (Smith & Pain, 2009). DEMs are most commonly produced - by three different methods; Synthetic Aperture Radar (SAR), photogrammetry and LiDAR (for a more complete summary see Oguchi *et al.*, 2011). Currently SAR provides the greatest coverage, LiDAR is most widely used for high resolution work and photogrammetry (covered later in the thesis) is rapidly developing as a cost efficient rival to both (Eisenbeib, 2007) through use of low resolution high coverage imagery from satellites such as ASTER (Toutin, 2008) and high resolution low coverage imagery from small format cameras (Neithammer *et al.*, in press).

The advantage of radar imagery is principally the longer wavelength's usability independent of weather and lighting. This weather independence allows repeat passes to be carried out and interferometric techniques to be used. Interferometric

synthetic aperture radar (IfSAR) uses the phase differences of two or more synthetic aperture radar (SAR) images to produce DEMs or maps of surface changes (Rosen *et al.*, 2000). A variety of satellites are currently used for this, including archive images from the ERS Tandem Mission (e.g. Muller *et al.*, 1996), ERS-2, ENVISAT ASAR and combination of ERS-2 and ASAR (Smith & Pain, 2009). Satellites are significantly more expensive than terrestrial and airborne sensing alternatives, but the all weather day/night capabilities mean development is ongoing in this field with new sensors such as TerraSAR-X and satellites like TanDEM-X coming into use with higher 1-2 m accuracies and 10-15 m resolution (Palmann *et al.*, 2008). One of the most important IfSAR uses for British Quanternary geomorphology has been the NextMap DEMs (5 m vertical accuracy) that was produced from airborne radar and initially for used in flood risk modelling. It has been particularly important as it is freely available to academic institutions and sufficiently high resolution to be used for most mapping and modelling work (Hughes *et al.*, 2010).

For high resolution sub-metric accuracy work, terrestrial and airborne laser scanning is usually seen as a better option. Pulsed laser systems record range and intensity which allows DEMs to be created from the point cloud data through interpolation, and a level of information about surface characteristics to be taken from the return (Rees, 2001). However, whilst producing accurate and dense point clouds, laser scanning remains expensive, particularly for those commissioning surveys rather than just obtaining previously processed data. The UK Environment Agency holds LiDAR data with 62% coverage of the country in resolutions between 0.25 m and 2 m (geomatics-group.co.uk). This is sold commercially, albeit at a lower rate to academic institutions. However as most Environment Agency data collection is focused on flooding risk, coverage outside urban, coastal and river valleys, if it exists, is only available at a spatial resolution of 2 m which may not be a large enough improvement on NEXTMap DEMs to reveal subtle geomorphic features.

2.1.3. Photogrammetry in Glacial Geomorphology

Photogrammetry, is applicable to geomorphology and particularly studies of morphology across all scales of landforms. As the DEM resolution is dependent on the

image resolution photogrammetry can be used to produce DEMs at the macro and micro scales (Chandler, 1999). Whilst photogrammetry is not a recent technique it required developments in computing power and programming in the 1990s that enabled automated or semi-automated DEM production before it became a useful technology for analytical geomorphology (e.g. Brunsden & Chandler, 1996; Pyle *et al.*, 1997; Butler *et al.*,1998).

Photogrammetry has three key benefits: 1) it is relatively cheap; 2) imagery is widely available and/or relatively easily gathered allowing a high temporal resolution and study of remote areas not covered by radar or LiDAR; 3) scale is only dependant on image resolution which can be varied easily via changing the proximity to the object or the quality of the camera (Chandler & Padfield, 1996). As with nearly every remote sensing method there are technical issues and limitations and these are presented in detail in the methodology section 5.2. Here it will suffice to state that the advantages of photogrammetry must often be weighed up against processing difficulties that include potentially onerous levels of supervision and variable levels of error.

In glaciology, perhaps the most obvious use of photogrammetry is to monitor mass change. It has been widely used for this purpose, initially in 2-D (e.g. Finsterwalder, 1954) and later in 3-D (e.g. Reinhardt & Rentsch, 1986; Etzelmuller *et al.*, 1993; Krabill *et al.*, 1999; Keutterling & Thomas, 2006; Barrand *et al.*, 2009) as computing power developed (Fox & Nuttall, 1997). One of the most effective uses of photogrammetry has been the exploitation of historical imagery to produce records of glacier change over time (e.g. Etzelmuller *et al.*, 1993; Fox & Nuttall, 1997; Hubbard *et al.*, 2000; Kohler *et al.*, 2007). However analytical application in glacial geomorphology has been limited. In glacial monitoring images have been actively collected for the task (e.g. Ahn *et al.*, 2010) but in glacial geomorphology studies have generally been carried out on pre-existing DEMs (e.g Clark *et al.*, 2009; Hess & Briner, 2009; Spagnolo *et al.*, 2010). It would be unrealistic to expect a glacial geomorphology study to have the resources to commission its own survey of a comparably large area to these studies, but it is worth noting that these data sets are not specifically designed for mapping bedforms.

2.2. UASs for Remote Sensing

Unmanned Aerial Vehicles have existed since the First World War (Newcome, 2004) and have grown to become a staple military system that is used for gathering imagery and as a weapons platform (Hardin & Jensen, 2011). For the purposes of this investigation they can be defined as aircraft that fly without a human being on board and are capable of autonomous flight. Civil and academic use of UASs has not been as extensive as the military use, largely due to legal reasons. For exmple, in the USA it is extremely difficult to obtain permits for UAS usage, and often it is helpful for pilots to obtain full flying licenses despite the discrepancy in scale between manned aircraft and most UASs (Laliberte & Rango, 2011). In the UK the CAA (Civil Aviation Authority) puts in place a series of regulations that limit, although do not prevent, the use of UAS's. These include a weight limit of 20 Kg, a flying ceiling of 400 Ft (125 m), a stipulation that line of site must be maintained between the pilot and platform at all times and limitation on flying in controlled airspace e.g. urban areas (CAA, 2004). In Europe similar rules apply and the EU are currently working on producing a full framework for UAS flying that will include additional stipulations about kinetic energy on impact that will effect airframe construction methods and materials (Hagner, 2011).

The key advantages of using a UAS platform are often financial, temporal and spatial benefits over established remote sensing platforms. These trade off against reduced flying time and consequential reduced coverage, weight and size related sensor limitations, platform stability and vibration issues, and weather related flight limitations (Hardin & Jensen, 2011). A common issue throughout the literature is maintaining spatial and temporal benefits and managing the difficulties without losing the financial benefits of using a UAS.

2.2.1. Sensors

UASs potentially could carry a variety of sensors, but weight is a key consideration. It requires miniaturisation of some sensing devices (multispectral, hyperspectral, LiDAR) and often these products are not available for purchase, or not available at a

reasonable price. For this reason most remote sensing from UASs is done with small format off-the-shelf digital cameras (Hardin & Hardin, 2010) operating in the visible spectrum, ultra-violet or near infra-red. They are both affordable and light, have long battery lives and data storage is simple and cheap. They can be used for a variety of purposes including simple image classification (e.g. Laliberte *et al.*, 2011), NDVI classification (e.g. Hunt *et al.*, 2010) and photogrammetry (e.g. Niethammer *et al.*, 2009). More complicated sensors have been used on UASs. For example, Rango *et al.* (2009) have made use of a Tetracam ADC-Lite (Tetracam, 2011) multispectral sensor, and Meggio *et al.* (2010) have used an AHS (airborne hyperspectral sensor) and thermal sensor. Active sensors have also been developed such as synthetic aperture radars (Zaugg *et al.*, 2006; Edrich & Weiss, 2008) and LiDAR systems (Archer *et al*, 2004; Vierling, 2006; Sugiura, 2007; Lambers *et al.*, 2007; Spiess *et al.*, 2007).

2.2.2. Applications in Photogrammetry & Geomorphology

Early UAS application has been concentrated gathering spectral information for vegetation analysis (e.g. Meggio *et al.*, 2010) or simple imagery for visual analysis (Aber *et al.*, 2002). Photogrammetry has been used from the outset (Przybilla & Wester-Ebbinghaus, 1979), but has only recently been widely used due to progress in photogrammetry that accommodates small format photography (Szeliski, 2010). Applications of UAS based photogrammetry in geomorphology have been limited and in glacial geomorphology there only appears to have been a few published examples of basic UAS use. They have been used for collecting oblique photography (Aber *et al.*, 2002; Aber & Ber, 2007; Smith *et al.* 2009; Aber, 2010) and some unpublished work on photogrammetry from UASs (Welty *et al.*, 2010; Westoby, 2011), but little else.

Possibly the first attempt at UAS based photogrammetry was by Przybilla & Wester-Ebbinghaus (1979) with a fixed wing UAS. This was not a success with the combustion engine powered UAS proving to vibrate too much for reliable image acquisition. This led to experimentation with small helicopters (Wester-Ebbinghaus, 1980) that was more successful, but also more complicated. A more simplistic approach was

attempted by Vozikis (1983) with use of a balloon. This was far less technical in terms of flying, but presented greater photogrammetric difficulty due to the unstructured and irregular nature of the images. A variety of balloon based (Marks, 1989; Johnson *et al.*, 1990; Mori *et al.*, 1996; Karras *et al.*, 1999; Visnovcova *et al.*, 2001), helicopter based (Miyatsuka, 1996; Tokmakidis *et al.*, 1998; Zischinsky *et al.*, 2000) and kite based (Aber, *et al.*, 2002; Smith *et al.*, 2009) platforms were used for photogrammetry, but overwhelmingly the application was for archaeology.

As UASs became more available the applications expanded. For example in natural resource management (Horcher & Visser, 2004), traffic monitoring (Puri, 2004), 3-D crop mapping (Rovira-Mas *et al.*, 2005), vehicle detection (Kaaniche *et al.*, 2005), forest fire monitoring (Zhou *et al.*, 2005), vegetation monitoring (Sugiura *et al.*, 2005), hyperspectral imaging (Laliberte *et al.*, 2011), precision farming (Reidelstuerz *et al.*, 2007; Meggio *et al.* 2010), river monitoring (Masahiko, 2007) and building inspection (Metni & Hamel, 2007). However, UAS photogrammetry has taken time to develop in geomorphology. Initial efforts were limited and largely restricted to kite based image capture (Muster & Boike, 2008; Smith *et al.*, 2009; Marzolff *et al.*, 2009) but whilst capable of carrying large payloads and working in remote areas this platform provides limited coverage. The complexity of using traditional photogrammetric methodologies with moderately unstructured image collections and normal cameras rather than the metric ones usually used in aerial photography certainly did not help the spread of UAS photogrammetry in geomorphology. Issues with exterior and interior information caused by low frequency GPS units, IMU inaccuracies and camera calibration discrepancies mean use of traditional photogrammetry packages is occasionally problematic, sometimes requiring alternative approaches and additional programming (Rango *et al.*, 2009).

In the last few years two key developments have opened UAS photogrammetry to a wider audience. The first was the expansion of open source UAS platforms and autopilots that has made them far more affordable and accessible. Fixed wing (Welty *et al.* 2010) and quadrocopter based designs (Niethammer *et al.*, 2009) have been used, and the variety of autopilots now available such as Paparazzi (Paparazzi, 2011) and

ArduPilot (diydrones, 2011) mean nearly any remote controlled airframe can be adapted through integration of thermocouples or an IMU. As a result, kite based imaging (Aber *et al.*, 2002; Smith *et al.*, 2009), has now been superseded as a low cost option by these UASs that can provide more structured image sets with consistent overlap and cover greater areas (Niethammer *et al.*, 2009). Kites will continue to play a role for some time though as they currently can take larger payloads than UASs, allowing better cameras, and can work in areas where UAS use is illegal (Muster & Boike, 2008) as well as sometimes being more practical for small scale projects (Verhoeven, 2009). The second development has been the use of SfM programmes that have simplified DEM production.

2.2.3.   Structure from Motion (SfM)

SfM is a computer vision approach to photogrammetry that involves determining the 3D structure of a scene from uncalibrated 2D perspectives (Szelsiki, 2010). As it does not require calibrated imagery it can be used with non-metric cameras and without ground control. Further detail on the exact methodology of the approach can be found in section 5.2.5. There are obvious advantages for pursuing a method with a low level of supervision and low technological requirements, and a number of workers have started to explore the potential of this approach. Within physical geography the uptake has not been overwhelming. It has been used to estimate landslide volume (Neithammer *et al.*, in press), ecohydrological research (Templeton *et al.*, 2010), landform size estimate in unsurveyed remote areas (Westoby, 2010) and for preliminary glacial mapping (Welty *et al.*, 2010). The method clearly has potential but is yet to fully integrate into the academic remote sensing repertoire. As such, this study addresses the two most commonly used SfM programmes; Bundler and PhotoSynth that have been used in the studies mentioned above and are both freeware. A third programme, AgiSoft PhotoScan, was also used as it was a recently produced commercial programme, but had shown itself to be a polished, usable and affordable approach to SfM (Verhoeven, 2011)

Chapter 3 Subglacial Bedforms

Work on drumlin formation can broadly be divided into three areas; modelling of the ice bed interface (e.g. Smalley, 1966; Boulton, 1987; Smalley & Warberton, 1994; Hindmarsh, 1998a, 1998b; 1999; Fowler 2000, 2009, 2010), sedimentological studies of drumlin internal structure (e.g. Slater, 1929; Hill, 1971; Dardis *et al*., 1984; Boyce & Eyles, 1991; Hart, 1997; Menzies & Brand, 2007; Stokes *et al.,* 2011) and direct observation/instrumentation of the processes occurring at the glacier bed (e.g Smith *et al*., 2009; Hart *et al*., 2011). Of those three, the third is still in its infancy and so the subject lacks substantive input from the modern analogue.

The lack of quantitative observation with statistically relevant sample sizes is an underlying problem with many theories of drumlin formation and Clark *et al*. (2009) go so far to dismiss the majority of drumlin theories as no more than "ideas, cartoons, concepts or diagrams" (Clark *et al*., 2009, p.679). They propose that future studies should concentrate on models based on physical principles (e.g. Fowler, 2009) and assessed against quantitatively defined landforms (e.g. Clark *et al*., 2009; Spagnolo *et al*., 2010) rather than just developing concepts (e.g. Smalley *et al*., 2000). Whilst recent work is encouraging, drumlins are yet to be modelled in 3-D, although recreation of 2-D ice-bed instabilities has been successful (Hindmarsh, 1998; Fowler, 2000, 2009; Chapwanya *et al*., 2011) and the wavelengths match our best understanding of drumlin length (Clark *et al*., 2009).
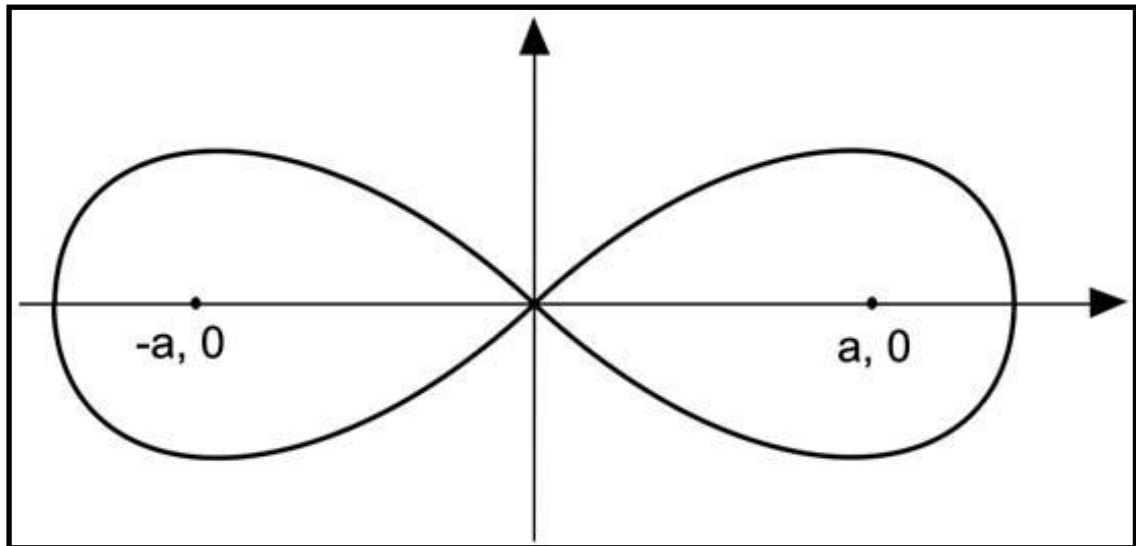
Figure 1: (Spagnolo *et al*. 2010). The lemniscite cosine function, which Chorley (1959) used half of as a representation of the idealised drumlin shape.

3.1.1. Drumlin morphology

Chorley (1959) suggested that the idealised drumlin shape can be described as half a lemniscate cosine function (Figure 1) and this was widely accepted (Smally & Unwin, 1968) and defined as the 'fundamental characteristic' of drumlin form in Menzies' review of drumlin literature (1979). The 'quantitative revolution' (Church 2010) and the elegance of the mathematical description (Smally & Unwin, 1968) made this mathematical description highly attractive. The concept of an ideal drumlin, featuring an asymmetric profile with a steep stoss face facing up ice and a gradual lee side facing down ice, is pervasive throughout the literature and in a variety of secondary education text books. However, this is an idealist view of the drumlin that does not reflect reality (Spagnolo *et al*., 2010). It certainly has impacted the identification of drumlins with authors possibly 'cherry picking' only the drumlins with the idealised shape, but actually when in the early literature there is no particular consistency in the shape of the drumlins identified. For exmple Hubbard (1906) noted some drumlins had a stoss-lee form, but there was no coherence to the direction they faced. Similarly, later papers (e.g. Reed *et al*. 1962; Barnett & Finke, 1971; Mills, 1980; Shaw, 1983; Shaw & Kvill, 1984; Harry & Trenhaile, 1987; Shaw *et al*. 1989; Shaw, 2002) noted departures from the lemniscates loop. However, efforts to provide a quantitative assessment of shape and/or morphology (e.g. Reed *et al*., 1962; Smalley & Unwin,

1968; Trenhaile, 1975; Doornkamp & King, 1971; Muller, 1974; Karczewski, 1976; Rose & Letzer, 1977; Evans, 1987; Coude, 1989; Stea & Brown, 1989) have arguably been hampered by assumption of a lemniscate loop, that may have influenced mapping, although some (Piotrowski & Smalley, 1987; Francek, 1991) do find significant departures from the traditional form.
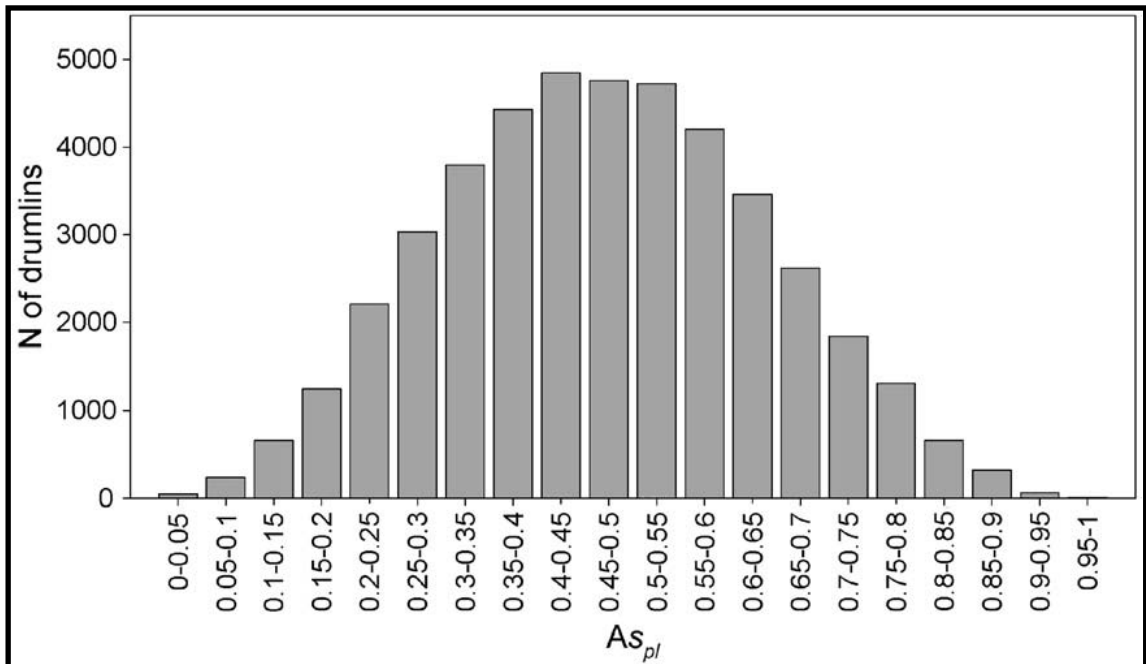
Figure 2: (Spagnolo *et al.*, 2010). A frequency histogram of drumlin parameter As$_{pl}$ in 0.05 bins. If the front of a drumlin is labelled A, the end of the drumlin *C*, and the point that lies on the line A-C at the widest point of the drumlin is labelled *B*, then the calculation of *AB/BC* gives As$_{pl}$ Therefore the parameter is a measure of asymmetry with 0.5 being perfectly symmetrical, values >0.5 indicating a 'classic' drumlin relative to ice flow, and values <0.5 indicating a reversed drumlins.

Recent mapping efforts that use relatively high resolution digital elevation models covering substantial areas (e.g. Greenwood & Clark, 2008; Hess & Briner *et al*., 2009; Hughes *et al*., 2010) have allowed a more statistically rigorous approach to quantification of drumlin size and morphology (Clark *et al*. 2009; Spagnolo *et al*., 2010). Spagnolo *et al*. (2010) examined drumlin shape over a sample of 44,500 drumlins from Northern Europe and Northern America. They found very little evidence of a consistent asymmetric shape, and the majority demonstrated a near symmetrical long profile with the transverse axis intersecting the longitudinal axis close to the midpoint and little difference in the size of the 'upstream' or 'downstream' halves (Figure 2). They also noted that whilst drumlins with the classic form are present, the opposite form is just as common. Often drumlins can be found within the same field with opposing asymmetric forms. This level of variance in the form of drumlins provides

further fuel for the debate over their formation. It would appear to either support theories that include multiple types of drumlin formation (e.g. Hart, 1997; Clark, 2010; Stokes *et al*., 2011), or could just suggest that they undergo change or remoulding after their initial formation (Spagnolo *et al*., 2010).

Clark *et al.* (2009) reviewed a large volume of literature that had quantified drumlin size alongside analysing the tens of thousands of drumlins mapped by Hughes *et al*. (2010) and Greenwood & Clark (2008) in order to produce a quantitative estimate for drumlin dimensions. They found a distinct cut off in horizontal length below 99 m (), a clear elongation/width limit of $E_{max} = L^{1/3}$ and similar distributions in lengths across several field areas (Figure 3: (Clark *et al.*, 2009). Bedforms <900 m long mapped in the Britain and Ireland. The data clearly trends towards an apex at ca 200 m with the shortest drumlins falling at 100 m. Dotted and solid lines are best-fit functions r^2 = 0.48.). They recognise that the validity of this as a lower bound for drumlin size is questionable in light of the usage of limited resolution DEMs for mapping (discussed below). However, they do speculate that finding an average size of 99 m with a 5 m DEM resolution suggests that resolution is not an issue as even at that resolution around 20 pixels are available to distinguish the feature. It is possible that they are right, but there are a number of observations throughout the literature of drumlins with low relief (see Table 1), and clearly this would present an opportunity for a smaller length drumlin to go undetected in a NextMap DEM. Indeed, throughout the literature, there are also frequent references to 'drumlinoid' features smaller than the recorded drumlins (e.g. Hubbard, 1906; Stea, 1989; Zelcs & Dreimanis, 1997; Hattestrand, 1999). However, due to the wide range of terminology used in drumlin literature the term 'drumlinoid' lacks a consistent definition. These would suggest that preconceptions about drumlin size have impacted sampling in a similar manner to the preconceptions of shape.
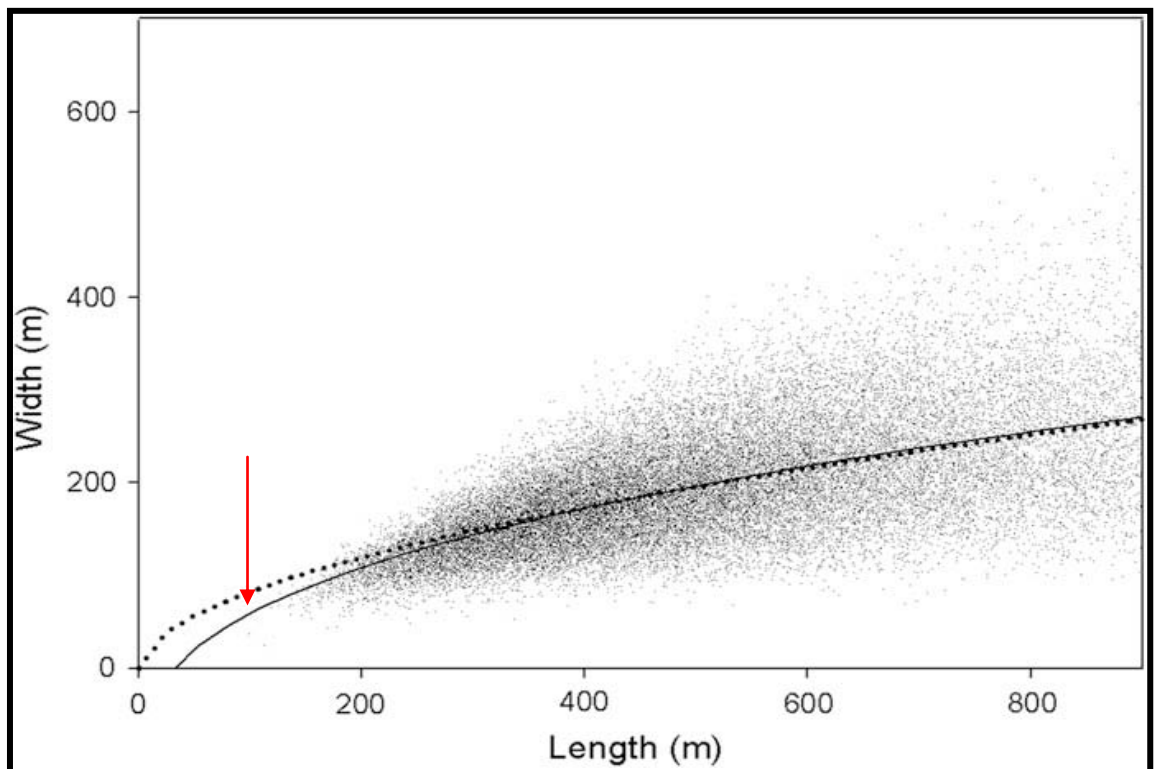
Figure 3: (Clark *et al.*, 2009). Bedforms <900 m long mapped in the Britain and Ireland. The data clearly trends towards an apex at ca 200 m with the shortest drumlins falling at 100 m. Dotted and solid lines are best-fit functions r^2 = 0.48.
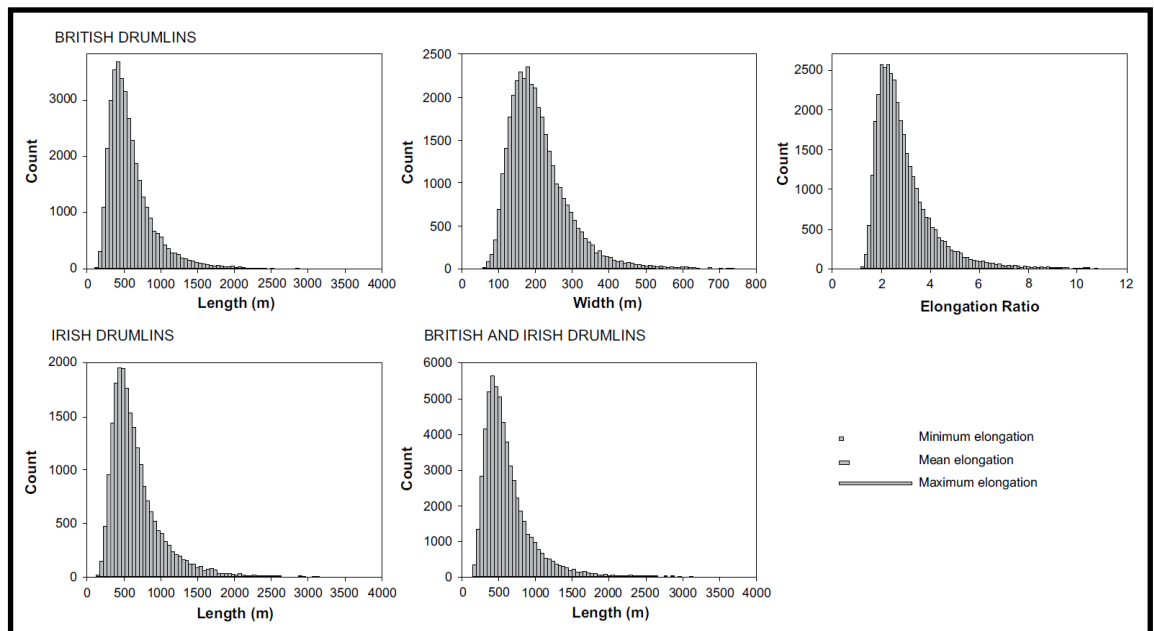
Figure 4: (Clark *et al.*, 2009). Histograms of the distribution of drumlin dimensions for Britain, Ireland and the combined data set studied. As with Figure 3: (Clark *et al.*, 2009). Bedforms <900 m long mapped in the Britain and Ireland. The data clearly trends towards an apex at ca 200 m with the shortest drumlins falling at 100 m. Dotted and solid lines are best-fit functions r^2 = 0.48., this clearly demonstrates the cut off in drumlin length at around 100 m.

Table 1: A brief sample of papers from the literature that record drumlins with low relief. The raw data is not always presented so it is probably sensible to assume that these may have come from qualitative observations.

Authors (year)	Country	Amplitude	Length	Width
Haavistohyvarinen (1987)	Finland	1 m	100 m	50 m
Rouk (1989)	Estonia	<2 m	N/A	N/A
Hattestrand (1999)	Sweden	1 m	100 m	10 m
Van Landeghem (2009)	Irish Sea	1 m	100 m	N/A
Velic (2011)	Croatia	5 m	71 m	25 m

Quantification of drumlin form through mapping attempts (e.g. Hughes *et al*. 2010; Wellner *et al*., 2006) are of great importance. However, if they are limited by the resolution of the elevation models, then the data will need to be used carefully. Smith *et al*. (2006) demonstrate that a resolution of at least 5 m is required to produce a good replication of field mapping, and that it produces significantly better results than efforts using contoured map data. Napieralski & Nalepa (2010) suggest that using a 10 m DEM might actually be the most effective for automated procedures. They show that for the area studied the features are still effectively extracted, and at with lower demands on computing power. Their conclusion may not have significant application though as their sample area only included 16 drumlins, none of which could be considered particularly small at 244 – 1279 m long. Perhaps the Smith *et al*. (2006) conclusion also has some vulnerability. Whilst the 5m DEM was shown to be suitable for identifying field mapped features with an effective resolution of 1 m, there is possibly a need to look at features that may not be distinguishable in the field. The ability to do so evidently is one of the primary benefits of remote sensing and so it would appear sensible to test Clark *et al*.'s (2009) conclusions by studying previously mapped areas with higher resolution DEMs.

3.1.2. Summary

Drumlins are a subset of subglacial bedforms and are the most studied of any glacial landform (Lowe & Walker, 1997). Despite this, an entirely satisfying theory of their formation is yet to be presented. The development of a formational theory has not been helped by, until recently (e.g. Clark *et al*., 2009; Spagnolo *et al*., 2010), a lack of quantitative and thorough investigations into drumlin morphology and size. The analysis (Clark *et al*., 2009) of Hughes *et al*.'s (2010) mapping of drumlins in the British Isles suggested that a key characteristic of drumlins may be a minimum length of 100 m, but potentially this characteristic is scale dependant due to the use of a 1 m accuracy 5 m resolution DEM in mapping. The minimum length of drumlins is potentially a key characteristic of their formation and is required for current modelling efforts (Fowler, 2009), therefore establishing whether Hughes *et al*.'s (2010) mapping was scale dependant is important. High resolution DEMs may allow us to do this and so photogrammetry will be used in this investigation for producing sub-metric accuracy, centimetric resolution DEMs of a small study area in NW England which lies within an extensive drumlin field.

Chapter 4 Study Site

The Eden Valley is well known for its complicated glacial history, with several flow reversals recognised during the Devensian and drumlins produced by ice flowing from the NW, W and SW (Riley, 1987; Clark, 2002). Erratics from Scotland, The Lake District, and Howgills, are all present in the area, but the extent and duration of each flow is not well constrained (Clark, 2002). Rosgill (Figure 5) lies to the west of possibly the most complicated area in the region, the Appleby Line, where drumlins appear to demonstrate convergent flow that produced now discredited theories of ice flowing in two directions (Evans *et al.*, 2009). Rather current ideas for the area around Appleby suggests over printing occurred due to variation in ice dispersal centres within a single glacial period (Rose & Letzer, 1977).
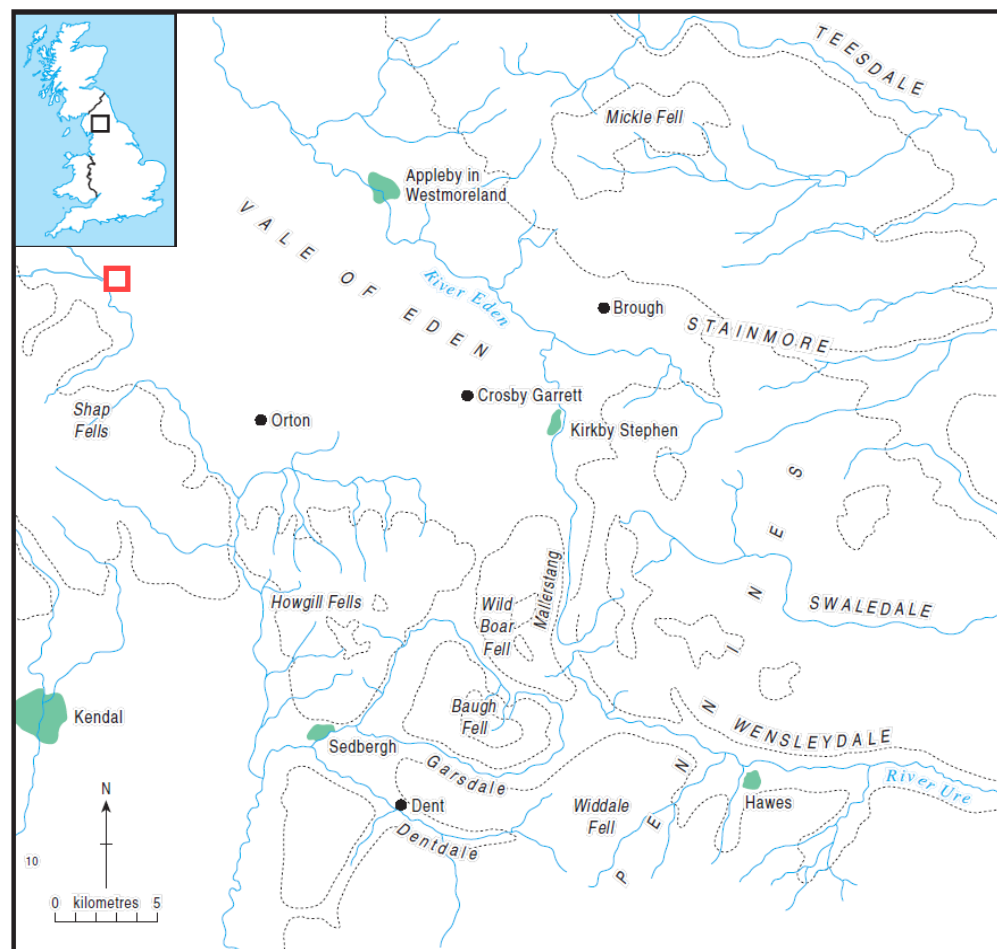
Figure 5: Map of the SE section of the Eden Valley, with the Rosgill site highlighted in red. Reproduced with amendments from Mitchell *et al.* (2006).
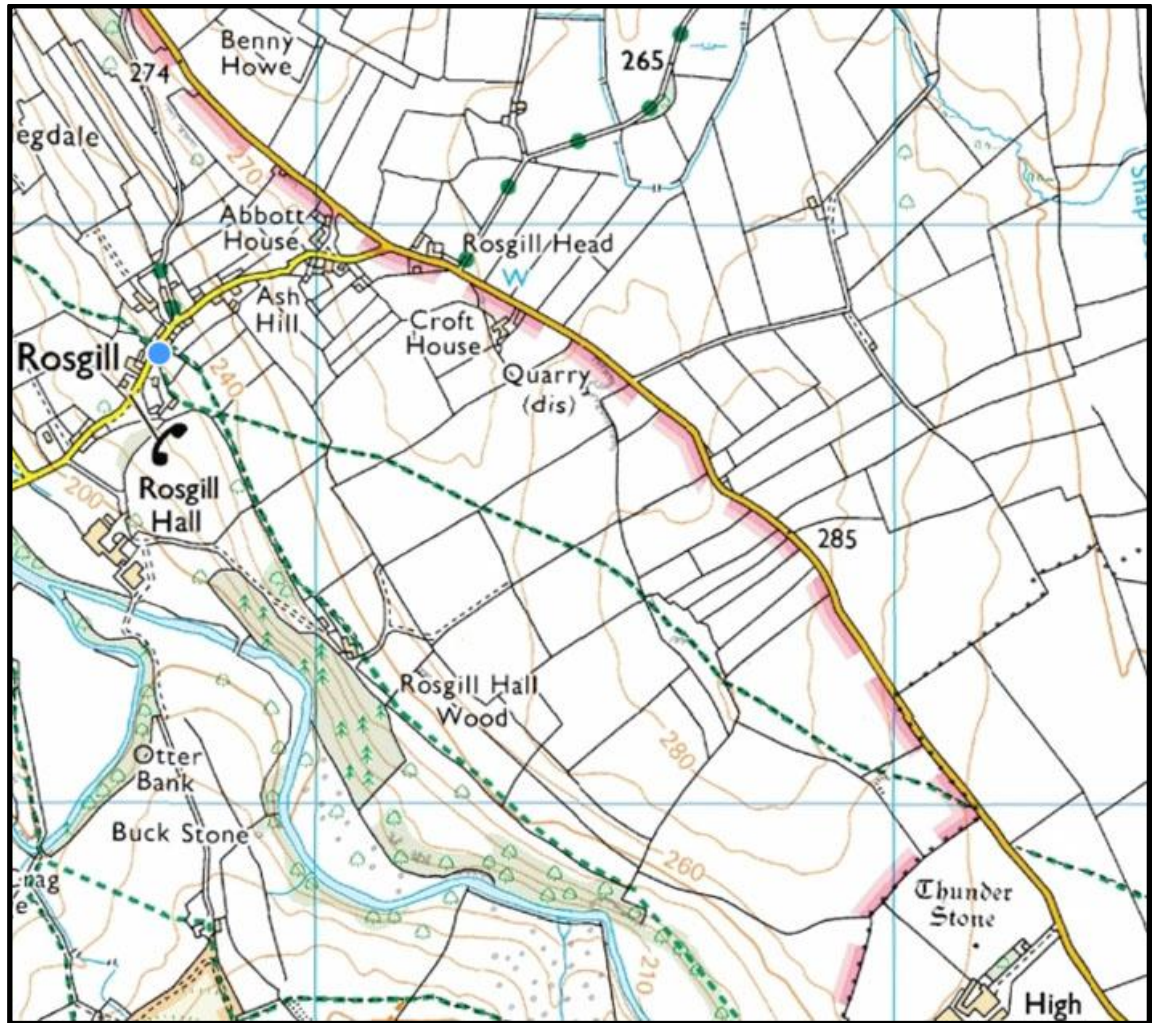
Figure 6: © Microsoft Corporation 2012. Ordnance Survey map (1 grid cell = 1km^2) showing the area around the flying site (centre).

Early observations of flowsets, groups of coherent bedforms, in the area around Rosgill by Trotter (1929) suggested that it had been subject to ice flowing NW from the Howgills, and NE from the Lake District. These ideas are supported and expanded on by Evans *et al*.'s (2009) modelling. They show initial unrestricted dispersal from upland areas into the Eden Valley and NW into the Solway Lowlands. With advance of Scottish Ice down the coast and into the Solway region, ice thickened in the Eden Valley resulting in a reversal and ice flowing over the Stainmore Gap. When the Scottish ice retreated again in deglacation the process was reversed and ice flowed into the Solway region again, before receding southwards onto the North Pennine plateau (Clark *et al*., 2006).

Therefore, it is likely that Rosgill has been impacted by local flows of ice into the lower areas of the Eden Valley during glaciation and deglaciation of the area, and also the major flows into the Solway and Tyne Valley. As deglaciation from the LGM is likely to have been rapid (Evans *et al.*, 2009) the dominant flowsets are likely to have been from the two major flows. This may explain why, from NextMap DEMs, the streamlining appears to be strongly focussed along a NW-SE axis, with little evidence of cross cutting composite landforms.

4.2. Justification for selection of study site

The survey area was chosen as the surrounding area suggests the presence of small drumlins. It was one of several areas where Hughes *et al.* (2010) mapped small (<200 m length) drumlins in the UK and was accessible by car from Durham in <2 hours. This allowed windows of weather conditions favourable to UAS flying to be capitalised on at short notice. The site is located relatively high within the Eden Valley and so will hopefully not have received as much postglacial fluvial erosion that can impact drumlin preservation (Riley, 1987). Its relatively high position in the valley also may have led to thinner ice and so smaller bedforms. The NextMap coverage of the area would appear to correlate with this and shows much less clear features. This could of course be due to a lack of bedforms in the area, but as bedforms surround the site in lower areas it would be sensible to hypothesise that was due to a reduction in amplitude of the features rather than a total absence.

The site is also suitable for UAS flying. It is largely open grass fields used for grazing livestock and divided by dry stone walls. The fields provide easy sites for landings, and individual stones within the walls can be resolved in the imagery increasing the tie points available during photogrammetry. There is also very little woodland, making flying easier and reducing post-processing difficulties. An additional benefit was the existence of Environment Agency LiDAR data of the area with a 1 m resolution and 1 m accuracy. The coverage of the site at Rosgill is due to its proximity to the River Lowther (approx. 1 km away) as the LiDAR was originally collected for use in the Eden Valley Rivers project. This data set is valuable as it provides a useful validation of the photogrammetric DEM produced in this study.

It is worth noting here that is not a large study site, with the survey area <1 km^2. This is a major limitation of the study from the perspective of the third aim. However, this study is primarily about establishing the suitability of the method, and this can be achieved without survey large areas, and indeed restricts the expansion of the study. Therefore, the choice of a small site is not a limitation to the study as a whole, but should be considered when drawing wider conclusions from the mapping of bedforms at the site.

Chapter 5 Methodology: Image Acquisition, Post Processing and Mapping

The methods used in this study can be divided into three sections; image acquisition (section 5.1), post processing (5.2) & mapping (section5.4). Image acquisition covers all usage of the UAS including an explanation of the flight process and technical details. Post processing involved the usage of four different photogrammetry programmes. The basic concepts of photogrammetry are presented followed by the key elements of the automated photogrammetry programmes used. The background and particulars of each programme is then introduced along with the exact manner of operation where suitable. Finally, mapping (section5.4) covers the use of ArcMap to compare bedform sizes between the DEMs produced and pre-existing NextMap and LiDAR DEMs.

Whilst the use of the four different photogrammetry programmes primarily focuses on simply producing DEMs from the imagery collected with the UAS, the requirement for the processing to be low cost and low complexity carries equal weight. This is reflected in the progression through the four different packages used, and the balancing of complexity vs price. Similarly it would have been more suitable to test a variety of UASs in varying conditions but unfortunately the project was restricted to one for financial reasons. With that in mind, and in the knowledge that UAS technology is improving constantly, the limitations of the UAS used are discussed and desirable future features are identified.

5.1. Image acquisition

5.1.1. General flying considerations

Before application can be considered it is essential to have an airframe and flight system capable of operating in the study area. Certain restrictions are mandatory. The

airframe must be capable of flying safely at or under 125 m. For fixed wing UASs, this means a high lift low stall speed airframe is required (Hardin & Jensen, 2011). Whereas flying at higher altitude allows for stalls to be corrected, at this lower altitude a stall could easily result in a crash. An additional benefit of low stall speeds and slow flying is improvement in image capture (Walker & Devore, 1995). Aside from the obvious benefit of greater image numbers, exposure length can be increased, which allows for imaging to take place in poorer lighting conditions. Sensors with long latency times, often a feature in meteorological applications, will also benefit (Reuder *et al.*, 2009). However, low speed flying does require payloads to be kept low, and also sensors to add limited drag. This requires sensors to be kept light and miniaturised. As well as limiting flying speed, payload also impacts range via fuel consumption and renders the already problematic take-off and landing phases even more difficult.

Alongside the technical aspects of the airframe construction, piloting is an aspect to be considered. Take-off and landing are areas that present potential for damaging crashes and may require a degree of skill from the pilot. An alternative to manual take off and landings is available with some autopilots (e.g. Kestrel: http://procerusuav.com). Once altitude has been achieved, flying tends to be relatively simple. There are a variety of autopilots available that will work off GPS and thermopile or intertial (IMU) stabilisation systems (Hardin & Jensen, 2011). These have been shown to be capable of accurately flying preset flight lines and are a relatively mature technology (Rosenburg, 2009).

Flight conditions can be challenging for UASs but, under low clouds, they do present a significant advantage to manned aircraft. If the UAS uses an IMU and is capable of flying in low light conditions they can be used whilst manned aircraft are grounded (Tomlins, 1983; Sugiura *et al.*, 2005; Jones *et al.*, 2006; Lewis, 2007). But, as winds increase, UASs become difficult or impossible to fly and take off and landing becomes particularly dangerous (Hardin & Jensen, 2011). Their ability to fly in winds is dependent on engine power and airframe design. Whereas an airframe designed for low stall speeds will be very stable in calm conditions it will tend to be buffeted

uncontrollably in higher wind speeds. A faster airframe will tend to work in higher wind speeds, but there is a direct trade off with general stability. For this reason, most airframes will be designed with stability in mind in order to maintain air photo quality. However, this limits the conditions that can be flown in, and even then, the platform may become too unstable for quality photography, even in light winds (Rango *et al.*, 2006; Dunford *et al.*, 2009). One approach to winds and thermals is to fly in the calm early morning and late evening. But whilst image blurring tends to be reduced, the long shadows caused by a low sun can effect image interpretation and impact analysis (Hardin & Hardin, 2010). Less obvious flight condition issues include difficulties with salt water (Jones *et al.*, 2006), electromagnetic interference with navigation systems and telemetry interference from other radio controlled devices in populated areas (Hardin & Jensen, 2011).

5.1.2. General imaging considerations

The camera used for imaging has significant consequences for both the resolution and accuracy of the DEM producible via photogrammetry. It may even impact whether the DEM creation is even a tractable calculation. Essentially the choice is defined by the payload of the UAS, although occasionally there are additional technological implications. For instance, aside from the payload restrictions of the UAS used in this study, the camera is controlled by a USB input from the UAS onboard control unit. This particular 'hack' is only available on Canon small format cameras.

5.1.3. Undoubtedly a DSLR (Digital Single-Lens Reflex) camera provides the best images. They tend to have better sensors than compact cameras, there are a range of lenses available minimising distortion, and they can be calibrated ensuring internal geometry stability. However, despite their clear advantages in terms of imagery they also weigh substantially more than compact cameras. As a result they are almost exclusively the preserve of platforms like kites (e.g. Aber *et al.*, 2002; Smith *et al.,* 2009). UAS information including previously known limitations

The PAMS (Personal Aerial Mapping System) Smart One B UAS (Figure 7) is designed to collect aerial images and accompanying geospatial information, primarily for creating orthomosaics and DEMs via photogrammetry. The UAS has a wing span of 1.2 m and weighs 1.1 kg including a Canon Ixus 70 camera. It is designed to be flown by one person, and is transported in a case measuring 0.85 x 0.40 x 0.15. It is capable of fully autonomous flight and it is controlled by a laptop via an 868 Mhz radio link. The control software is the open source autopilot programme Paparazzi (Paparazzi, 2011) that is developed by a number of contributors and a research stream at ENAC (Ecole Nationale de l'Aviation Civile). Alongside the UAS module the kit includes a remote control, radio transmitter and ruggedized laptop, which holds flight and post-processing software.

Figure 7: The PAMS SmartOne B UAS assembled along with its case

Flying at 200 m above ground level, it captures images with 0.10 m resolution. However, due to flying restrictions in the UK, UASs are required to be flown under 125 m. Whilst flying at 100 m produces imagery with 0.05 m resolution, there is a trade off with image sharpness due to the relative ground speed increasing. To balance these factors, flying at 125 m is generally the best compromise, but flying lower than this is

often necessary to reduce the impact of wind. The UAS is powered by a 200 w electric motor run off an 11.1 v Li-Po battery and generally achieves a flight period of 30 – 45 mins depending on the wind conditions. Flying at 125 m and at an average 13 ms^{-1} this usually means imaging an area 400 x 400 m.

The UAS airframe is relatively resistant and made of shock absorbing plastic and polystyrene parts. It does not have an undercarriage and is designed to be launched by hand and, effectively, 'belly landed'. Whilst it is very resilient and easily repaired, it helps to land it on soft and even surfaces to minimise damage through impact or snagging. If the surface is particularly rough or otherwise unsuitable, it is possible to catch the UAS rather than landing it.

The autopilot system is dependent on infrared thermopiles for sensing attitude. Three pairs of sensors are used and cover the x, y and z axis in order to monitor pitch and roll (x and y) and provide absolute values (z). The sensors work on the principal that the sky is cold relative to the Earth. Therefore at 0° pitch or roll there will be no difference in signal between the two sensors, but at 90° it will be at its maximum. A linear regression can be calculated from this and pitch and roll can be calculated and corrected during flight. Although earlier models of the PAMS UAS flew with just the x and y axis sensors, the z axis sensors further improve the accuracy through provision of a reference value for the ground and sky. Furthermore, a safeguard is in place ensuring that a minimum radiative temperature difference exists between the ground and the sky, preventing the UAS from 'arming' if this is not met. In practice, this means that the UAS can only be flown on bright clear days or with sparse or thin clouds. With a low ceiling of relatively warm clouds, the thermal contrast with the ground drops and the platform becomes increasingly unstable. The UAS will automatically sense this and communicate the values back to the laptop via the radio link. This information is also recorded in the geospatial data used later for constructing DEMs and orthomosaics. In the latest version of the SmartOne, the thermopiles have been replaced with an IMU. As well as providing greater accuracy this also removes the lighting restrictions to flying.

The Canon Ixus 70 camera is perhaps the primary limitation of the platform. Changing it is not possible due to the firmware in the UAS. Whilst it has a relatively good sensor and lens, calibrations display that it is relatively unstable. The level of this instability has not been tested within this study, just the alteration from the initial calibration, but it is possible that within a survey the internal geometry changes due to lens retractions between flights and also landing impacts.

5.1.4. UAS flying

There are a variety of different UASs and autopilot systems available and so it is worth documenting the PAMS SmartOne B UAS flight process for comparison.

1. Flight location choice.

The first step is to identify a location for take-off and landing. There are three factors to consider here. It must be in a suitable and preferably central location if multiple flights are planned. For landing there should be a stretch ideally 100+ m of open grass that faces into the wind (if there is any). If there is wind, this will also be ideal for take-off, but in the absence of wind it is useful to find a raised area for launch, to allow more time and vertical fall distance for the UAS to accelerate and develop lift.

2. Set up and flying.

With the area selected, the UAS is assembled. In its case it consists of: 2 wings, 2 wing tips, 2 joining rods for the wings, fuselage, camera with programmed SD Card, 2250 mA Lithium Ion battery and laptop radio transmitter. In a separate case there is the remote control, a radio band checker and a variety of spares such as propellers, nose sections and fabric tape. A laptop is required for the running of the flight programme, and a ruggedized lap top has been used for the flights in this study. The set up and flying procedure then continues as follows (Figure 8):

Assembly	• The wing joining rods are placed into one wing (figure), the second wing is slotted onto these rods (figure) and a Velcro strap is done up to hold the wings together (figure). • Wing tips are attached via a wire rod (figure) and a Velcro strap (figure). • The fuselage is slipped over the wings (figure) and secured at the nose with two Velcro straps (figure). • The battery is secured in the nose section (figure), connected (figure) and the nose section closed. • In the central section of the fuselage the wing servos are plugged in (figure). The camera is turned on, plugged in, and secured (figure). The UAV is then turned on (figure) and the fuselage closed and secured.
Laptop set up	• The radio link is attached and via usb. • The flight programme is launched. • A georeferenced image of the flight area is loaded (figure). • A 'new flight' is selected (figure). • The survey area is defined. This is done by setting the flight height and then dragging a box to the desired size and position. If there is any wind the flight lines should be positioned across the wind. Flying with the wind will often result in the UAV going faster than desirable and increase motion blur in the images (figure). • A 'park zone' is selected. This is where the UAV will fly to when set under automatic control but not carrying out a survey or if contact is lost between the UAV and laptop. It is helpful to have it near the landing zone (figure). • The UAV is then turned on. This should establish a link to the laptop via the radio link.
Pre-flight Checks	• Battery levels should be checked, and if fully charged will be close to 12.5 v (figure). • The UAV should be placed a few metres away from the operators on the ground. It should then establish a GPS lock. This will result in a UAV symbol appearing on screen on the georeferenced image, and the GPS symbol going green (figure). • It will also detect contrast levels. If this is over 100 the contrast levels will be deemed suitable for flying and the contrast symbol will go green (figure). • The RC is now turned on and the UAV is 'armed'. The engine is revved to full throttle, and then the aerilon control is tested.
Flight	• The RC is set to 'semi-auto'. • The UAV is thrown into the wind by one operator, and the second operator controlling the RC goes to full throttle and flies the UAV upwards. • Once altitude of around 25 m is achieved the RC can switch to 'full auto' and the UAV will fly to its 'park' zone. • The survey can then be started at from the laptop. • During the survey one operator is required to maintain eye contact with the UAV. Because of this it is useful to have the second operator watching the laptop to monitor battery levels. If the danger of collision with another aircraft does arise the UAV can be put down with the RC or the laptop. • Once the survey is completed the UAV will return to the 'park' zone. The operator then switches to semi-auto control, reduces the UAV altitude and lands the UAV. • Post flight checks (throttle, aerilons) are carried out again to check no damage was sustained in the landing. • The UAV is disarmed at the laptop, switched off at the fuselage, and packed away.

Figure 8: Flow chart of UAS flight process.

5.1.5. Rosgill Survey

Imagery of the Rosgill field site was gathered in four separate flights on the 8th February 2011. Due to the use of different age batteries with variable capacities, flights 1 and 2 were slightly larger than 3 and 4. Inclement weather prevented flying until early afternoon, and Flight 4 suffered from slightly poorer lighting than the previous flights. This prevented further flying that might otherwise have been undertaken in addition to the planned flights. As multiple flights cannot be planned out at once, it was judged sensible to err on the side of caution and plan overlap between each flight. The full area covered and level of overlap between flights is displayed in Figure 10.

5.1.6. Ground Control

Ground control was required for some stages of the post processing, namely image triangulation in LPS. Whilst not strictly necessary it was also a useful addition to PhotoScan. A Leica differential GPS was used to collect 24 points across the study area. The DGPS was set to capture points with an accuracy of >0.025 m and so particular efforts were made to select location that would allow a similar level of accuracy to be maintained in the post processing stage whilst selecting the control points in the images. Due to the homogeneity of the area this largely meant the use of walls, drain covers, large rocks and fixed location farm machinery. These were easily identifiable in the UAS imagery and a suitable spread across the site was still achieved.

Figure 9: Ground control was collected with a differential GPS with accuracy >0.025 m. Due to the high resolution of the imagery, individual rocks were easily distinguishable and so these were used as control points during the survey.

5.2. Post processing

Photogrammetry was used to produce 3-D models from the imagery acquired with the UAS. A brief introduction to the technical principles of the subject is presented in section 3.3.2. A more specific section then covers the particular programmes used and their approaches to photogrammetry.

5.2.1. A simple introduction to technical details of photogrammetry

Photogrammetry can be thought of as a geometric problem. For 2-D measurements that lie parallel to the plane of an image; distance on the image can be converted into real distance if the scale is known. 3-D measurements are more complicated and require two perspectives of the object under consideration. Given the position of the

object on the image, the position and orientation of the camera (exterior orientation) and the properties of the camera (interior orientation), the position of the object can be calculated via triangulation. If the interior and exterior parameters are known, the complexity of the process is primarily due to the repeated translation of coordinates through different Cartesian coordinate systems that refer to the object's position on the image (image space) and in real life (object space). If the parameters are not known, the complexity increases significantly and requires a least squares approach to generating a solution.

As photogrammetry is, these days, rarely done manually, the need to have an in-depth knowledge of the exact equations is not required to produce results, and so the topic is not covered here for the sake of brevity. Understanding the interior and exterior parameters remains extremely important though as these continue to be user-supplied. Thus, this section covers some of the technical details of the parameters, but for a more consummate and mathematical coverage of the subject Wolff & Dewitt (2000) provide an excellent account.

5.2.2. Interior orientation

The interior orientation regards five metric characteristics of the camera. Cameras can be either metric or non-metric. For a metric camera internal orientation is highly stable, lens distortion is minimal, principal point offset is zero and there is an image coordinate system defined by fiducial marks. Using a metric camera for photogrammetric tasks is obviously preferable as it removes a number of unknowns from the calculations, but in the case of this study a non-metric camera digital camera is used. This means that at best, the interior orientation of the camera can be regarded as 'initial'. With most digital cameras this data is available as an .exif file associated with the images, but a more accurate initial set of values can be obtained by calibrating the camera before use. The parameters are:

1. Focal length

2. Radial distortion

3. Coordinates of the ficudial marks

4. Position of the perspective centre respective to the fiducial marks

5. Image resolution

Essentially, these parameters allow the user to reconstruct how the points on an image relate to the actual points on the ground, or in more precise terms, how the photo-coordinate system relates to the measuring coordinate system. A photo-coordinate system is used in addition to the measurement coordinate system because it is only defined mathematically and cannot be measured, preventing it from being described by the 'real' measurement coordinate system.

We can depict the relationship between the two coordinate systems graphically or through a variety of mathematical transformations. At the simplest level, a similarity transformation can be used. However, in most cases this does not consider all variables. Therefore, in general, a more complicated transformation such as an affine transformation is used and additional calculations are done to correct for a variety of factors such as radial distortion, refraction and Earth curvature.

5.2.3. Exterior orientation

Exterior orientation defines the position of the camera within the measuring coordinate system. It is defined by the location of the perspective centre, expressed in terms of the measuring coordinate system, and the attitude of the camera expressed as three angles.

For an image with known position 'control points' it is possible to calculate the six exterior orientation parameters via a collinearity model. However, with only a single image, it is not possible to reconstruct the object space, but with the addition of a second image with a different perspective on the same area this is possible. There are then a number of options for the user to use the collinearity model to convert the images into different coordinate systems. Generally, the procedure is to convert the

coordinates into a relative coordinate system based on the first image in a strip. The entire image set can be converted into an absolute system based on ground control points.

5.2.4. Automated photogrammetry

Automated photogrammetry takes a number of forms. All use feature-based alignment, but do so with varying amounts of supervision and a number of unknowns. The automated photogrammetry market is dominated by SOCET SET and LPS, but, in recent years a number of alternatives to classical photogrammetry have become available including Bundler (Snavely *et al.*, 2008), PhotoSynth (PhotoSynth, 2011) and AgiSoft PhotoScan. This study has used all of these programmes with the exception of SOCET SET which was not available and is prohibitively more expensive than the other commercial packages LPS and AgiSoft PhotoScan.

There are four different methodologies that are used in automated photogrammetry, and all are versions of a non-linear parameter minimization (Szeliski, 2010). Pose estimation regards the determination of a camera's position with regard to a scene; intrinsic calibration involves the calculation of the internal camera parameters such as focal length and radial distortion; and triangulation regards estimating 3-D point structure from 2-D matches. The final method is Structure from Motion (SfM) that involves simultaneously estimating all of the above at once. Of the programmes used LPS is the only one not capable of SfM.

Structure from motion is a technique developed in the late 1980s, which involves reconstructing a 3-D scene whilst also constraining internal and external camera information via feature correspondence between images (Longuet-Higgins, 1981). Initially, this was for pairs of images (Longuet-Higgins, 1981) but it was further developed in to a multi-frame technique (Tomasi & Kanade, 1992) and then for global situations (Spetsakis & Aloimonos, 1991; Szeliski & Kang, 1994; Oliensis, 1999). A key progression in the multi frame and global SfM approaches is the use of bundle

adjustment algorithms. These are responsible for the refinement that allows production of the jointly optimal 3-D scene and camera parameter estimates (Triggs *et al.*, 1999).

The primary advantage of the SfM approach is that it can be used for unstructured collections of images that may not initially have been taken for use in 3-D reconstructions. The PAMS SmartOne UAS does record camera position and attitude, but the data is only available via PAMS processing the flight log files. Even when exterior information is available from the UAS issues such as a low frequency GPS unit can mean the positions are far less accurate than required (Laliberte & Rango 2011). Therefore, these programmes present an opportunity to circumnavigate these restrictions. Reconstructions such as those by Neithammer *et al*. (in press) face similar issues as they do not have a structure to their imaging of the site, they only aim for coverage with some degree of overlap.

Bundle adjustment is a robust non-linear minimization of the re-projection errors and the most accurate manner in which to recover SfM (Szeliski, 2010). It takes its name from the 'bundles' of light from 3-D features that converge on the camera centre (Triggs *et al*., 1999). Effectively it is a large sparse geometric parameter estimate problem, with the three parameters being 3-D feature co-ordinates, exterior camera information and interior camera orientation (Szeliski, 2010). This type of problem is used extensively throughout empirical sciences such as meteorology and surveying, and the principal remains exactly the same. To adapt the problem to suit a particular application just requires changing the optimization scheme to one that works best with the structure and sparsity of the application (Triggs *et al*., 1999). Bundle adjustment has become the preferred adjustment method in computer vision/photogrammetry because of three characteristics (Triggs *et al*., 1999). It is flexible, coping with a variety of feature locations and types (points, lines, curves, surfaces), different and unusual cameras, and can cope with missing data. It is accurate, using a consistent and defined methodology that produces precise and easy to interpret results. And, finally, it is efficient, even with large problems, using the sparse nature of the problem to its

advantage. Bundle adjustment is not unique to SfM. It is used in all automated photogrammetry and so in all of the programmes used in this study. The difference between LPS and the other programmes is that more unknowns are included in the bundle adjustment and so less information has to be provided to the programme (Szeliski, 2010).

One potential issue with bundle adjustment is that it is not actually possible to recreate internal information entirely without some form of external information about the scene (Szeliski, 2010). Such information might be parallel lines converging on a point within the scene. With three or more of these in the image, focal length and orientation can be recovered by establishing the homography of the plane at infinity. Without such information, it is not possible to fully recreate the internal camera information. Instead, assumptions, such as internal information not changing between frames, must be made (Hartley & Zisserman, 2004). This can lead to warping of the recovered scene, which then requires 3-D adjustment to control points. Most scenes do have the required features and so this is not always and issue, but it is worth noting why warping does occasional arise in SfM generated DEMs. There are also a variety of algorithmic adaptations that must be used to help solve SfM problems and stop them become intractable.   These are too complicated to be usefully covered here, but Szeliski (2010) presents an excellent review of the subject.

5.2.5. Programmes used for post processing

Bundler and Photosynth are freeware and mostly opensource. AgiSoft PhotoScan is a commercial package, but it is priced affordably for academic use at around £350 and so is relatively accessible. LPS is included in the UK CHEST agreement and is therefore available to UK academia at a reduced cost. Here each piece of software is introduced and their processing methodologies explained.

5.2.5.1.   Freeware packages

5.2.5.1.1.   Bundler toolkit (Bundler, CMVS, PMVS)

The Bundler toolkit (PhotoTour, 2010) utilises three programmes to produce the 3-D reconstruction. Firstly, Bundler is used to calculate the camera positions and attitudes and produce a sparse 3-D construction, then CMVS (Clustering Views for Multi-view Stereo) removes unnecessary images with poor quality or lighting that duplicate areas, and finally PMVS2 (Patch-based Multi-view Stereo Software 2) uses these images to increase the point density of the initial sparse reconstruction (Snavely *et al.*, 2007).

The key to Bundler is, as the name suggests, bundle adjustment. Bundler somewhat improves on the basic bundle adjustment by providing camera information imbedded in the EXIF tags of images. This provides an initial set of values, but is not absolute, because they are often inaccurate due to limited initial calibration of variance over the camera's lifetime. There is no requirement here for expensive or highly calibrated cameras but, evidently, they will help.

Bundler starts by using the Scale Invariant Feature Transform algorithm (SIFT) (Lowe, 2004), a key point detector. This excels at finding features despite differences in scaling, rotation, illumination and 3-D viewpoint. Additionally, the features are distinctive, making matching between different images relatively reliable. Typically, a 500 x 500 pixel image would yield around 2000 stable features (Lowe, 2004). After the SIFT algorithm has finished, keypoints are matched between each pair of images using an approximate nearest neighbour approach (Arya, *et al*. 1998). This is then used to estimate a fundamental matrix for the pair using the RANSAC (RANdom Sample Consensus) algorithm (Fischler & Bolles, 1987). Outlying matches are then removed from the fundamental matrix, and if the number of remaining matches drops to less than twenty, the pair is discarded. With the remaining pairs, matches between pairs are then organized into 'tracks' of matching keypoints across multiple images. This is

again vetted, and if a track contains more than one keypoint in a single image it is discarded.

From this information, the camera parameters and the 3-D location for each track is determined. To improve the consistency of the reprojection error, the sum of the distances between the track and corresponding image feature positions is minimized using a non-linear least squares problem that is solved with the Levenberg-Marquardt algorithm (Nocedal & Wright, 1999). This stage is particularly helpful to the SfM algorithms, as they often get stuck due to poorly constrained local minima, and so this helps by providing the better initial values.

Bundler then estimates camera parameters. To increase the robustness of this stage, this is not done *en masse* but, rather, the cameras are added incrementally. The initial pair of cameras are selected based on the number of matches between them and also their baseline which helps improve the quality of the 3-D locations observed. Next, any camera that observes 75% of the currently projected tracks is added, and tracks observed by this new camera are added into the optimization. As well as the extrinsic parameter calculation, intrinsic parameters are also calculated for each camera. This does require the image file to include EXIF tags that provide an initial value for focal length, but this information can be added separately, if necessary. This continues until all cameras are projected, and to increase the accuracy high reprojection error key points are removed between each camera addition.

An additional tweak to the standard programme is the inclusion of radial distortion parameters for the camera. Radial distortion can produce significant errors in the reconstruction and is quite common when not using expensive cameras and lenses. Therefore, by estimating two radial distortion parameter k_1 and k_2 the model is improved significantly.

5.2.5.1.2. CMVS – Clustering view for Multi-View Stereo

CMVS is an important addition to the Bundler package because it improves the efficiency of the model reconstruction as more images are added. The Bundler toolkit is already computationally intense, and PMVS2 (discussed below) uses a large amount of memory. This means there are scaling issues as we progress to modelling larger areas. CMVS improves the efficiency of the model in two ways (Furukawa *et al.*, 2010). Firstly, it uses the SfM output to cluster groups of images into manageable chunks for processing. Secondly, it identifies whether images are present that have poor resolution or lighting, or duplicate another image, and so are not needed. Therefore, the inclusion of CMVS in the toolkit limits the impact of scaling and allows models to be produced from large numbers of images without the need for very powerful computers.

5.2.5.1.3. PMVS2 – Patch-based Multi-View Stereo software (version 2)

PMVS2 is a multi-view stereo programme that produces dense 3-D reconstructions from calibrated images, which in this case are produced by Bundler. It ignores non-rigid structures such as pedestrians, cars and moving vegetation. The model outputs are a set of oriented points (P_i) with associated 3-D location, surface normal, the relevant images, and a photometric consistency score (Furukawa *et al.*, 2010). PMVS2 can produce very dense clouds, but does struggle in two situations. If the area has little texture it struggles to find tie points. Similarly, if the area's surface is not Lambertian then the results may be unreliable (Furukawa *et al.*, 2010).

5.2.5.1.4. Photosynth Toolkit

Photosynth is an online photo-tourism website run by Microsoft (Photosynth, 2011). It is based on work by Noah Snavely that is also used in his Bundler programme (Snavely *et al.*, 2006; Snavely *et al.*, 2007), but also includes additional features for viewing photos that are aided by Microsoft Silverlight. For 3-D reconstructions, Photosynth

can be used in the same manner as Bundler; to produce camera positions and information from unstructured sets of photos. Photosynth does not work in the same co-ordinate system as Bundler, but the output can be converted with Henri Astré's Photosynth Toolkit (Visual Experiments, 2010) and then used with PMVS2 to produce dense point clouds.

There are advantages and disadvantages apparent when using Photosynth rather than Bundler. It provides a relatively easy user interface and online processing that may reduce computer time providing a suitable internet connection is available. However, Microsoft reduce all images to 1.5 Megapixels and limit each 'synth' to around 300 images to reduce the storage and processing burden on their servers. Similarly, at this stage in its development, the Photosynth Toolkit does not use CMVS. Without CMVS the computational burden of PMVS2 is higher due to the inclusion of superfluous images. This means that the method does not scale well. PhotoSynth's most pressing limitation, however, is that it is designed for phototourism. Whilst this means that usability is high, it also may limit the potential quality of the point cloud generated.

### 5.2.5.2.	Commercial packages

#### 5.2.5.2.1.	AgiSoft PhotoScan

PhotoScan is a commercial SfM software package. It is produced by AgiSoft and advertised as 'an advanced image-based solution for creating professional quality three-dimensional content from still images' (AgiSoft LLC, 2010). It is available in two editions, 'standard' for $179 and 'professional' for $549. The main difference between the two editions is the geo-tools available in the professional version that allow 2-D and 3-D transformations of the models to match ground control or to georeference it.

The main advantages over Bundler and Photosynth, and the reasons to pay for the programme, are usability and speed. PhotoScan will work with a variety of image formats (JPEG, TIFF, PNG, BMP & MPO), has a simple three step approach to point cloud construction and can output the point cloud in a number of formats for further

manipulation including in PDF format for easy inclusion in reports. Whilst it works in a similar manner to Bundler with an initial sparse SfM approach followed by a dense reconstruction, it uses different algorithms that achieve a faster and arguably higher quality reconstruction than the Bundler – CMVS – PMVS approach.

The initial feature identification is very similar to the SIFT algorithm but results in a slightly higher accuracy. The exact details of this are not known outside the company, but it is noticeable that it appears to map a higher number of features. For example, for a 3.5 MB .jpeg files run on 'high' alignment it will find 30-40,000 feature per image which is far higher than SIFT tends to manage at a similar computational burden, although running on 'medium' produces a more comparable 3-4,000 features. Pushed to 'ultra high' it is even capable of getting close to one point per pixel. Similarly, the process for calculating external and internal parameters is slightly different. Here, PhotoScan initially runs a greedy algorithm before refining results with a bundle adjustment algorithm. The greedy algorithm is far simpler than the bundle adjustment algorithm, and will not be as accurate, but would appear to be a good way of decreasing the process time by giving the bundle adjustment algorithms an initial set of values to process. Finally, the dense reconstruction does not use a multi-view approach, instead preferring a pair-wise depth map algorithm. There is a multi-view approach available, but only for the 'fast' reconstruction that is less accurate, suggesting the pair-wise approach is a better way of approaching the process.

PhotoScan provides a range of options for the dense reconstruction; exact, smooth, height field and fast. These allow the user to optimise the reconstruction for the task in hand as, evidently, reconstructions from close range images of an object will differ from aerial photography. The two settings recommended for aerial photography are 'Height field' and 'exact' (Verhoeven, 2011). Exact produces the greatest level of terrain details, but also tends to have holes in the DEM. Height field automatically fills holes, potentially at the expense of some accuracy. It is possibly to run the exact reconstruction and then fill holes manually afterwards, if a precise knowledge of the DEM detail is required. If an image set is too large to be processed, it is possible to

process it in 'chunks' and then combine these afterwards. This can be done in Bundler, but is far more complicated because a third party programme such as MeshLab (Meshlab, 2011) has to be used for the chunk combination. Meshlab is designed for viewing and manipulating point clouds, but the task here is non-trivial and the results are generally unimpressive. At all stages (photo alignment, geometry densification, model texturing), it is also possible to adjust the reconstruction quality. Settings available are; Very High, High, Medium, Low. Similarly to quality choice when running PMVS these settings refer to using the image at full size (very high), ½ size (high), ¼ size (medium) and 1/8 size (low). Therefore, there is a significant processing saving by switching down a category. Alongside this, the final model size can be varied by choosing the number of faces present. This can be useful when exporting into some post processing programmes, for example MeshLab struggles with point clouds with >3,000,000 faces.

5.2.5.1. Hardware requirements

PhotoScan 0.8.3 is available in a 64-bit version and is optimised for multiple core use. RAM requirements are dependent on the amount of data being processed, which in turn is dependent on the number of images, image resolution, and quality of processing specified. It is also Open CL (computer language) compatible and so is capable of using the graphics card for processing if a suitable one is available. Visualisation of point clouds is dependent on the graphics card size. The computing requirements can be summarised to the speed of the job being reliant on processor speed and number of CPUs, and the size of the job being dependant on RAM. When processing, it is advisable to use all cores, if possible, but not to exceed the RAM limit and use page file memory. Doing this drastically slows the programme to the point where it is worth restarting the model.

The computer used in this study is a Dell Precision T1500 running Windows 7 64-bit. It has an Intel i7 processor with 4 CPUs (8 virtual) running at 2.8 GHz, 16 GB RAM and a 4 GB NVIDIA Quadro FX 580 graphics card. This is adequate for running models, but not

ideal. With the 500-1000 image data sets, some compromises over image quality have to be made in order to run the dense reconstruction stage. Preferably, the user would have access to 24 GB RAM or more for running UAS data sets on full resolution, and if more cores or a faster processor is available, then that is obviously beneficial.

5.2.5.2. Programme settings for speed vs quality optimisation

PhotoScan can potentially use a huge amount of RAM and take days to process even on the relatively quick computer used in this study. Because of the limits on UAS flying height in the UK, UAS surveys will always consist of a large number of images. For instance, one survey at Rosgill produced 353 images for an area spanning roughly 400 x 400 m. Because of this, running multiple flight surveys through PhotoScan may not be possible due to limitations on the RAM available. This leaves three options. Resolution can be reduced via the quality settings in 'geometry reconstruction', the number of images can be reduced effectively lowering the overlap, and the area can be processed as several chunks and then combined later.

Evidently, it is preferable to process imagery at the highest resolution possible in order to generate the maximum number of tie points, constrain camera positions as accurately as possible, and produce the best resolution DEM. This means the obvious processing power optimisation is to split the area into chunks. Unfortunately, there is currently a quality issue bug in the chunk process. When combining the chunks there are no options for quality, and PhotoScan appears to run it at a preset low quality. This results in fairly significant down-sampling of the DEMs and, effectively, removes the incentive for initially running the chunks at a high resolution. This leaves the other two options, reducing quality and reducing the numbers of images processed. The best option to pursue first is reducing the number of images. The PAMS UAS achieves 80% overlap but PhotoSynth will work quite comfortably with half that. This means that a simple trim of the image collection to 50% of the original size decreases RAM usage drastically. If processing time is not a concern, the next step is to identify the highest quality level it is possible to run the imagery at without using page file memory. This

47

will generally be 'medium' for large collections of >400 images. If time is a consideration then 'medium' is again the best option. Run times will be in the order of 3 hours for a 500 image set from our UAS (3.5 MB image files). Lifting the quality to high will generally result in an approximately 8 fold (also noted by Verhoeven, 2011) increase in processing time and so may not be feasible.

The density of the final pointcloud is, effectively, graphics limited. Although the user may specify the number of faces desired in the final point cloud, this only defines the decimation of the mesh and PhotoScan will actually produce a full density mesh regardless. It is desirable, where possible, to try and output the full density point cloud, save it, and then decimate it to a workable size in order to leave the full version intact for archive purposes. For the computer used in this study, a sensible size for smooth visualisation was around 5,000,000 points. This was used for georeferencing and quick visual checking, and the full model was used for DEM export.

5.2.5.3. Georeferencing and export

Models can be exported straight after production in a variety of formats with euclidean coordinates. But for export as a DEM in GeoTiff, Arc/Info ASCII Grid or band interlieved file format (BIL) spatial reference is first required. Georeferencing can be done in three ways. Camera positions can be added, GCPs can be added to individual photos and/or GCPs can be placed on the model after it has been generated. The latter approach was found to be the most effective. Using camera coordinates was ruled out due to concerns over the accuracy of the low frequency standard GPS; and placing markers directly on images was too laborious due to each control point appearing on 4 or more images. Placing the GCP on the model also automatically places it on the relevant position within all images. Initial accuracy was not that high, but it is quick and easy to adjust the marker positions within the image.

The georeferencing process illustrates a key difference between SfM and photogrammetry. In photogrammetry, GCPs are introduced at the onset of the process

and the resulting DEM is directly produced in a georeferenced frame of reference. Errors in the GCPs will be minimised in a least-squares sense but will still propagate in the DEM. However, in SfM, position information is only introduced after a DEM is produced in an arbitrary coordinate system. Therefore, the position of information in the GCPs is used in a least-squares sense in order to calculate a 7 parameter rigid transform that will translate, rotate and scale the DEM to the correct frame of reference. The crucial point is that errors in the GCPs will not introduce warp in the DEM. The 7 parameter transform is 100% rigid.

With spatial data added and the arbitrary frame of reference transformed, the model can then be output as a georeferenced DEM. A variety of resolution and projection options are available at this stage but are generally not needed. Whilst a 5,000,000 point model may be difficult to visualise smoothly in PhotoScan, the resulting c.4000x3000 is easily projected in ArcMap.

5.2.5.3.1.   Leica Photogrammetry Suite (LPS)

Leica Photogrammetry Suite, now officially known as LPS, is a photogrammetry package associated with ERDAS. The workflow in LPS is triangulation, followed by DTM extraction and, finally, the use of stereo vision to edit the extracted DTM. LPS is widely used by national mapping agencies and can produce extremely accurate results. For users, this additional accuracy compared to SfM photogrammetry packages is balanced by the requirement for additional data and greater levels of supervision. For metric survey usage it is undoubtedly excellent, but whether it is suitable for non-metric use is less certain. The absence of a SfM approach means that although some parameters can be set as initial, and bundle adjusted to produce a result, LPS will not manage if too many parameters are set as unknown or initial.

Triangulation, the first stage of processing, requires a high level of supervision. LPS requires at least six tie points to be identified in each image, including three ground control points, before automatic tie point generation can then be implemented. After

automatic tie point generation, points should also be checked manually to ensure no false ties have been created. Further to this, LPS is principally designed to be used with metric cameras and so interior camera information is a requirement. When working with un-calibrated small format cameras, this means a calibration must be carried out before triangulation begins. LPS can deal with some error here, if the interior information is set as 'initial', but this increases the likelihood of error occurring elsewhere in the process. For the calibration, the Caltech camera calibration routine was used that runs in Matlab (Caltech Vision, 2010).

It should be noted here that Laliberte *et al.* (2011) have had some success using UAS imagery with LPS by introducing two extra stages. Firstly they use AutoPano Pro to produce automatic tie points across the image set. They then use a programme they have written themselves to convert the coordinates outputted by AutoPano Pro into a format suitable for LPS. With this density of tie points across the data set they do manage to extract good DEMs from their small format photographs. Similarly Eisenbeiss *et al.* (2005) have had problems with LPS stemming from uncalibrated cameras, variable lighting conditions, and poorly constrained camera positions. They too have been able to extract DEMs from LPS but only after also introducing their own programme 'BUN' which carried out additional bundle adjustments to the initial tie points. Smith *et al.* (2009) also used LPS successfully, but their workflow differs from the two projects above as the imagery was collected with a camera with a more stable interior orientation (a DSLR rather than a compact camera). They also benefited from a more structured flight line design. Both of these elements helped them circumnavigate some of the difficulties encountered in this research.

From this previous work it appears that the weakness in LPS's workflow is in tie point generation and matching. LPS's version is far less effective than the SIFT algorithm used in most SfM based programmes, and with poorer tie point generation it becomes difficult to accurately recreate image geometry. It also appears to lead to a higher dependence on other information supplied, making LPS more dependent on precise inputs. Unfortunately, in this study there was not have time to produce an additional

programme or combine AutoPano Pro into the workflow. Therefore, LPS is tested in the project as a standalone piece of software.

5.3. DEM validation

Validation of the resultant DEM is an important step in the process of assessing the quality of any given software package. Primarily, this was achieved by comparison to an existing LiDAR DEM of the area. The LiDAR DEM has 1 m vertical accuracy, so the photogrammetric DEM with a sub-metric resolution has to be downsampled first to match the LiDAR DEM. Error between the two DEMs will then be calculated in MATLAB and values will be given for the precision and strength of relationship of the photogrammetric DEM against the LiDAR DEM.

5.4. Mapping

Once the final DEM was produced, features that could be bedforms were mapped in ERDAS. As with most previous mapping efforts from DTMs (e.g. Clark & Meehan, 2001; Smith & Clark, 2005) hillshading with five times vertical exaggeration was used to enhance the visibility of landforms. Features, roughly defined as any enclosed area of raised ground, were mapped as GIS vector polygons through identification of their bounding break in slope.

Hillshading needs to be conducted with care as it can introduce bias into the mapping process. Smith & Clark (2005) make recommendations for illumination direction, but because this is a small area there was no need to limit the mapping to just a couple of angles. Therefore, to insure full illumination of all features, eight hillshaded DTMs were produce at 45° intervals. Mapping was then initially conducted on with a NW illumination, and then each feature was examined under each illumination angle and adjusted accordingly to reach the best representation of the bounding break in slope. Crestlines and the widest section of each feature were then identified and mapped to

provide the drumlin dimensions. Spagnolo *et al* (2010) actually automatically extract width, but again as the area is small there was no need to replicate this, and they note that the tool achieved excellent correspondence to their manual measurements.

It is worth noting that although utmost care was taken to capture the break in slope surrounding each feature, the mapping will probably be subtly different to mapping styles of previous workers (e.g. Greenwood & Clark, 2008; Hess & Briner *et al*., 2009; Hughes *et al*., 2010). A quantitative automated approach to mapping would be preferable to the inherently subjective approach used here and in most previous work. Whilst techniques for basic 2-D extraction (Napieralski & Nalepa, 2010) and quantitative extraction of 3-D morphology (Smith *et al.* 2009) have been proposed, neither are implemented in this study as testing automated extraction methods was not a key aim. If only minor differences exist between the features mapped in this study and previous work then the influence of mapping will be considered before making conclusions, but if the differences are relatively large the mapping influence will be assumed to be a negligible influence due to the care taken. Therefore whilst automated methodologies should certainly be a focus for future work in order to try and reach a level of standardisation, it is not entirely relevant to this work which could be seen more as a guide to design of future automated techniques.

Chapter 6 Results

As with Chapter 4 this section is presented in three parts. In section 6.1 the imagery collected with the UAS is presented, section 6.2 presents the resulting outputs from each of the programs presented in section 5, and section 6.3 presents the final morphological maps.

6.1. Imagery

As detailed in section 5.1 the Rosgill site was surveyed over four separate flights on the 8th February 2011. Figure 10 shows the extent of each flight. Again, as mentioned in the methodology, the light deteriorated towards the end of the day preventing any additional imagery from being collected. The impact of the lighting change is displayed in Figure 11 with a drop in saturation of the later images.
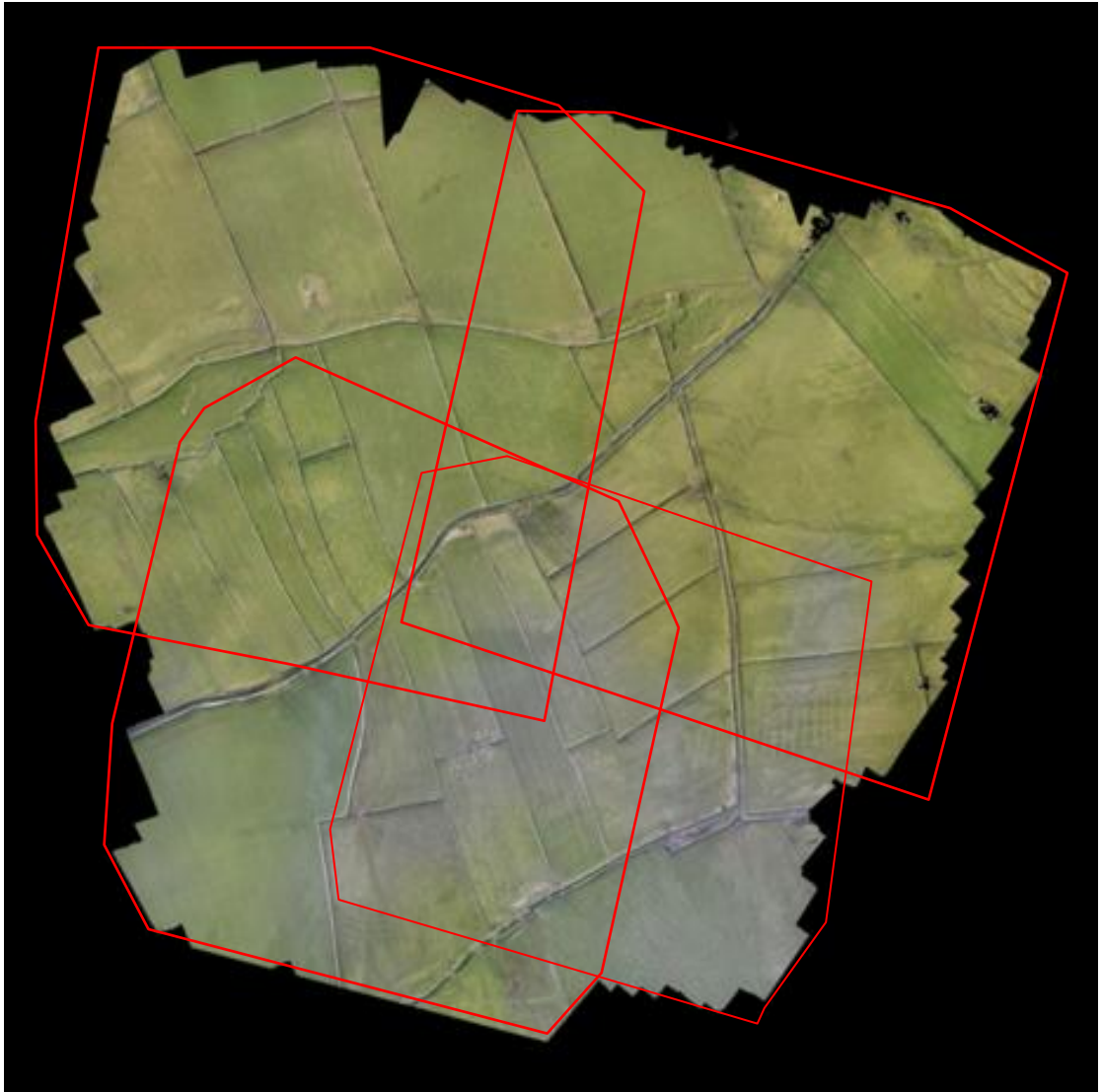
Figure 10: Projected mosaic of the Rosgill site, showing the overlap between each flight.
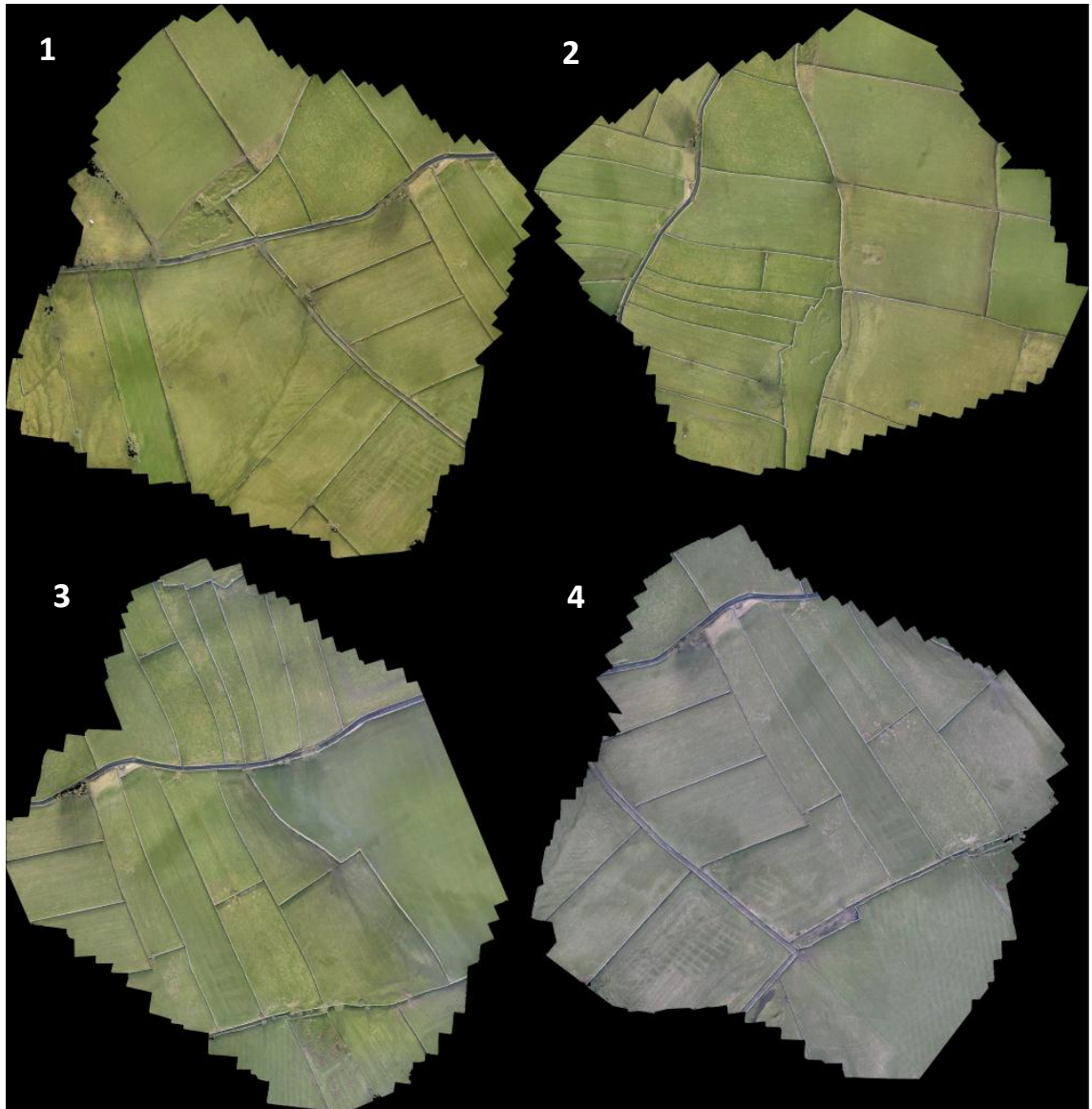
Figure 11: Mosaics of each flight at Rosgill that demonstrate the change in lighting conditions that eventually limited flying. The mosaics do not have spatial data at this stage as no georeferencing has been carried out, but can effectively be judged an orthophoto in that the image positions are a product of the bundle adjustment calculations and actually projected rather than just simply mosaiced via stitching.

6.2. Photogrammetry

As detailed in section 5.2.5, four programmes were used in this study to process the imagery collected with the UAS. Only PhotoScan and PhotoSynth actually produced any results, and only PhotoScan produced any useable results. Whilst, evidently, the three programmes not used do not contribute usefully towards the study, the steps undertaken in them and stage at which they were discarded is documented in order to provide a suitable rationale for the choice of PhotoScan.

6.2.1. LPS

LPS was not found to be suitable for DEM production. The level of supervision in LPS is high, and for a project with 500-1000 images per site it was judged to be prohibitive. Additionally, triangulation was extremely problematic, to the extent that a suitable accuracy was not achieved for DTM extraction to occur.

Numerous attempts were made to use the programme, and various approaches were used. For instance, re-calibrating the camera and running triangulation repeatedly with parameters set as initial, fixed or unknown. The number of GCPs and inputted tie points was varied as well, with no success. The final attempt made was with a small subsection of the images collected, just 5 in total, with 3 GCPs visible in each image, and >8 tie points inputted per image. This still resulted in a total RMSE of 200.5 which was unacceptable considering the level of supervision relative to other software packages.

6.2.2. Bundler

Bundler was not pursued due to its lack of usability. Primarily this was due to the programme requiring a working knowledge of Linux programming and so being unfamiliar to the majority of potential future users. Because of the command line style of operation, and lack of a debug option, the programme is also prone to bemusing and unexplained crashes, often frustratingly coming after several hours of processing.

6.2.3.   Microsoft PhotoSynth

Microsoft PhotoSynth was successfully used to produce a pilot point cloud (Figure 12 A and B), but not pursued due to the low quality. This is at least partially due to the resolution limits (1.5 MPix) on the online 'synths', and also the algorithms used being optimised for photo-tourism rather than photogrammetry. The low quality was an issue, not only because error was obviously high, but also because it appeared to prevent PMVS2 producing a dense reconstruction of anything other than the walls. Extensive post-processing of the initial sparse mesh may have improved the quality, but that level of supervision is not desirable and so the decision was made to not pursue the programme any further.
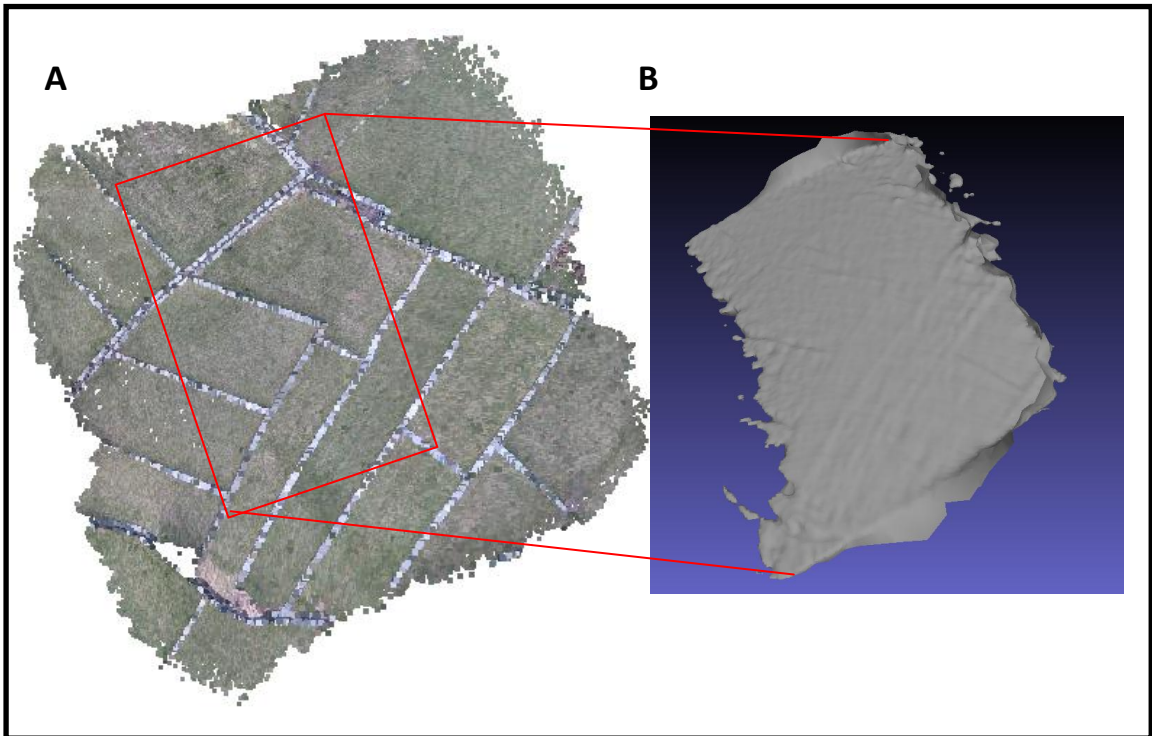
Figure 12: Results from PhotoSynth processing of imagery from Flight 2 at Rosgill. Figure 12 A is the basic coloured point cloud displayed in MeshLab. Figure 12 B is a section of the same point cloud again displayed in MeshLab but shown as a surface. The level of noise is quite apparent from the lack definition of the walls. Post processing issues are also aptly demonstrated by the edges of the surface. As mentioned elsewhere these are not insurmountable issues, but certainly impact the usability of the programme.

6.2.4. AgiSoft PhotoScan

AgiSoft PhotoScan was successfully used to produce DEMs from the small format photographs taken from the UAS. It was more accurate, faster and far easier to use than any of the other programmes. This more than merited its selection and the small cost of its purchase ($549 ex. VAT). Here the DEMs are presented along with their validation against GCPs collected with a differential GPS and pre-existing LiDAR data for the site.

6.2.4.1. DEMs produced

Figure 13 shows the DEMs final model of the Rosgill site in AgiSoft, with and without texture. To illustrate the level of detail achieved, Figure 14 shows the close up section of the model in an area with relatively complex terrain. **Error! Reference source not found.** again shows the whole DEM, but after export to ArcMap, and with a variety of different shading directions to illuminate the landscape. Although the DEM was outputted at roughly half the resolution that could be achieved with the imagery used due to computing constraints, resolution was 0.12 m^2.
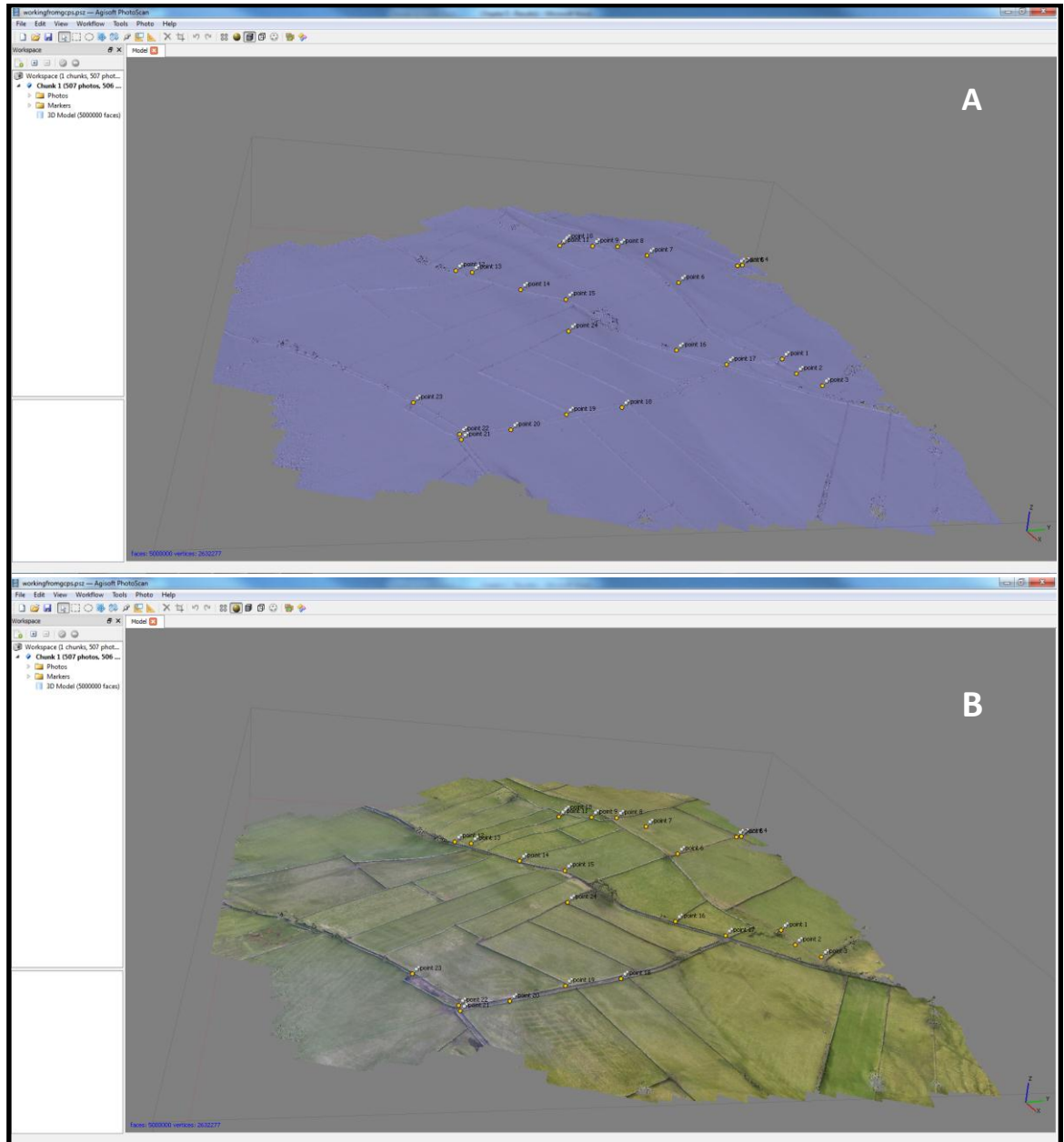
Figure 13: Final model for the Rosgill site, pictured after georeferencing has been carried out. Figure 13 A is the basic model with shading applied to the point cloud. Figure 13 B is the textured model. Labels on the model represent GCPs.
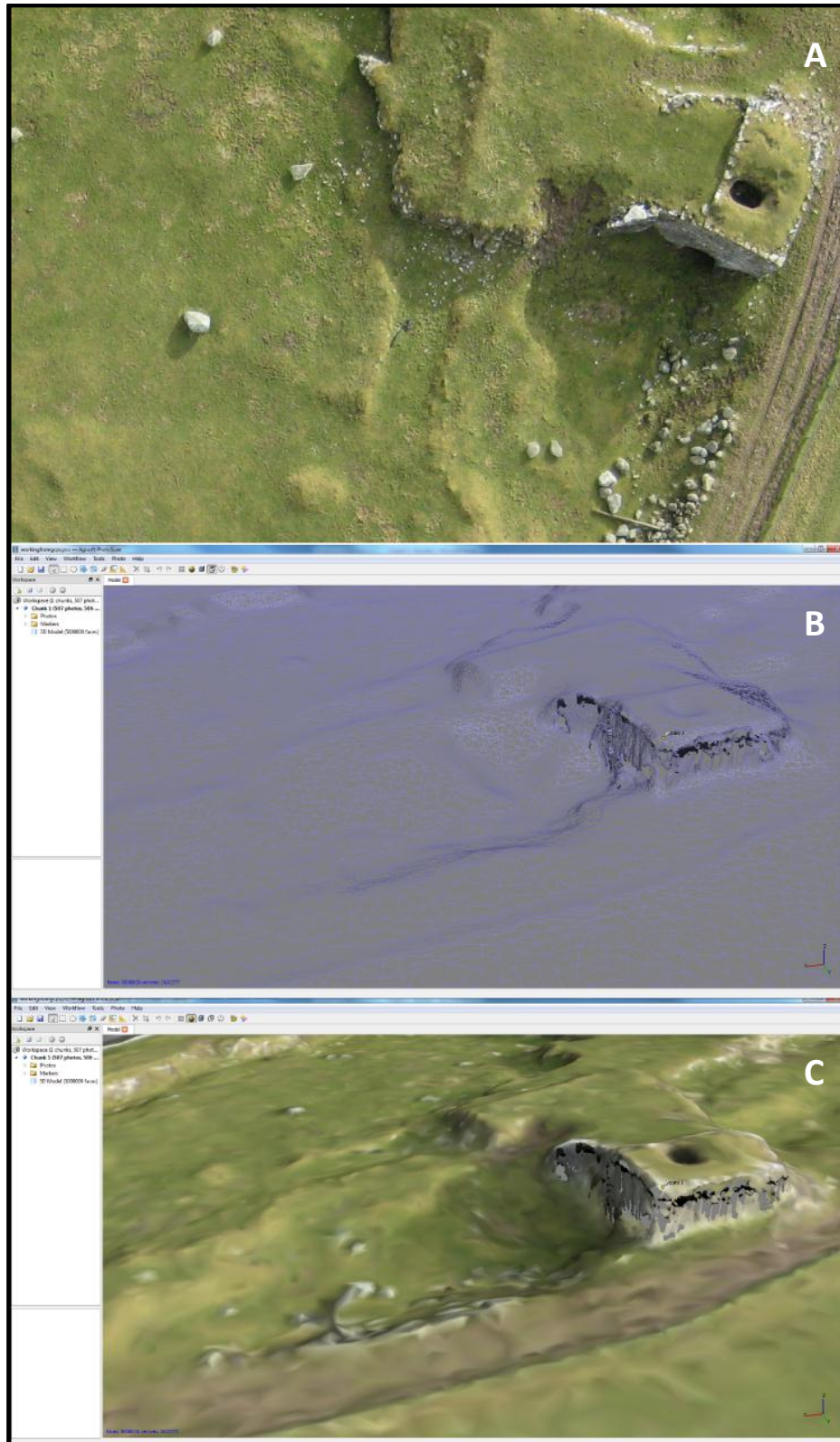
Figure 14: Displaying the level of detail achieved on a complex section of terrain within the final model, an abandoned quarry and lime kiln. Figure 14A shows one of the images used for this area of reconstruction and the level of detail captured. Figure 14B shows the wire mesh of individual points produced. Figure 14C shows the final shaded model. Overall point density is good, but there is an obvious and understandable drop off in point density on vertical surfaces due to the relatively poor perspective achieved from the air.
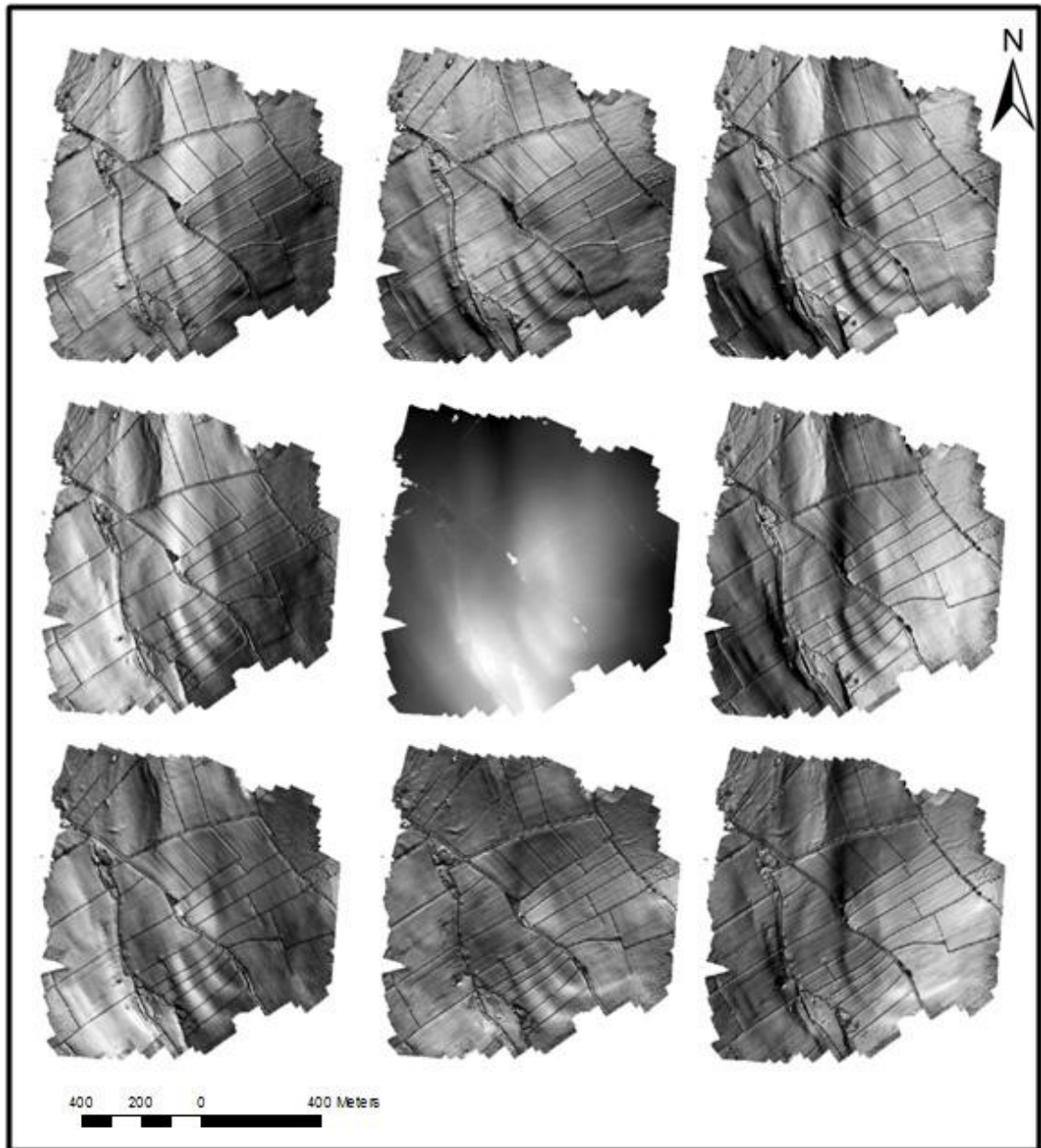
Figure 15 The final DEM produced in PhotoScan (centre) shaded at 45° intervals from a 45° perspective with 5 times vertical exaggeration.

6.2.4.2.   DEM validation

The DEM produced was validated against GCPs collected with a differential GPS, and pre-existing LiDAR data (1m vertical accuracy). The GCPs were used within PhotoScan, and so as such do not provide a proper validation of the programme. Average vertical error against them was 0.761 (

Table **2**) at the DEMs raw resolution of 0.12 m^2 (DEM outputted at 5,000,000 points).

Table 2: Error between PhotoScan model and GCPs.

Point	X Error (m)	Y Error (m)	Z Error (m)
1	-0.077	0.071	-1.162
2	-0.132	0.078	-0.391
3	0.167	-0.054	-0.282
4	-0.172	-0.161	1.74
5	-0.253	0.097	1.099
6	0.057	0.061	0.365
7	-0.047	0.249	0.073
8	-0.04	-0.098	-0.589
9	0.197	0.423	-1.548
10	0.009	-0.104	-1.226
11	-0.033	-0.078	-0.365
12	0.206	-0.026	0.785
13	0.062	-0.088	0.222
14	0.081	0.146	0.443
15	-0.158	0.13	0.689
16	0.046	-0.028	0.007
17	0.201	-1.56	-0.228
18	-0.16	0.402	-0.391
19	-0.054	0.201	-0.285
20	0.162	0.201	0.571
21	0.056	0.044	0.073
22	-0.104	-0.061	0.885
23	-0.015	0.154	-0.486
Average	0.129	0.366	0.761

Validation against the LiDAR data was done with a down-sampled version of the DEM so both had the same (1 m vertical) resolution. For further details see section 5.3.
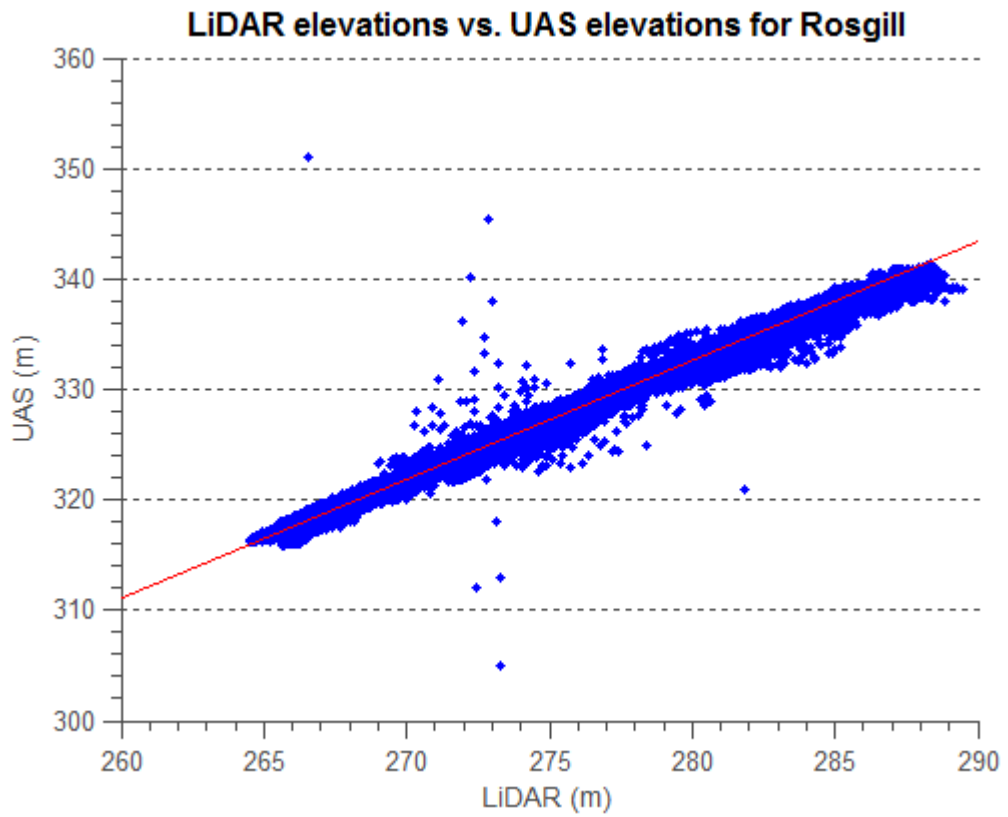
Figure 16: Scatter plot of the two DEMs along with a linear regression: $y = 1.0697x$ +33.12 The R^2 relationship of the datasets is 0.96.

Grayscale DEM of Difference between LiDAR and PhotoScan DEMs
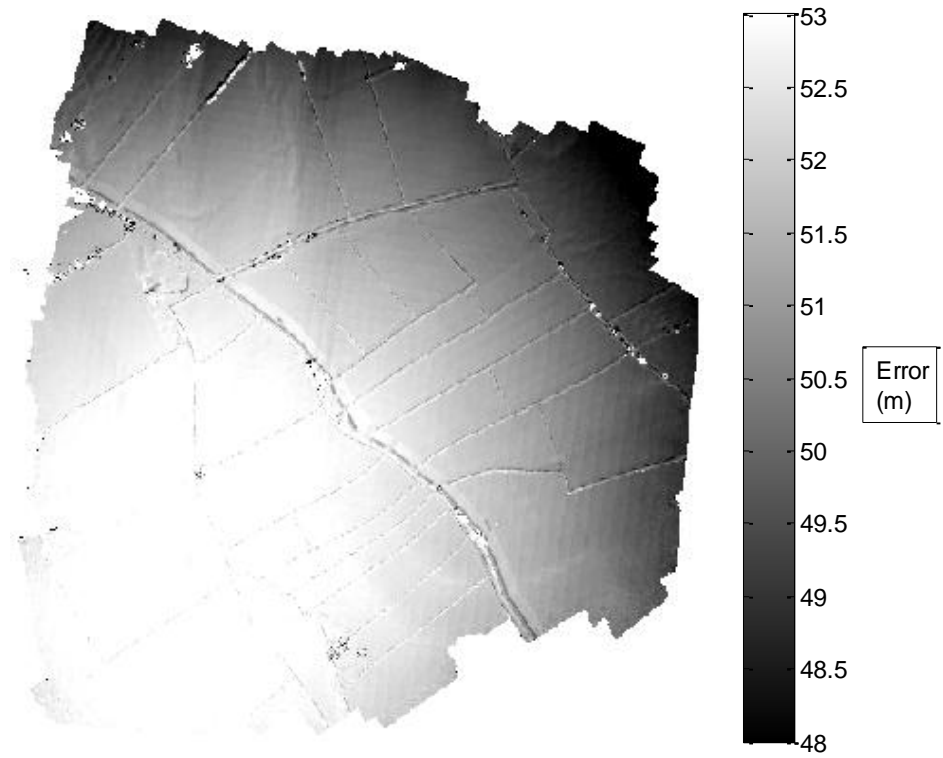
Figure 17: DEM of difference showing the spatial representation of error between the LiDAR and PhotoScan DEMs.
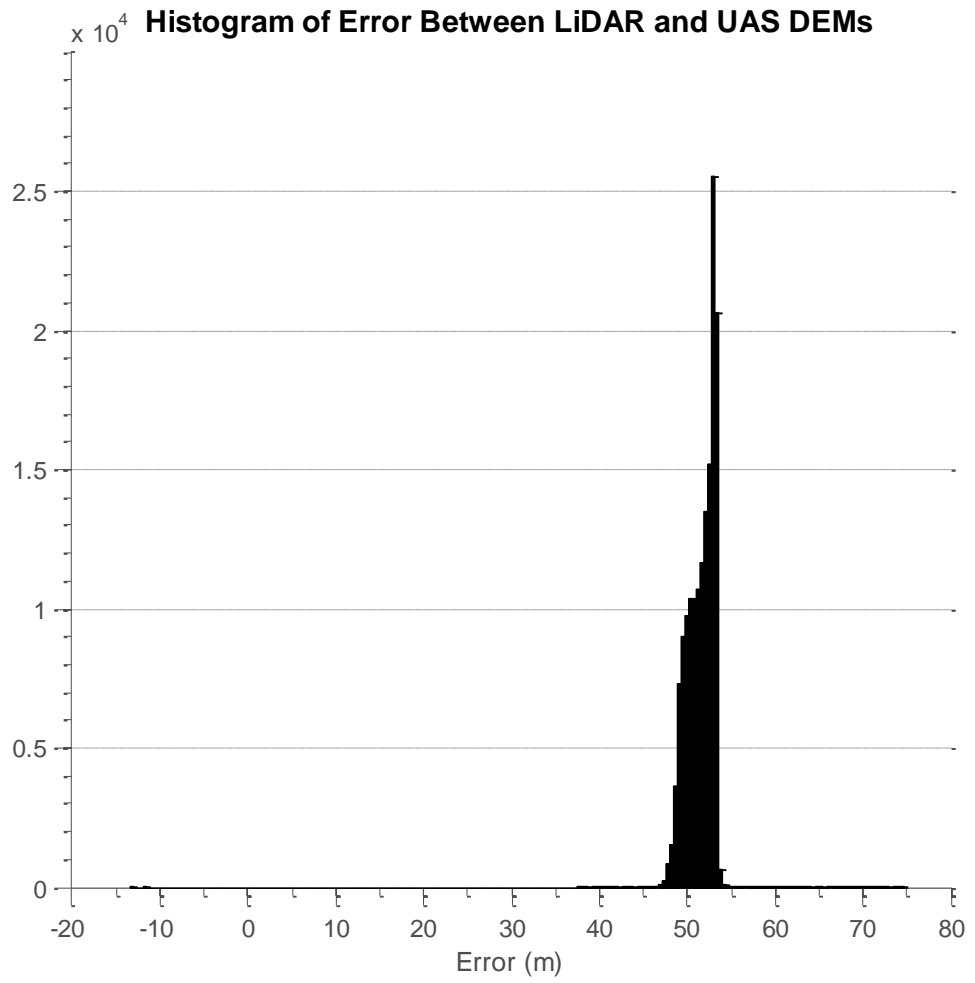
Figure 18: Histogram of the error between the LiDAR DEM used for validation and the PhotoScan DEM.

Average error of the UAS DEM against the LiDAR DEM is 51.58 m.

6.3. **Bedform mapping**

All discernible features were mapped using the shading shown in **Error! Reference source not found.**, and the results are presented alongside NEXTMap (Figure 19) and LiDAR data (Figure 20) for comparison in Figure 21. Care was taken not to map features that appear to be largely delineated by noise around the edge of the DEM, such as in the SW corner. The dimensions of the features mapped can be seen in Table 3 below, with average values of 132 m, 43 m and 3.15 for length, width and elongation ratio respectively.
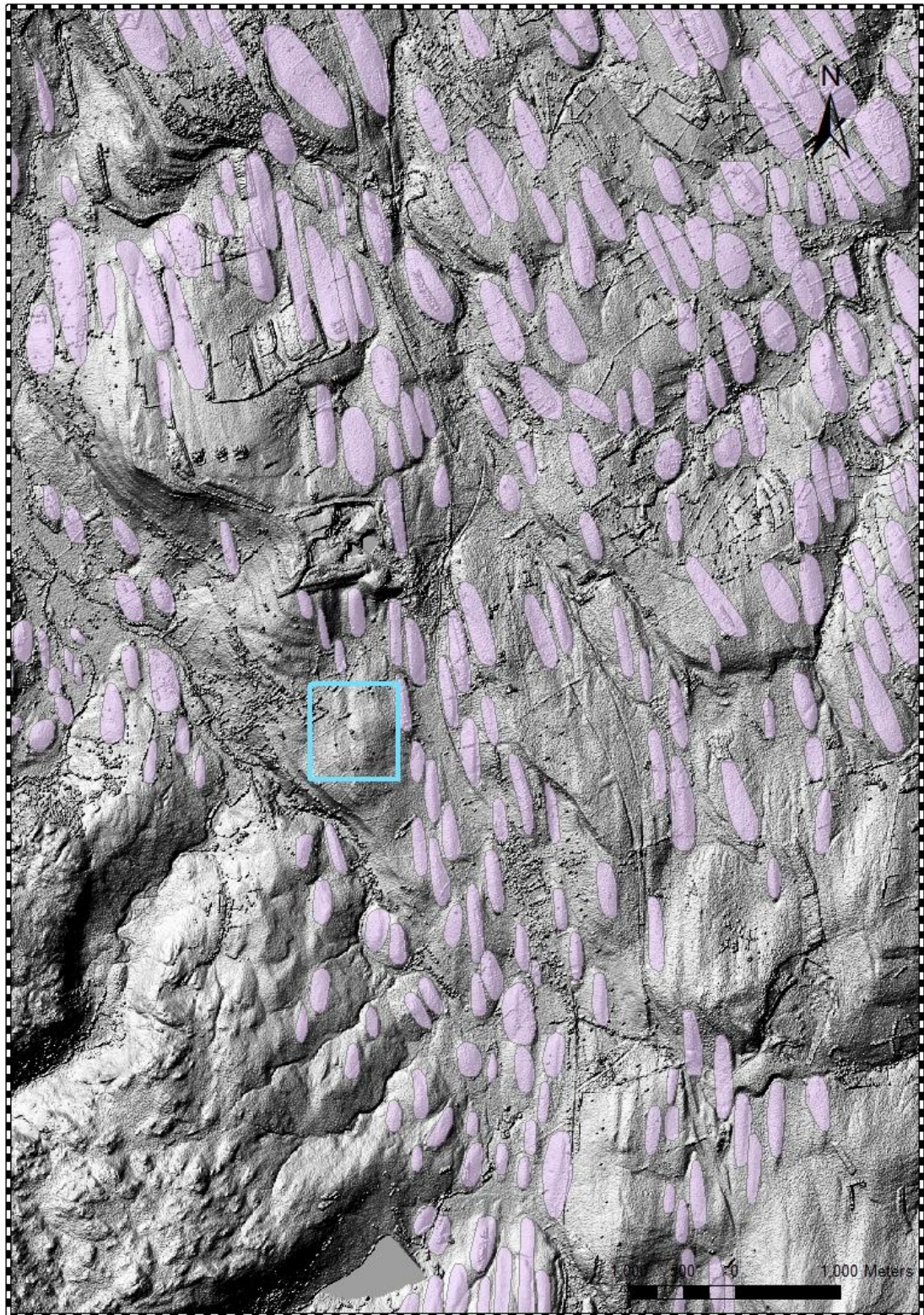
Figure 19: NEXTMap (5 m resolution, bare Earth) of area around the field site, hillshaded from the NW with five times vertical exaggeration (as used by Hughes *et al.* 2010 to map from). Bedforms mapped by Hughes *et al.* (2010) are included in pink, and the extent of figure 18 is depicted in light blue.
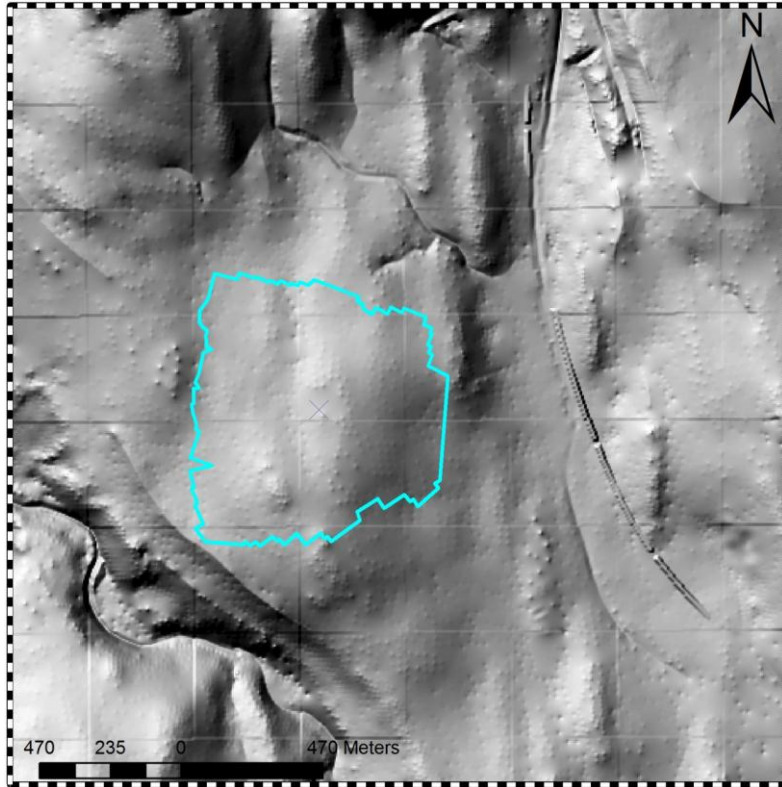
Figure 20: LiDAR bare Earth DEM of the area around the Rosgill Site, with the area flown depicted in blue. Hillshading has been applied with illumination from the NW and five times vertical exaggeration.
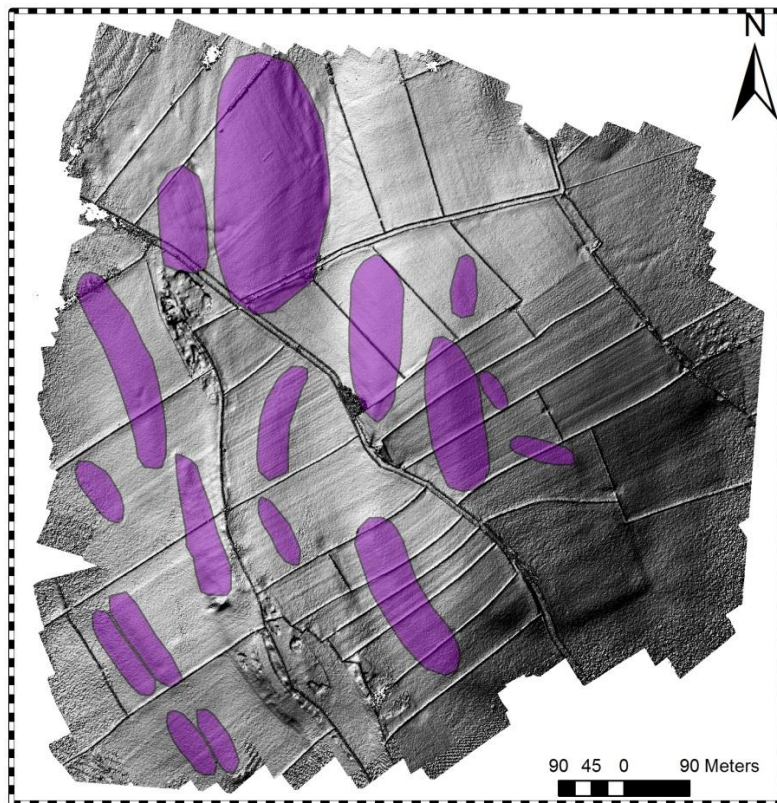
Figure 21: Mapped features presented on top of the PhotoScan DEM shaded at 315° with five times vertical exaggeration.

Table 3: A table of the dimensions of the features mapped in Figure 24.

Length	Width	Elongation Ratio
303.4	134.3	2.3
119.1	55.4	2.1
239.6	47.5	5.0
175.4	60.7	2.9
72.2	31.9	2.3
134.5	36.1	3.7
173.9	65.0	2.7
48.0	21.7	2.2
75.3	26.0	2.9
78.8	35.8	2.2
165.0	38.0	4.3
110.6	25.6	4.3
112.4	29.5	3.8
85.7	26.6	3.2
84.9	31.0	2.7
84.6	25.3	3.3
186.8	52.3	3.6

Chapter 7 Interpretation & Discussion

7.1. General remarks on the study

This study has demonstrated the variety of pitfalls that await UAS photogrammetrists. Image acquisition was successful in terms of the application of UAS technology, but remains limited by legal barriers and aspects of the UAS design that are specific to the UAS used here. Image processing was far more problematic, and three of the four programmes used were not suitable, mostly due to complexity and unreasonable time requirements. Encouragingly though, PhotoScan demonstrated how SfM can produce high quality DEMs whilst also maintaining a simple and efficient workflow.

Mapping from the DEM of Rosgill revealed a number of features that could be glacial bedforms, and generally a North West – South East streamlining of the landscape that is opposed to the more dominant North – South streamlining mapped on NEXTMap by Hughes *et al.* (2010). Equifinality remains a serious issue and without an additional investigation, perhaps into internal structure of the features, it is difficult to expand on. A number of mapped features were <100 m in length, but perhaps more significantly several were extremely thin at <40 m wide. In the context of Clark *et al.*'s analysis the <40 m wide bedforms fall outside of two standard deviations of the mean width of drumlins, and very few drumlins with widths <100 m were mapped by Hughes *et al.* (2010).

7.2. UAS use for image acquisition

The PAMS SmartOne B proved to be an extremely effective tool for aerial survey. It is robust, simple, and easy to fly, and so carries a number of advantages over adapted amateur airframes (DIY Drones, 2011) and kite based methodologies (Aber *et al*. 2002; Smith *et al.,* 2009). It does have a number of weaknesses related to restrictions on operating conditions, but, the alternative platforms largely share these due to common engineering difficulties and legal issues. The principal issue to consider when

comparing it to other platforms is the financial penalty of opting for its off-the-shelf technology over cheaper experimental DIY options. This discussion focuses on the technical issues, as financial considerations of future users are unknown.

If UASs are considered as a survey method, and here we argue that they should be, then motorised fixed wing modules such as the PAMS Smartone B UAS are the best choice in a number of scenarios. Powered flight is much more efficient for surveying than unpowered options such as kites. It allows larger areas to be covered and requires less user supervision. For Rosgill, it also would not have been possible to carry out a survey with kites as the farmers specifically requested that we did not enter certain fields. Using a fixed wing airframe rather than a helicopter based model is preferable too. Whilst helicopters can be useful for sites with restricted flying areas, they also require far more power and so have shorter flight duration. The fixed wing airframe is more efficient and so can cover greater areas or, at least, can cover the same area in a less fragmentary fashion and this simplifies photogrammetric processing. Therefore, for surveys of sites like Rosgill, where there are no topographical restrictions such as steep valley sides, or location restrictions that prevent access to power, it is the preferred platform.

Aside from the airframe, other elements of the UAS need to be considered when selecting one. In this study a major limitation of the PAMS SmartOne B was the use of thermopile stabilisation that prevents flying in overcast conditions. This placed unnecessary limitations on surveying in the UK due to the changeable weather. Thankfully, future editions of the SmartOne are to be made with an IMU, and so flying will become insensitive to lighting conditions. When considering any form of UAS this should be a priority. With a good enough camera, image quality is generally suitable for photogrammetry in a wider range of lighting conditions than can be flown in with a thermopile stabilisation system.

When considering the UAS as a whole, the ground control software is of some significance. Here there was not a comparison of different software, but the software used was more than satisfactory. It shows the UAS position, displays all relevant information such as contrast, wind speed, GPS signal, and battery charge, and it is easy

to define the survey area. It also works as a safeguard by not allowing the UAS to start until all essential elements such as GPS signal and contrast are good enough. In a more recent version of the software which has not been used, the same features are retained, but the presentation has been improved and a survey area can now be altered whilst the UAS is in flight which can sometimes be useful when surveying several small areas or reacting to a dynamic situation.

In summary, the PAMS SmartOne B UAS is a simple to use survey tool, and its quality is commensurate with its price. Its principal disadvantage is its dependence on thermopiles for stabilisation, but, for any future user this is not an issue due to the new versions replacing this with an IMU. There is no reason why any user could not use it for conducting aerial surveys of suitably sized and located sites. In some circumstances where the terrain prevents flying or location restricts access to power, other technologies such as kites would be more appropriate, but in every other situation powered UASs remain superior.

7.3. Photogrammetry programme selection

This study used both an established photogrammetry programme, LPS, and a variety of more recently developed programmes based on SfM techniques. From the results it is clear that the developments in SfM are the key reason that small format photography has become a viable surveying method. Here, as with the discussion over image acquisition, we have focussed primarily on usability which is also heavily intertwined with accuracy in the SfM programmes. The strength of the UAS survey method is its flexibility, and so in order to preserve that throughout the processing, the photogrammetry software ideally had to mirror that. SfM provides the opportunity to overcome technical difficulties with small format photogrammetry, such as an inability to constrain internal and external parameters, and because it achieves this through automated sections of programming it is easier to use than LPS's workflow.

7.3.1. LPS

LPS proved to be entirely unsuitable in this study. This was due to its inability to cope with the level of error in the intrinsic and extrinsic camera parameters. LPS performs poorly with too many unknowns, as noted by Aber (2010), due to a weak feature matching algorithm, limiting its ability to compensate for imprecise user inputs during triangulation.

Efforts to calibrate the camera used with the Caltech calibration toolbox (Caltech Vision, 2010) were of limited use because while they did help constrain camera geometry, the results did not appear to be good enough to be used as a fixed known value within LPS. Whilst small format cameras have been shown to be relatively stable (Laebe & Foerstner, 2004; Habib *et al.,* 2004) there is still some variation and that may be enough to force the value to be set as initial within LPS. The only way to circumnavigate this obstacle would be to either use a metric camera with a fixed lens (e.g. Smith *et al.*, 2009), or perform a calibration after turning the camera on before each flight. Both of these options are impractical. Whilst using a metric camera is evidently preferable, it is not possible due to weight restriction. Moreover, the nature of the UAS landing would more than likely change the calibration over time. Performing a calibration before flight is more feasible, and there are a number of SfM based automated calibration programmes that can be used with an object/scene of known dimensions, but this is still an additional layer of complexity that arguably does not need to be introduced to the flight process.

The extrinsic parameters were more problematic. Whilst the UAS collects camera positions and orientations the accuracy did not appear to be workably high enough. Other authors (Laliberte *et al.*, 2011) have had issues with GPS accuracy due to a low sampling rate and it is likely that a similar issue is also present here. This lack of camera positions can be overcome with good ground control and well constrained intrinsic parameters but, as discussed above, the intrinsic parameters are difficult to constrain and collecting suitably accurate GCPs is not always feasible.

These issues were further compounded by the general difficulty of using LPS. It is not a user friendly system, and requires a relatively high level of training before a user

becomes competent. Whilst this is hardly unique amongst GIS programmes, it does pale in comparison to the ease with which users pick up AgiSoft PhotoScan and added weight to the decision not to pursue LPS further. It is not impossible to get LPS to work with UAS imagery, and Laliberte *et al*. (2011) demonstrate this, but this study did not have the resources or capability to introduce the additional layers of programming that their methodology required.

7.3.2. Bundler

Bundler is an attractive option for small format photogrammetrists. It is proven in numerous studies (Snavely *et al.,* 2006; Snavely *et al.,* 2007; Neithammer *et al.*, in press) and also free. Being 64-bit compatible, designed for multiple CPUs, and with the addition of CMVS, it provides an extremely scalable approach to photogrammetry.

Bundler's primary limitation, and the reason it was not pursued, was the complexity of the programme. Bundler has to be compiled before use, and then run from the command line. This is further complicated by the Linux nature of the programming which is not familiar to all potential users. Additionally, it requires extra programmes to produce a final DEM, with a major problem being georeferencing (Westoby, 2011). Whereas in PhotoScan georeferencing markers can be adjusted on the actual photos, in Bundler georeferencing has to be done in a separate programme after the point cloud is created and so must be done on the DEM. As the resolution of the point cloud is always lower than the source images, accuracy will be commensurately lower. Westoby (2011) has used meter square yellow markers for georeferencing to make spotting the markers in the point cloud easier, but this tends to limit the accuracy achievable to the size of the markers.

Whilst Bundler remains an option for future users and will probably continue to improve due to its open source nature and popularity amongst online communities, it was felt that it does not provide the level of usability required and PhotoScan remains a better option despite its cost.

7.3.3. PhotoSynth

PhotoSynth was initially a promising option because of its usability, but, whilst it is easy to produce a point cloud with it, the accuracy was lower than required for mapping purposes. This was partially due to the limit on the resolution of uploaded images, but also the algorithms used in the programme. Although these are based on those used in Bundler, they are understandably optimised for photo tourism rather than photogrammetry. In photo tourism aligning the images is the primary concern and this requires a lower point density than used in photogrammetry. Therefore, cloud density is sacrificed to speed up the processing.

As well as limiting the resolution of uploaded images, PhotoSynth limits the number that can be uploaded to around 300. This is still a relatively large number and, by reducing the overlap between images from the UAS to the minimum required, it would be possible to cover a substantial area in one block. It should also be possible to combine multiple point clouds to cover a larger area. Unfortunately, the process is complicated by the presence of severe warping on the DEM. This means that it is basically impossible to create point clouds of large areas with PhotoSynth without carrying out complicated 3-D transforms to GCPs after they have been initially produced. Whilst PhotoSynth was promising in that it was relatively easy to use, it clearly is not fit for purpose for high resolution photogrammetry.

7.3.4. AgiSoft PhotoScan

AgiSoft PhotoScan was the preferred programme for DEM production because it scores highly on usability, speed, and accuracy. The SfM approach, combined with an interface that is intuitive and familiar to users, makes for an exceptionally easy to use software package. In addition, whilst the basic workflow is simple, there are opportunities to provide data for internal and external parameters if it is available. This means that if one is working with partially metric data that potentially could work in LPS, but with a significant processing time penalty, it can be quickly processed in PhotoScan. As well as being able to provide additional information, PhotoScan is preferable to other SfM based programmes because it deals with the data more

efficiently through use of slightly different algorithms and alternative approaches. For instance, the use of a simplistic greedy algorithm before the bundle adjustment shortens the processing time by reducing the number of iterations required during the bundle adjustment.

The spatial resolution of the DEMs produced is excellent. Defined as pixel size, resolution is 0.12 m^2 in the DEM produced. However, this does not reflect the potential resolution attainable in PhotoScan, but rather the computational limits of the study. The DEM was reduced, from a maximum raw output of 11,000,000 points, to 5,000,000 points due to graphical restrictions. An even higher resolution would have been possible had the model reconstruction been run on 'ultra high' rather than 'high' where there SIFT algorithm gets close to one point per pixel. Despite this the outputted model is an extremely high resolution for a DEM, although validation is problematic here due the lack of a comparable resolution pre-existing DEM.

Validating the DEMs accuracy is problematic as there appears to be four different sources of error within the DEM and precisely defining the scale of each error is difficult. In order of scale, there is a systematic datum error introduced by the DGPS survey, a systematic error due to warping of the DEM by PhotoScan, variable levels of error due to misalignment of the two DEMs and error due to different handling of vegetation (predominantly trees) between the two methodologies.

The datum error introduced by the DGPS survey is the most significant. It was created due to a poor survey design that focused on relative positions rather than absolute positions. As a result, whilst the GCPs are relatively accurate (±0.0025 m) there is a large amount of error between them and the LiDAR data used for validation. A key oversight in the research design here is the usage of all the GCPs in the production of the DEM. Had some been left unused they could have provided an additional validation which circumnavigated the datum issue. Establishing the size of the error is difficult as whilst the GCPs are easy to identify on the imagery, and so easy to use in the production of the PhotoScan DEM, they are difficult to identify on the LiDAR dataset with any accuracy. Given to suitable level of accuracy the error is 52 m.

With the deduction of 52 m, average error on the DEM is 0.58 m with a precision (defined as one standard deviation from the mean) of 1.68 m. However, further analysis suggests that these are poorly applied metrics due to the nature of the data. The DEM of difference between the LiDAR and PhotoScan DEMs displays what appears to be an underlying parabolic trend of error across the DEM. This is perhaps better displayed if a limited range of the data is plotted as seen below in Figure 22: A DEM of difference showing the distribution of error between the LiDAR and PhotoScan DEMs after the removal of the 52 m of systematic error introduced by the GCPs. The colourmap has been limited to -2 to 5 m in order to display the systematic nature of the error introduced by PhotoScan that appears to be parabolic.
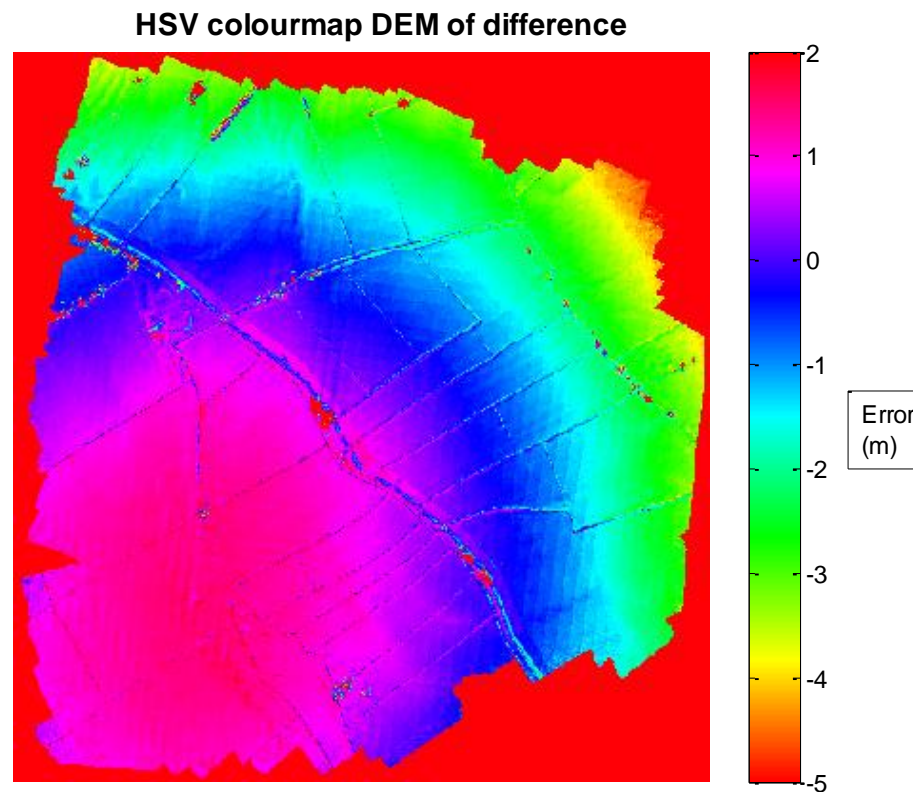
Figure 22: A DEM of difference showing the distribution of error between the LiDAR and PhotoScan DEMs after the removal of the 52 m of systematic error introduced by the GCPs. The colourmap has been limited to -2 to 5 m in order to display the systematic nature of the error introduced by PhotoScan that appears to be parabolic.

Therefore, due to this systematic polynomial error, ascribing an average error to the dataset is relatively pointless. Equally, using one standard deviation from the mean as a definition of precision appears to be unsuitable as demonstrated by another DEM of difference below in Figure 23: A DEM of difference showing the distribution of error between the LiDAR and PhotoScan DEMs after the removal of the 52 m of systematic error introduced by the GCPs. The colourmap has been limited to one standard deviation from the mean and displays how this description of precision fails to properly categorise error within the DEM due to the systematic error introduced by PhotoScan. limited to those values:

HSV colourmap DEM of difference for one standard deviation from the mean
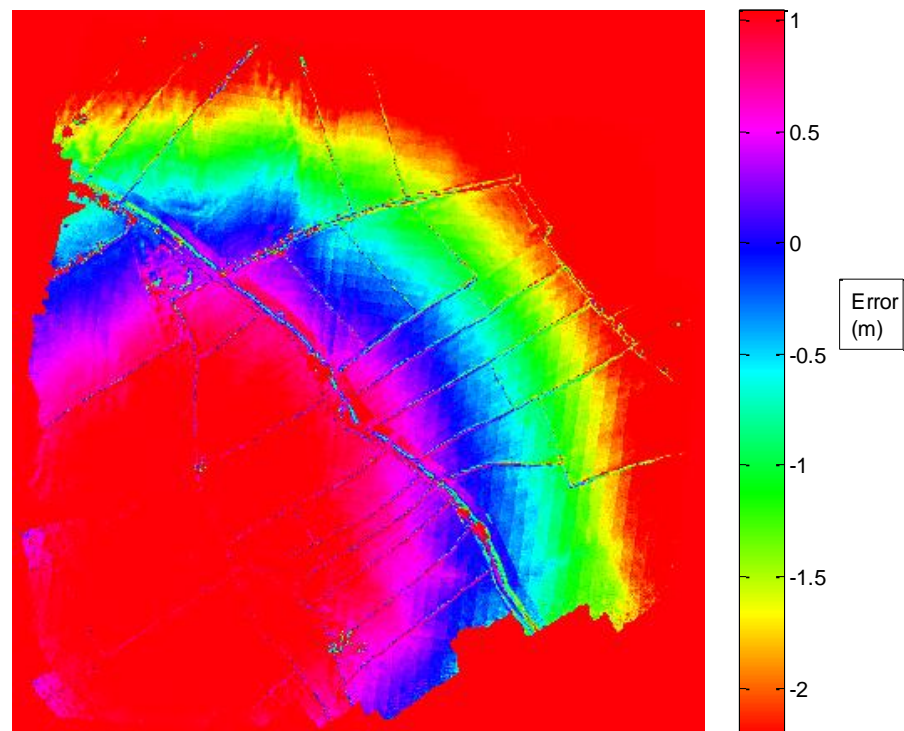
Figure 23: A DEM of difference showing the distribution of error between the LiDAR and PhotoScan DEMs after the removal of the 52 m of systematic error introduced by the GCPs. The colourmap has been limited to one standard deviation from the mean and displays how this description of precision fails to properly categorise error within the DEM due to the systematic error introduced by PhotoScan.

This error is similar to the DGPS error in that it is systematic and so correctable. Although this will not be done in the course of this project, de-trending the DEM is essentially a simple task in MATLAB, and presumably as it is a systematic error

PhotoScan will at some point remove it from the programme. However, for the moment it is a key limitation of the software.

The third and fourth sources of error in the DEM are difficult to separate at without the aforementioned de-trending. There is certainly error present due to inaccuracies in the co-registration of the two DEMs as features and terrain are visible in the DEMs of difference. There is also error wherever trees are present and these appear to count for the majority of outliers although it is difficult to quantify this. This error will have occurred due to the differences in dealing with vegetation between photogrammetry and LiDAR, with LiDAR providing an option of including ground or vegetation returns and so the final DEM being dependant on the processing of the raw data. This difference in data generation almost certainly manifests itself in error on the grassy areas, but both of these sources of error are inherent in photogrammetry and so difficult to use as a critique of PhotoScan based on this validation.

In summary, the DEM produced in this study is not accurate, demonstrating systematic error of 52 m due to an error in the GCP survey design. Even with this resolved the DEM is not accurate due to a systematic polynomial error introduced by PhotoScan during processing. Furthermore this is difficult describe in normal terms. However, whilst the validation technique does not have the means to quantify it, qualitatively the DEM is accurate with those systematic errors removed as evidenced by the rough validation via comparison of wall heights. Clearly though, for moment the DEM remains classified as inaccurate.

Aside from assessing PhotoScan by the quality of the data produced, the main disadvantage to using it is that it is a commercial package. Fortunately, the cost is affordable under an education license, and considering the time saved in processing, which could easily be measured in hours if not days, it is more than merited. Cost apart, the commercial nature also impacts on the level of documentation on the software. Whereas Bundler has a number of papers published on its structure due to its academic nature (e.g. Snavely *et al.*, 2006; Snavely *et al.,* 2007), quite understandably there are no papers published by AgiSoft. Fortunately this is in some way compensated

by AgiSoft employees being particularly involved in the PhotoScan online community and being more than happy to answer any queries about the software.

Alongside the substantially problem of the systematic error the programme appears to introduce, there are two additional bugs that restrict PhotoScan's performance. PhotoScan does often struggle with visualisation of large point clouds, to the point where processing will crash at the final stage. Additionally, it cannot currently align 'chunks' without a substantial drop in quality. Fortunately, and perhaps due to the programme being relatively young, AgiSoft are constantly producing new versions with bug fixes and are willing to provide advice when bugs such as visualisation can be circumnavigated within the current version.

PhotoScan almost realises the potential of the SfM approach to photogrammetry. It provides the flexibility of the SfM approach, matched with an intuitive interface and the ability to provide known parameters where appropriate. However, unfortunately the existence of a bug that introduces a systematic polynomial error into the DEM means it is not currently fit for purpose as an all encompassing technique for producing DEMs and must rely on post-processing before the outputs can be used for many quantitative applications that rely on vertical accuracy. However, within the remit of this study the DEMs produced are suitable for mapping bedforms as the spatial resolution is very good, and whilst it is not quantified, the vertical accuracy without the systematic error appears very good.

7.4. Decimetric resolution DEMs for drumlin mapping.

The DEM produced (Figure 21) clearly shows a far higher level of detail than NEXTMap (Figure 19). Around the edges of the DEM there are well defined areas of noise, where there has been sufficient image overlap or coverage to produce points, but not enough to constrain them accurately. These areas were not used when mapping and care was taken not to interpret features created by the boundaries of these areas.

Before continuing the discussion, it is worth remembering the small size of the study area. As discussed previously (see section 4.2) this obviously limits the conclusions that

can be drawn. The size of the region is a consequence of the photogrammetric processing. Flying additional areas remained a secondary focus until the initial area could be processed, but with the processing methodology now certain, there is the option to easily expand on the discussion here by flying a variety of other areas in future studies.

Clearly, from the mapping (Figure 21), and just looking at the DEM (**Error! Reference source not found.**), there are large numbers of potential bedforms present. Initially all raised topographic features were mapped. They vary in size from 48 m to 303 m and average 132 m (

Table 3). Two flow sets appear to be present, with the features roughly grouping into a N-S alignment and a NW-SE alignment. Both of these make sense with a N-S alignment being very dominant in Hughes *et al.*'s (2010) mapping, and a deep river valley running NW-SE just to the west of the site. As the NW-SE features are smaller, it is possible that these are a product of a later and less extensive phase of glaciations that skirted the high ground as Rosgill and was more topographically influenced than the earlier phase that produced the dominant N-S features. Hughes *et al*. (2010) do not pick up on a NW-SE trend in the immediate proximity of the site, but further up the same valley they map bedforms oriented in that direction.

Are the features mapped in this study actually subglacial bedforms? Whilst mapping resolution impacts the range of forms produced by a particular geomorphic process that are visible, it also impacts the number of geomorphic processes that are visible. When mapping with NEXTMap, the geomorphology can be assumed to be a product of tectonic, glacial or fluvial processes. These are usually relatively easy to differentiate between, but when mapping with this higher resolution there are far more processes that could have affected the landscape, making interpretation more difficult.

 Figure 24 highlights three obvious examples. In the south of the DEM the blue box highlights a road cutting. The cutting sits in the middle of two features. The two features may be one feature split by the cutting, but from the DEM it is not possible to

tell. Both features appear to taper out slightly before reaching the cutting, but this could be due to anthropogenic reworking around the road. In the centre of the DEM the red box highlights a short feature, in fact the shortest feature mapped at 48 m long. It is an elongate form and tapered at each end, but it also runs perfectly orthogonal to two walls and sits roughly in the middle of a particularly long field. Therefore, it is quite possible it is the remnant of an old wall. In the north of the DEM, a yellow box highlights what appears to be to be an area of fluvial incision. It forms the boundary of the largest feature mapped (303 m in length). Without further information it is particularly difficult to ascertain whether the clearly fluvial features have formed in the valley beside the feature after it was formed, or whether fluvial processes are solely responsible for forming the valley. If the former is true then the feature has been mapped correctly, but, if the latter is true then the mapping should interpolate over the valley. Evidently from this DEM alone it is not possible to reach a conclusion.
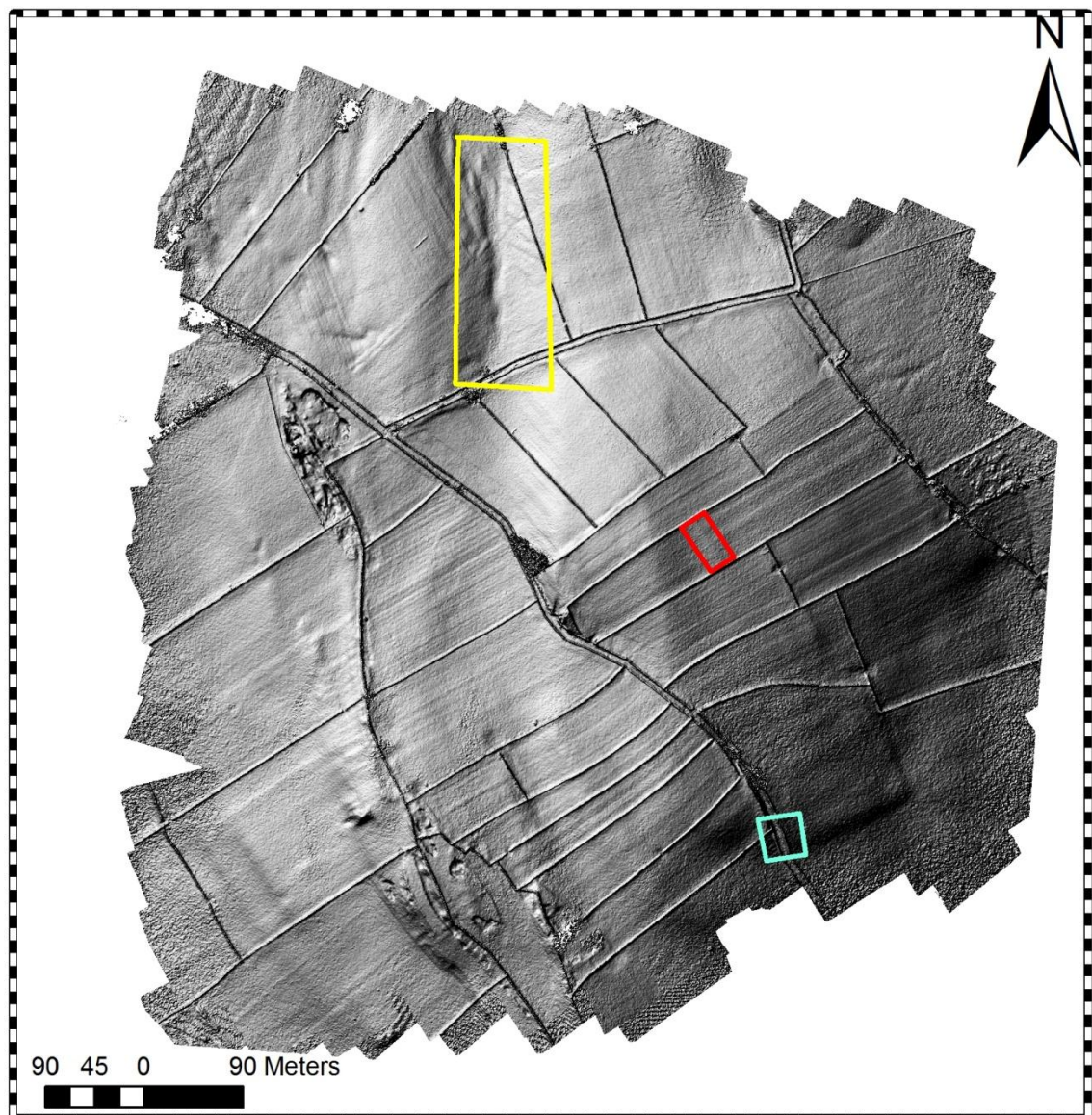
Figure 24: Issues with mapping from the DEM are highlighted in three locations. The yellow box highlights an area of fluvial incision, the red box highlights a possible former field boundary, and the blue box highlights a road cutting.

A further mapping complication involves potentially compound forms. Several of the features mapped are in relatively close proximity on an area of high ground. If mapped on a lower resolution DEM they would be regarded as a single feature. Here they were mapped as individual features, but, potentially both the smaller and larger features could be mapped, or perhaps just the larger feature. It is difficult to discern whether they represent the signature of different glacial phases, or just complex features (e.g. Clapperton, 1989). Spagnolo *et al.* (2010) choose not to include superimposed and cross cut features in their analysis of drumlin form, and perhaps analysis of poorly resolved bedforms as compound forms resulted in many small drumlins being

discarded. Obviously it is sensible to omit poorly resolved bedforms when attempting to quantify the true shape of drumlins, but at the higher resolution of the UAS DEM it is less a case of not being able to distinguish whether a form is a single bedform or not, and more a case of deciding which of several well defined forms to map. In this case it seems sensible to map the smallest form unless it evidently has been truncated by cross cutting, and here that never appears to be the case.

Clearly, equifinality is a serious issue and one that remote sensing alone is unable to answer. Whilst mapping from remote sensing is appropriate at poorer resolutions, a field investigation may be required to establish the genesis of the features mapped. It brings about an interesting question about what we can map as a bedform. Clearly there is a deficiency when mapping solely from remotely sensed data, but whether further data, such as feature sedimentology, is required is not clear, and even that might not clarify the issue. Despite the current deficiencies though, the sizes of the mapped features remain of interest.

Discarding the particularly short 48 m long feature, there are six 'short' features that could be regarded as small 'baby drumlins' that are <100 m. They are well within the resolution of the DEM, but average 80 m in length. Whilst this is slightly less than the 100 m lower bound established by Clark *et al.* (2009) it actually matches well to a number of published studies (e.g. Kupsch, 1955; Mitchell, 1994; Velic, 2011). This is a particularly small study site, but none of these features were visible on NEXTMap. Perhaps this suggests that whilst there is no apparent need for a wholesale revision of drumlin length, it might be sensible to acknowledge a slightly lower bound.

It is worth considering why the small features are not visible on NEXTMap DEMs. Largely it appears that the width is more significant than length. The average width of the mapped features is 43 m and because NEXTMap has a 5 m horizontal resolution, the features could be only be represented by 6-12 pixels. This is obviously difficult to map from, and the amplitude of the features makes the task even harder. Whilst NEXTMap has a 1 m vertical accuracy, the effective smoothing of the horizontal resolution means that the edges of the drumlin are not distinguishable and so the feature is actually only depicted by perhaps 2 pixels. Another possible complication is

the presence of bedforms on slopes, as seen in the Western section of the DEM. In this situation, the smoothing of the 5 m horizontal makes the drumlins difficult or impossible to see because the magnitude of the slope is similar to the amplitude of the drumlins. So certainly, it does appear that there are benefits to mapping at this higher resolution.

Although not included in the aims of this study, the width of the mapped bedforms could be just as significant a metric as the length, and there is more evidence that there the mapping on NEXTMap is less suitable. Whereas Hughes *et al.* (2010) only mapped a small number of bedforms with a width <100 m (see Figure 3) the features mapped here have an average width of 43 m. Furthermore, eleven of the seventeen features mapped were <37 m wide and so outside two standard deviations of Clark *et al.*'s (2009) mean. Whilst they are particularly narrow, they remain similar in elongation (3.15) to Clark *et al.*'s (2009) bedforms (2.9) and so cannot be considered just a series of flutes, which would be expected to exhibit much higher elongation ratios.

As discussed above, narrow drumlins are difficult to map on NEXTMap, and the presence of 11 features <37 m wide within such a small area does suggest that there might be a number of bedforms across the UK of a similar size not mapped by Hughes *et al.* (2010). Additionally, whilst the literature review conducted by Clark *et al.* (2009) does correlate well with their findings about length (e.g. 8 sites from the literature were found where length was <100 m which is similar to their findings from mapping), the same cannot be said of drumlin width. For drumlin width, the literature review revealed 13 sites where drumlins with widths <100 m were mapped of which 12 were <56 m wide (Table 4). This seems at odds with the small number mapped in their study and so again suggests that NEXTMap's resolution may have influenced the mapping of narrow drumlins.

Table 4: Selections from the literature review of observed drumlin sizes in Clark *et al.* (2009). Published work that records drumlins with widths <100 m.

Authors (year)	Site	Length (min.)	Width (min.)	Spatial Resolution (if mapped)
Kupsch (1955)	Dollard, Saskatchewan, Canada	76 m	23 m	Mapping in the field and fron unspecified resolution aerial photography
Gluckert (1973)	Central Finland	100 m	50 m	Unspecified
Rose & Letzer (1977)	Glasgow and Vale of Eden, UK	100 m	50 m	1:10,560
Kruger & Thomsen (1984)	Myrdalsjokull, South Iceland	20 m	15 m	Field mapping
Zakrzewska Borowiecka & Erickson (1985)	Eastern Wisconsin, USA	116 m	55 m	Field mapping
Clapperton (1989)	Patagonia, Chile	200 m	80 m	Field mapping
Mitchell (1994)	West Pennines, UK	135 m	50 m	Unspecified
	Upper Dentdale, UK	95 m	55 m	Unspecified
	Wensleydale, UK	90 m	40 m	Unspecified
Wysota (1994)	Koziary, Poland	23 m	15 m	1:10,000
	Gorzno, Poland	55 m	15 m	1:10,000
	Trepki-Samin, Poland	50 m	25 m	1:10,000
	Janowko, Poland	25 m	15 m	1:10,000

7.5. Implications for future work

7.5.1. Use of UASs & small format photogrammetry

UASs currently are a niche remote sensing technology in the study of glacial geomorphology. This study shows that their technology has advanced to a stage where they are suitable for imaging applications in numerous studies of glacial geomorphology. The technology has now become so accessible that arguably they extend the role of high resolution imagery beyond specialist users, and into the domain of any geomorphological researcher.

Combined with photogrammetry tools such as AgiSoft PhotoScan, the glacial geomorphologist has the ability not only to quantify morphology, but simply to depict their site in 3-D. Whilst quantifying morphology and process impact over time is

obviously the primary scientific application of this technology, the wider implications of increased use of 3-D mediums for research dissemination are significant. With growing use of alternative media online, the use of 3-D models will continue to expand and help make glacial geomorphology and geomorphology as a whole more accessible to the wider public.

As discussed at length previously, neither photogrammetry nor UASs are new technologies, but it appears that finally they have reached a stage where they can play a larger role in this area of research. When available, and increasingly UASs are available, it would seem sensible to include them in research into glacial geomorphology wherever possible.

7.5.2. Drumlin Mapping

The scale of this study limits the strength of its findings, but it suggests there are several fruitful avenues for future work. Primarily a larger scale study is needed to establish the dimensions of these features. Clark *et al.* (2010) argue that their data suggests drumlins are a separate population of landforms unlike Rose's (1987) proposal of a continuum of forms, but the results of this work hints that their conclusion may not be so clear. The narrow features mapped in this study potentially are indicative of drumlins fining into flutes. Establishing whether this is the case would be a useful contribution to the development of instability based models of drumlin formation that assume 'emergence' at a given size (Clark, 2010).

A second area that requires further work is on establishing an automated, or at least more thorough, mapping technique. The difficulties surrounding mapping at high resolution stem both from equifinality and simply the number of forms that are visible. However, perhaps a more sensible approach here is to move away from the palaeo forms and to concentrate on the modern analogue where there is less potential for non-glacial geomorphic processes to contribute to the landscape.

Therefore, the most appropriate extension to this work might be a series of high resolution studies of the glacial foreland of retreating Icelandic glaciers, and perhaps

particularly the foreland of Múlajökull where drumlins have recently emerged (Johnson *et al.*, 2010). That would limit the impact of equifinality when mapping, and offer the opportunity to examine the relationship between drumlins and flutes without having to worry unduly about whether the more delicate forms have been eroded from the landscape. For future studies in the UK, now the method of UAS survey has been established, it would also be sensible to simply extend the coverage of this study and simply examine sub-metric DEMs of different drumlinised areas across the country. Unfortunately this study cannot scale its findings to identify the potential number of drumlins unmapped by Hughes *et al.* (2010) as no drumlins were mapped by her in the area surveyed. This was essentially a product of the research design that focused on finding small bedforms outright rather than aiming to produced a scaled estimate. Initially a study covering just a few kilometres, and possibly over a variety of different sites, would allow a scaled estimate of unmapped bedforms in the UK, but there is merit in a full scale study mapping the entire glaciated area of the UK.

Chapter 8 Conclusions

UAS based photogrammetry was shown to be a low cost, low complexity method for producing DEMs of small areas (circa 1km^2) but accuracy remains a concern. The use of a UAS provides flexibility to the glacial geomorphologist as it can be deployed quickly and easily to survey small areas that do not merit the commissioning of other methodologies such as LiDAR. Specifically the PAMS SmartOne B proved simple to fly and suitably robust. It was limited by its thermopile based flight stabilisation that prevents flying in low light levels, but, as new versions now feature an inertial system this will not be an issue in future.

Of the photogrammetry programmes tested, PhotoScan was shown to be the most suitable. It provides a simple interface, efficient processing, and requires minimal user training which satisfies this study's aim to identify a low complexity method for photogrammetric DEM creation. Frustratingly it currently introduces a systematic polynomial error into the DEMs produced, but this could be easily resolved by detrending the DEM in future work. Because of this systematic error it was difficult to assess the accuracy of the DEM produced, but an estimate puts it at around 0.5 m after the systematic error has been resolved. Further work is required to establish the exact accuracy of this DEM.

The DEM produced was successfully used for mapping geomorphic features, and demonstrated that NEXTMap imagery does not show a number of features that could be glacial bedforms. These features were measured and it was found that whilst they did not differ greatly from Clark *et al.*'s (2010) 100 m lower limit on drumlin length, they were considerably thinner than bedforms mapped in that study. The 17 mapped bedforms had an average width of 43 m and 11 measured <37 m, which is outside two standard deviations of Clark *et al.*'s (2010) average. Despite this, they remained within the elongation ratio of drumlins, and so could conceivably be considered as such, rather than flutes.

The presence of these features tentatively suggests that drumlins may fine into flutes as hypothesised by Rose (1987). However, the sub-metric resolution of the DEM also highlighted that, alone, it may not be suitable for mapping glacial geomorphology. The noise in high resolution DEMs from small scale processes complicates mapping, making it difficult to determine whether bedforms are of a glacial origin. This issue of equifinality prevents solid conclusions from being drawn from this mapping and highlights the requirement for such resolution DEMs to be used alongside other techniques such as field validation. Despite this, the level of additional detail visible at this resolution does demonstrate the limitations of using DEMs such as NEXTMap, with lower resolution, for mapping of glacial geomorphology.

References

Aario, R. (1977). *Classification and terminology of morainic landforms in Finland*. Boreas 6(2): 87-100.

Aber, J. S., K. Aaviksoo, E. Karofeld and S. W. Aber (2002). *Patterns in Estonian bogs as depicted in color kite aerial photographs.* Suo (Helsinki) 53(1): 1-15.

Aber, J.S. and A. Ber (2007). *Glaciotectonism*. Developments in Quaternary Science Series Volume 6. Amsterdam, Boston, Heidelberg.

Aber, J.S., I. Marzolff and J.B. Ries (2010). *Small-Format Aerial Photography. Principles ,techniques and geoscience applications.* Elsevier, Amsterdam.

AgiSoft LLC (2011). PhotoScan Proffesional [online] Available at <http://www.agisoft.ru/products/photoscan/professional/> Accessed: 10.12.11.

Alden, W.C. (1905). *The drumlins of southeaster Wisconsin*. U.S. Geological Survey 273: 18.

Ann, Y. and J. E. Box (2010). *Glacier velocities from time-lapse photos: technique development and first results from the Extreme Ice Survey (EIS) in Greenland*. Journal of Glaciology 56(198): 723-734.

Archer, F., A. M. Shutko, T. L. Coleman, A. Haldin, E. Novichikhin, and I. Sidorov (2004). *Introduction, overview, and status of the Microwave Autonomous Copter System (MACS)*. In: Proceedings of IGARSS 200, Anchorage, Alaska, USA.

Arya, S., D.M. Mount, N.S. Netanyahu, R. Silverman and A.Y. Wu (1998). *An optimal algorithm for approximate nearest neighbour searching fixed dimensions*. Journal of the ACM *45*(6): 891–923.

Avery, T.E. and G.L. Berlin (1985). *Interpretation of Aerial Photographs*. Burgess Publishing Co., Minneapolis, MN.
Barrand, N. E., T. Murray, T. D. James, S. L. Barr and J. P. Mills (2009). *Optimizing photogrammetric DEMs for glacier volume change assessment using laser-scanning derived ground-control points.* Journal of Glaciology 55(189): 106-116.

Barnett, H.F. amd P.G. Finke (1971). *Morphometry of landforms: drumlins*. Army Natick Labs Mass Earth Science Lab Technology Report ES-63, 1–34.

Benn, D. I. and D. J. A. Evans (2010). *Glaciers and glaciation*. London, Hodder Education.

Bingham, R. G., E. C. King, A. M. Smith and H. D. Pritchard (2010). *Glacial geomorphology: Towards a convergence of glaciology and geomorphology*. Progress in Physical Geography 34(3): 327-355.

Boulton, G. S. (1985). *Ice sheets, their fluctuations and some of their geological effects*. Geophysical Journal of the Royal Astronomical Society 81(1): 310-310.

Boulton, G. S. (1987). *A theory of drumlin formation by subglacial sediment deformation*. In: Menzies, J. and J. Rose, (Eds.) Drumlin Symposium. Rotterdam, A.A. Balkema, 25–80.

Boulton, G. S. and C. D. Clark (1990). *A highly mobile laurentide ice-sheet revealed by satellite images of glacial lineations*. Nature 346(6287): 813-817.

Boyce, J. I. and N. Eyles (1991). *Drumlins carved by deforming till streams below the laurentide ice-sheet.* Geology 19(8): 787-790.

Brunsden, D. and J. H. Chandler (1996*). Development of an episodic landform change model based upon the black ven mudslide 1946-1995.* In: Advances in Hillslope Processes, Anderson, M.G. and S. M. Brooks (Eds.), J. Wiley, Chichester, UK, 869-896.

Bryce, J. (1833). *On the evidences of diluvial action in the north of Ireland.* J. R. Geol. Soc., Dublin 1: 34-44.

Butler, J. B., S. N. Lane and J. H. Chandler (1998). *Assessment of DEM quality for characterizing surface roughness using close range digital photogrammetry*. Photogrammetric Record 16(92): 271-291.

Caltech Vision (2011). Camera Calibration Toolbox for Matlab. [online] Available at: <http://www.vision.caltech.edu/bouguetj/calib_doc/ > Accessed: 03.02.11.

Carbonneau P.E. and Piégay H. (in press). *Fluvial Remote Sensing for River Science and Management.* Wiley and Sonc, Chichester.
Civil Aviation Authority – CAA (2004). UK-CAA Policy for Light UAV Systems. [online] Available at: <http://www.caa.co.uk/docs/1416/srg_str_00002-01-180604.pdf> [Accessed 15.04.2011]

Chamberlin, T.C. (1883). *Terminal moraines of the second glacial epoch.* United States Geological Survey, 3rd Annual Report: 291-402.
Chandler, J. (1999). *Effective application of automated digital photogrammetry for geomorphological research.* Earth Surface Processes and Landforms 24(1): 51-63.

Chandler, J. H. and C. J. Padfield (1996). *Automated Digital Photogrammetry on a Shoestring*. The Photogrammetric Record 15(88): 545-559.

Chapwanya, M., C. D. Clark and A. C. Fowler (2011). *Numerical computations of a theoretical model of ribbed moraine formation.* Earth Surface Processes and Landforms 36(8): 1105-1112.

Charlesworth, J. K. (1957). The Quaternary Era, with special reference to its glaciation. Clark, C. D. (1993). *Mega-scale glacial lineations and cross-cutting ice-flow landforms.* Earth Surface Processes and Landforms 18(1): 1-29.

Chorley, R.J. (1959). *The shape of drumlins.* Journal of Glaciology 3: 339–344.
Church, M. (2010). *The trajectory of geomorphology*. Progress in Physical Geography 34: 265-287.
Clapperton, C.M. (1989). *Asymmetrical drumlins in Patagonia, Chile*. Sedimentary Geology 62, 387–398.

Clark, C.D. (1993). *Mega-scale glacial lineations and cross-cutting ice-flow landforms*. Earth Surface Processes and Landforms 18(1): 1–29.

Clark, C. D. (1994). *Large-scale ice-molding - a discussion of genesis and glaciological significance.* Sedimentary Geology 91(1-4): 253-268.

Clark, C. D. (1997). *Reconstructing the evolutionary dynamics of former ice sheets using multi-temporal evidence, remote sensing and GIS.* Quaternary Science Reviews 16(9): 1067-1092.

Clark, C. D. (2010). *Emergent drumlins and their clones: from till dilatancy to flow instabilities*. Journal of Glaciology, 56(200): 1011-1025.

Clark, C.D. and R. T. Meehan (2001). *Subglacial bedform geomorphology of the Irish Ice Sheet reveals major configuration changes during growth and decay.* Journal of Quaternary Science 16: 483–496.

Clark, C.D., S.L. Greenwood and D.J.A Evans (2006). *Palaeoglaciology of the last British-Irish ice sheet: challenges and some recent developments*. In: Knight, P.G. (Ed.), Glacier Science and Environmental Change. Blackwell, Oxford, pp. 248–264.

Clark, C. D., A. L. C. Hughes, S. L. Greenwood, M. Spagnolo and F. S. L. Ng (2009). *Size and shape characteristics of drumlins, derived from a large sample, and associated scaling laws*. Quaternary Science Reviews 28(7-8): 677-692.

Clark, R., (2002). *The Solway region in the Late Pleistocene*. Proceedings of the Cumberland Geological Society 6: 553–586.

Close, M. H. (1867). *Notes on the general glaciation of Ireland*. Royal Geological Society of Ireland Journal 1: 207-242.

Coudé, A., (1989). *Comparative study of three drumlin fields in western Ireland: geomorphological data and genetic implications*. Sedimentary Geology 62: 321–335.

Dardis, G. F., A. M. McCabe and W. I. Mitchell (1984). *Characteristics and origins of lee-side stratification sequences in late pleistocene drumlins, northern-ireland*. Earth Surface Processes and Landforms 9(5): 409-424.

Davis, W. M. (1884). *The distribution and origin of drumlins*. American Journal of Science 28: 407–416.

DIYDrones (2011). ARDUPilot home page. [online] Available at: <http://diydrones.com/notes/ArduPilot > Accessed: 24.05.11.

Doornkamp, J.C. and C.A.M. King (1971). *Numerical Analysis in Geomorphology*. Edward Arnold, London.

Dunford, R., K. Michel, M. Gagnage, H. Piegay and M. L. Tremelo (2009). *Potential and constraints of Unmanned Aerial Vehicle technology for the characterization of Mediterranean riparian forest*. International Journal of Remote Sensing 30(19): 4915-4935.

Ebers, E. (1926). *Die bisherige Ergebnisse der Drumlinforschung.* Neues Jahrbuch Geol. Palaontol. Adh. 53B: 153-270.

Edrich, M., G. Weiss and Ieee (2008). *Second-Generation Ka-Band UAV SAR System.* New York, Ieee.

Eisenbeiss, H., K, Lambers, M. Sauerbier, L. Zhang (2005). *Photogrammetric documentation of an archaeological site (Palpa, Peru) using an autonomous model helicopter.* Proceedings of the XXth CIPA International Symposium, Torino, Italy, 26 September - 1 October, In: International Archives of Photogrammetry, Remote Sensing and Spatial Information Sciences 34(C34): 238-243.

Eisenbeiss, H., (2007). *Applications of photogrammetric processing using an autonomous model helicopter.* Symposium ISPRS Commission Technique I Des capteurs a l'Imagerie, n°185, Saint-Mande Cedex, France.

Etzelmuller, B., G. Vatne, R. S. Odegard and J. L. Sollid (1993). *Mass-balance and changes of surface slope, crevasse and flow pattern of Erikbreen, Northern Spitsbergen - an application of a Geographical Information-System (GIS).* Polar Research 12(2): 131-146.

Evans, D. J. A., S. Livingston, A. Vieli and C. O'Cofaigh (2009). *The palaeo Glaciology of the central sector of the British and Irish Ice Sheet: reconciling glacial geomorphology and preliminary ice sheet modelling.* Quaternary Science Reviews 28:739-759.

Evans, I.S. (1987) *A new approach to drumlin geomorphometry*. *In*: Menzies, J., and Rose, J., eds. Drumlin Symposium. Balkema, Rotterdam, 119-147.

Fischler, M.A. and R.C. Bolles (1987). *Random Sample Consensus: A Paradigm for Model Fitting with Applications to Image Analysis and Automated Cartography*. In: Readings in Computer Vision: Issues, Problems, Principles, and Paradigms, Martin, A.F. and F. Oscar (Eds.). Morgan Kaufmann Publishers Inc., London, 726-740.

Finsterwalder, R. (1954). *Photogrammetry and glacier research with special reference to glacier retreat in the eastern Alps*. Journal of Glaciology 2(15): 306-315.

Fowler, A. C. (2000). *An instability mechanism for drumlin formation*. Deformation of Glacial Materials. A. J. Maltman, B. Hubbard and M. J. Hambrey. Bath, Geological Soc Publishing House. 176: 307-319.

Fowler, A. C. (2009). *Instability modelling of drumlin formation incorporating lee-side cavity growth.* Proceedings of the Royal Society a-Mathematical Physical and Engineering Sciences 465(2109): 2681-2702.

Fowler, A. C. (2010). *The instability theory of drumlin formation applied to Newtonian viscous ice of finite depth*. Proceedings of the Royal Society a-Mathematical Physical and Engineering Sciences 466(2121): 2673-2694.

Fox, A. J. and A. M. Nuttall (1997). *Photogrammetry as A Research Tool for Glaciology*. The Photogrammetric Record 15(89): 725-737.

Francek, M.A., (1991). *A spatial perspective on the New York drumlin field*. Physical Geography 12: 1-18.

Furukawa, Y. and J. Ponce (2010). *Accurate, dense, and robust Multi-View Stereopsis*. IEEE Trans. on Pattern Analysis and Machine Intelligence 32(8): 1362-1376.

Getmapping (2011). Products – NEXTMap. [online] Available at: <http://www2.getmappig.com/Products/NEXTMap> [Accessed 10.06.11].

Goodchild, J.G. (1875). *Glacial erosion*. Geology Magazine 12: 323-328.

Gluckert, G. (1973). *Two large drumlins field in central Finland*. Fennia 120: 37.

Greenwood, S. L. and C. D. Clark (2008). *Subglacial bedforms of the Irish Ice Sheet*. Journal of Maps, 332–357.

Greenwood, S. L. and J. Kleman (2010). *Glacial landforms of extreme size in the Keewatin sector of the Laurentide Ice Sheet.* Quaternary Science Reviews 29(15-16): 1894-1910.

Haavisto-Hyvarinen, M., (1987). *Mapping of drumlins of the Mikkeli district, southeastern Finland.* In: Rose, J., Menzies, J. (Eds.), Drumlin Symposium. Balkema, Rotterdam, 295-307.

Habib, A.F., A.M. Pullivelli and M. Morgan (2004). *Quantitative measures for the evaluation of camera stability*. International Archives of Photogrammetry, Remote Sensing and Spatial Information Sciences. 35(B1): 63–69.

Hagner, O. (2011) *Discussion on UAV design.* [conversation] Personal Communication, 8.7.2011.

Hardin, P. J. and T. J. Hardin (2010). *Small-Scale Remotely Piloted Vehicles in Environmental Research.* Geography Compass 4(9): 1297-1311.

Hardin, P. J. and R. R. Jensen (2011). *Introduction-Small-Scale Unmanned Aerial Systems for Environmental Remote Sensing*. Giscience & Remote Sensing 48(1): 1-3.

Harry, D.G. and A.S. Trenhaile (1987).The morphology of the Arran drumlin field, southern Ontario, Canada. In: Rose, J., Menzies, J. (Eds.), Drumlin Symposium. Balkema, Rotterdam, 161–173.

Hart, J. K. (1997). *The relationship between drumlins and other forms of subglacial glaciotectonic deformation*. Quaternary Science Reviews 16(1): 93-107.

Hart, J.K., K.C. Rose and K. Martinez (2011). Subglacial till behaviour derived from *in situ* wireless multi-sensor subglacial probes: Rheology, hydro-mechanical interactions and till formation. Quaternary Science Reviews 30: 234-247.

Hattestrand, C., D. Goodwillie and J. Kleman (1999). *Size distribution of two cross-cutting drumlin systems in northern Sweden: a measure of selective erosion and formation time length.* Annals of Glaciology. J. Kleman. Cambridge, Int Glaciological Soc. 28: 146-152.

Hess, D. P. and J. P. Briner (2009). *Geospatial analysis of controls on subglacial bedform morphometry in the New York Drumlin Field - implications for Laurentide Ice Sheet dynamics*. Earth Surface Processes and Landforms 34(8): 1126-1135.

Hill, A.R. (1971). *The internal composition and structure of drumlins in North Down and South Antrim, Northern Ireland.* Geografiska Annaler 53(A): 14-31.
Hindmarsh, R. C. A. (1998). *Drumlinization and drumlin-forming instabilities: viscous till mechanisms.* Journal of Glaciology 44(147): 293-314.

Hindmarsh, R. C. A. (1998). *The stability of a viscous till sheet coupled with ice flow, considered at wavelengths less than the ice thickness*. Journal of Glaciology 44(147): 285-292.

Hindmarsh, R. C. A. (1999). *Coupled ice-till dynamics and the seeding of drumlins and bedrock forms.* Annals of Glaciology. J. Kleman. Cambridge, Int Glaciological Soc. 28: 221-230.

Hitchcock, C.H. (1876). *Lenticular hills of glacial drift*. Proceedings of the Boston Society of Natural History 19: 63-67.

Horcher, A. and R. J. M. Visser (2004). *Unmanned Aerial Vehicles: Applications for Natural Resource Management and Monitoring.* In: Council on Forest Engineering Annual Meeting, Hot Springs (AR), USA.

Hubbard, G. D. (1906). *Drumlinoids of the Catatonk Folio.* Bulletin of the American Geographical Society 38(6): 355–365.

Hughes, A. L. C., C. D. Clark and C. J. Jordan (2010). *Subglacial bedforms of the last British Ice Sheet*. Journal of Maps: 543-563.

Hunt, E. R., W. D. Hively, S. Fujikawa, D. Linden, C. S. Daughtry and G. McCarty (2010). *Acquisition of NIR-Green-Blue Digital Photographs from Unmanned Aircraft for Crop Monitoring.* Remote Sensing 2(1): 290-305.

Jansson, K. N. and N. F. Glasser (2005). *Using Landsat 7 ETM+ imagery and Digital Terrain Models for mapping glacial lineaments on former ice sheet beds*. International Journal of Remote Sensing 26(18): 3931-3941.

Johnson, G., Meisner, D. & Johnson, W. (1990). *Aerial photography of the Nasca lines*. In Aveni (Ed.), The lines of Nasca: 271-283. Philadelphia: American Philosophical Society.

Johnson, M. D., A. Schomacker, I. O. Benediktsson, A. J. Geiger, A. Ferguson and Ó. Ingólfsson (2010). *Active drumlin field revealed at the margin of Múlajökull, Iceland: A surge-type glacier*. Geology 34(10): 943-946.

Jones, G. P., L. G. Pearlstine and H. F. Percival (2006). *An assessment of small unmanned aerial vehicles for wildlife research.* Wildlife Society Bulletin 34(3): 750-758.

Kaaniche, K., B. Champion, C. Pegard and P. Vasseur (2005). *A vision algorithm for dynamic detection of moving vehicles with a UAV.* In: IEEE International Conference on Robotics and Automation: 1878-1883.

Karczewski, A. (*1976). Morphometric features of drumlins in Western Pomerania*. Quastiones Geographicae 3, 35–42.

Karras, G. E., D. Mavromati, M. Madani, G. Mavrelis, E. Lymperopoulos, A. Kambourakis and S. Gesafidis (1999). *Digital orthophotography in archaeology with low-altitude non-metric images.* In: International Archives of Photogrammetry & Remote Sensing, WG V/2 & 5 Photogrammetric Measurement, Object Modelling and Documentation in Architecture and Industry, Thessaloniki, Greece, XXXII-5/W11, 8-11.

Keutterling, A. and A. Thomas (2006). *Monitoring glacier elevation and volume changes with digital photogrammetry and GIS at Gepatschferner glacier, Austria.* International Journal of Remote Sensing 27(19): 4371-4380.

King, E. C., R. C. A. Hindmarsh and C. R. Stokes (2009). *Formation of mega-scale glacial lineations observed beneath a West Antarctic ice stream*. <u>Nature Geoscience</u> 2(8): 585-588.

Kleman, J., C. Hattestrand, I. Borgstrom and A. Stroeven (1997). *Fennoscandian palaeoglaciology reconstructed using a glacial geological inversion model*. <u>Journal of Glaciology</u> 43(144): 283-299.

Kohller, J., T.D. James, T. Murray, C. Nuth, O. Brandt, N.E. Barrand, H.F. Aas and A. Luckman (2007). *Acceleration in thinning rate on western Svalbard glaciers*. <u>Geophysical Research Letters</u> 34.

Krabill, W., E. Frederick, S. Manizade, C. Martin, J. Sonntag, R. Swift, R. Thomas, W. Wright and J. Yungel (1999). *Rapid Thinning of Parts of the Southern Greenland Ice Sheet.* <u>Science</u> 283(5407): 1522-1524.

Kruger J., H.H. Thomsen (1984). Morphology, stratigraphy, and genesis of small drumlins in front of the glacier Myrdalsjokull, South Iceland. <u>Journal of Glaciology</u> 30: 94–105.

Kupsch, W.O. (1955). *Drumlins with jointed boulders near Dollard, Saskatchewan. <u>Geological Society of American Bulletin</u>.* 66: 327–338.

Laebe, T. and W. Foerstner (2004). *Geometric stability of low-cost digital consumer cameras.* <u>International Archives of Photogrammetry, Remote Sensing and Spatial Information Sciences</u>. 35(B1): 528–534.

Laliberte, A. S. and A. Rango (2011). *Image Processing and Classification Procedures for Analysis of Sub-decimeter Imagery Acquired with an Unmanned Aircraft over Arid Rangelands.* <u>Giscience & Remote Sensing</u> 48(1): 4-23.

Lambers, K., H. Eisenbeiss, M. Sauerbier, D. Kupferschmidt, T. Gaisecker, S. Sotoodeh and T. Hanusch (2007*). Combining photogrammetry and laser scanning for the recording and modelling of the Late Intermediate Period site of Pinchango Alto, Palpa, Peru.* <u>Journal of Archaeological Science</u> 34(10): 1702-1712.

Le Heron, D. P. (2008). *Review of Glaciotectonism* by Aber, J. & Ber, A. <u>Geological Magazine</u> 145(6): 892-a-893.

Lewis, G. (2007). *Evaluating the Use of a Low-Cost Unmanned Aerial Vehicle Platform in Acquiring Digital Imagery for Emergency Response.* <u>Geomatics Solutions for Disaster Management</u>. J. Li, S. Zlatanova and A. Fabbri. Berlin, Springer-Verlag Berlin: 117-133.

Lo, C.P. (1976). *Geographic Applications of Aerial Photography*. <u>Russak Company, New York.</u>

Longuet-Higgins, H. C. (1981). *A computer algorithm for reconstructing a scene from two projections*. Nature 293: 133-135

Lowe, D. (2004). *Distinctive image features from scale-invariant keypoints*. International Journal of Computer Vision 60 (2): 91–110.

Lundqvist, J. (1970). *Studies of drumlin tracts in central Sweden*. Acta Geographica Lodziensia 24: 317-326.

Marks, A. R. (1989). *Aerial photography from a tethered helium filled balloon*. The Photogrammetric Record 13(74): 257-261.

Marzolff, I. and J. Poesen (2009). *The potential of 3-D gully monitoring with GIS using high-resolution aerial photography and a digital photogrammetry system*. Geomorphology 111(1-2): 48-60.

Masahiko, N. (2007). *UAV borne mapping system for river environment*. In: 28th Asian Association of Remote Sensing Conference, Kuala Lumpur, Malaysia.

Meggio, F., P. J. Zarco-Tejada, L. C. Nunez, G. Sepulcre-Canto, M. R. Gonzalez and P. Martin (2010). *Grape quality assessment in vineyards affected by iron deficiency chlorosis using narrow-band physiological remote sensing indices*. Remote Sensing of Environment 114(9): 1968-1986.

Menzies, J. (1979). *Review of the literature on the formation and location of drumlins*. Earth-Science Reviews 14(4): 315-359.

Menzies, J. and U. Brand (2007). *The internal sediment architecture of a drumlin, Port Byron, New York State, USA*. Quaternary Science Reviews 26(3-4): 322-335.

MeshLab (2011). MeshLab – open source processing of 3-D meshes. [online] Available at: <http://meshlab.sourceforge.net/> Accessed 10.02.2011.

Metni N. and T. Hamel (2007) *Visual Tracking Control of Aerial Robotic Systems with Adaptive Depth Estimation*. *International Journal of Control, Automation and Systems 1*(5).

Millington, A.C. and J. R. G. Townshend (1987). *The potential of satellite remote sensing for geomorphological investigations: an overview.* In: Gardiner, V., (Ed.) International geomorphology, Chichester: Wiley, 331-42.

Mills, H. H. (1980). *An analysis of drumlin form in the Northeastern and North-Central United-States - summary.* Geological Society of America Bulletin 91(11): 637-639.

Mitchell, W.A. (1994). *Drumlins in ice sheet reconstructions, with reference to the western Pennines, northern England*. Sedimentary Geology 91, 313–332.

Mitchell, W.A. and Riley, J.M. (2006). *Drumlin map of the western Pennines and southern Vale of Eden, northern England*. Journal of Maps: 10-16.

Miyatsuka, Y. (1996). *Archaeological real time photogrammetric system using digital still camera.* In: The International Archives of the Photogrammetry, Remote Sensing and Spatial Information Sciences, XVIII ISPRS Congress, Vienna, Austria, XXXI-B5, 447-452.

Mori, M., Masahiro, S., Akamatsu, Y., Yamana, R. and Yahara, T., (1996). *Discussion on the automatic measurement of traffic flow by video camera mounted on balloon.* International Archives of the Photogrammetry, Remote sensing and spatial Information Sciences. ISPRS Congress, Vienna, Austria, XXXI, B5, 378-381.

Muster, S., J. Boike, W. Bolton, M. Grüber, M. Langer, K. Piel, T. Sachs, G. Stoof, S. Westermann (2008). *Monitoring permafrost patterned ground with small-formst aerial photography: Classification of a polygon landscape on Samoylov Island, Lena Delta, Siberia*. General Assembly European Geosciences Union (Vienna, Austria 2008).

Muller, E.H., (1974). *Origins of drumlins*. In: Coastes, D.R. (Ed.), Glacial Geomorphology. State University of New York, Binghamton, New York, 187–204.

Napieralski, J. and N. Nalepa (2010). *The application of control charts to determine the effect of grid size on landform morphometry*. Computers & Geosciences 36: 222-230

Neithammer U., M.R. James, S. Rothmund, J. Travelletti, M. Joswig (in press). *UAV-based remote sensing of the Super-Sauze landslide: Evaluation and results.* Engineering Geology.

Newcome, L.R. (2004). *Unmanned Aviation: A Brief History of Unmanned Aerial Vehicles*. American Institute of Aeronautics and Astronautics, Inc. Reston, VA

Nocedal, J. and S. Wright (1999). *Numerical Optimization*. New York, NY: Springer.

Oguchi, T., Y. Hayakawa, T. Waslewicz (2011). *Chapter 7: Data Sources*. In: Smith, M.J., P. Paron and J. Griffiths (Eds.), Geomorphological Mapping: Methods and Applications. Elsevier, London.

Oliensis, J. (1999). *A multi-frame structure-from-motion algorithm under perspective projection*. International Journal of Computer Vision 34(2–3): 163–192.

Paine, D. P. and J. D. Kiser (2003). *Aerial photography and image interpretation*, John Wiley.

Palmann, C., S. Mavromatis, M. Hernandez, J. Sequeira and B. Brisco (2008). *Earth observation using radar data: an overview of applications and challenges*. International Journal of Digital Earth 1(2): 171-195.

Paparazzi (2011). Paparazzi autopilot wiki homepage. [online] Available at: <http://paparazzi.enac.fr/wiki/Main_Page > Accessed 24.05.11.

PhotoSynth (2011). PhotoSynth home page. [online] Available at: < http://photosynth.net/> Accessed 24.01.11.

PhotoTour (2010). Bundler: Structure from Motion (SfM) for Unordered Image Collections. [online] Available at: < http://phototour.cs.washington.edu/bundler/ > Accessed 21.03.11.

Piotrowski J. A. and I.J. Smalley (1987). *The Woodstock drumlin field, southern Ontario, Canada.* In: Menzies J. and J. Rose, (Eds), Drumlin Symposium, A.A. Balkema, Rotterdam (1987), 309–321.

Przybilla, H.J. and Wester-Ebbinghaus, W. (1979). *Biuldflug mit ferngelenktem Kleinflugzeug.* In: Bildmessung und Luftbildwesen, Zeitschrift fuer Photogrammetrie und Fernerkudung. 47(5): 137-142.

Puri, A. (2004). *A Survey of Unmanned Aerial Vehicles (UAV) for Traffic Surveillance.* Internal Report, Department of Computer Science and Engineering, University of South Florida, Tampa, FL, USA, 29.

Pyle, C. J., K. S. Richards and J. H. Chandler (1997). *Digital Photogrammetric Monitoring of River Bank Erosion.* The Photogrammetric Record 15(89): 753-764.

Rabus, B., M. Eineder, A. Roth and R. Bamler (2003). *The shuttle radar topography mission - a new class of digital elevation models acquired by spaceborne radar*. Isprs Journal of Photogrammetry and Remote Sensing 57(4): 241-262.

Rango, A., A. Laliberte, C. Steele, J. E. Herrick, B. Bestelmeyer, T. Schmugge, A. Roanhorse and V. Jenkins (2006). *Using Unmanned Aerial Vehicles for Rangelands: Current Applications and Future Potentials.* Environmental Practice 8(03): 159-168.

Reed, B., C. J. Galvin and J. P. Miller (1962). *Some aspects of drumlin geometry.* American Journal of Science 260(3): 200-&.

Rees, G. (2001). *Physical principles of remote sensing*, Cambridge University Press.

Reidelstuerz, P., J. Link, S. Graeff, W. Claupein (2007). *UAV (unmanned aerial vehicles) für Präzisionslandwirtschaft*. 13. Workshop Computer-Bildanalyse in der Landwirtschaft & 4. Workshop Precision Farming*, In:* Bornimer Agrartechnische Berichte, 61, 75-84.

Reinhardt, W. and H. Rentsch (1986). *Determination of changes in volume and elevation of glaciers using digital elevation models for the Vernagtferner, Otztal Alps, Austria*. Annals of Glaciology 8: 151-155

Reuder, J., P. Brisset, M. Jonassen, M. Muller and S. Mayer (2009). *The Small Unmanned Meteorological Observer SUMO: A new tool for atmospheric boundary layer research.* Meteorologische Zeitschrift 18(2): 141-147.

Riley, J.M., (1987). *Drumlins of the southern Vale of Eden, Cumbria, England*. In: Rose, J., Menzies, J. (Eds.), Drumlin Symposium. Balkema, Rotterdam, 323–333.

Rose, J. (1987). *Drumlins as part of a glacier bedform continuum*. In Menzies, J. and rose, J. (Eds.), Drumlin Symposium. Balkema, Rotterdam, 103-116.

Rose, J. and Letzer, J.M. (1977). *Superimposed drumlins*. Journal of Glaciology. 18: 471-480.

Rosen, P. A., S. Hensley, I. R. Joughin, F. K. Li, S. N. Madsen, E. Rodriguez and R. M. Goldstein (2000). *Synthetic aperture radar interferometry* - Invited paper. Proceedings of the IEEE 88(3): 333-382.

Rouk, A. M. and A. Raukas (1989). *Drumlins of estonia*. Sedimentary Geology 62(2-4): 371-384.

Rovira-Más, F., Q. Zhang and J. F. Reid (2005). *Creation of three-dimensional crop maps based on aerial stereoimages.* In: Biosystems Engineering 90: 251-259.
Scheritz, M., Dietrich, R., Scheller, S., Schneider, W., Boike, J. (2008). *High Resolution Digital Elevation Model of Polygonal Patterned Ground on Samoylov Island, Siberia, Using Small-Format Photography.* Proceedings of the 9th International Conference on Permafrost, June 29 - July 3, 2008, University of Alaska, Fairbanks, USA, 1589-1594.

Shaw, J. (1983). *Drumlin formation related to inverted melt-water erosional marks*. Journal of Glaciology 29(103): 461–479.

Shaw, J. (2002). *The meltwater hypothesis for subglacial bedforms.* Quaternary International 90: 5-22.

Shaw, J. and D. Kvill (1984). *A glaciofluvial origin for drumlins of the Livingstone Lake area, Saskatchewan*. Canadian Journal of Earth Sciences 21: 1442–1459.

Shaw, J., D. Kvill and B. Rains (1989). *Drumlins and catastrophic subglacial floods*. Sedimentary Geology 62(2-4): 177-202.

Slater, G. (1929). *The structure of drumlins exposed on the south shore of Lake Ontario.* New York State Museum Bulletin 281: 3-19. Smalley, I.J., P. Lu and I.F. Jefferson (2000). *The golf ball model and the purpose of drumlin formation.* Studia Quaternaria 17: 29–33.

Smalley, I. and J. Warburton (1994). *The shape of drumlins, their distribution in drumlin fields, and the nature of the sub-ice shaping forces*. Sedimentary Geology 91(1-4): 241-252.

Smalley, I. J. (1966). *Drumlin formation - a rheological model*. Science 151(3716): 1379-&.

Smith, A. M. and T. Murray (2009). *Bedform topography and basal conditions beneath a fast-flowing West Antarctic ice stream*. Quaternary Science Reviews 28(7-8): 584-596.

Smith, M. J. and C. D. Clark (2005*). Methods for the visualization of digital elevation models for landform mapping*. Earth Surface Processes and Landforms 30(7): 885-900.

Smith, M.J., J. Rose and S. Booth (2006). *Geomorphological mapping of glacial landforms from remotely sensed data: An evaluation of the principal data sources and an assessment of their quality*. Geomorphology 76: 148-165.

Smith, M. J., J. Chandler and J. Rose (2009). *High spatial resolution data acquisition for the geosciences: kite aerial photography*. Earth Surface Processes and Landforms 34(1): 155-161.

Smith, M. J. and C. F. Pain (2009). *Applications of remote sensing in geomorphology*. Progress in Physical Geography 33(4): 568-582.

Snavely N, S.M. Seitz & R. Szeliski (2006). *Photo Tourism: Exploring image collections in 3-D.* ACM Transactions on Graphics (Proceedings of SIGGRAPH 2006).

Snavely N, S.M. Seitz & R. Szeliski (2007). *Modelling the World from Internet Photo Collections.* International Journal of Computer Vision. 2007.

Spagnolo, M., C. D. Clark, A. L. C. Hughes and P. Dunlop (2011). *The topography of drumlins; assessing their long profile shape.* Earth Surface Processes and Landforms 36(6): 790-804.

Spagnolo, M., C. D. Clark, A. L. C. Hughes, P. Dunlop and C. R. Stokes (2010). *The planar shape of drumlins*. Sedimentary Geology 232(3-4): 119-129.

Spetsakis, M. E. and J.Y. Aloimonos (1991). *A multiframe approach to visual motion perception*. International Journal of Computer Vision *6*(3): 245–255.

Spiess, T., J. Bange, M. Buschmann and P. rsmann (2007). *First application of the meteorological Mini-UAV 'M2AV'*. Meteorologische Zeitschrift 16(2): 159-169.

Stokes, C. R. and C. D. Clark (2002). *Are long subglacial bedforms indicative of fast ice flow?* Boreas 31(3): 239-249.

Stokes, C.R., M. Spagnolo and C.D. Clark (2011). *The composition and internal structure of drumlins: Complexity, commonality and implications for a unifying theory of their formation*. Earth-Science Reviews 107(3-4): 398-422.

Stea, R.R. and Y. Brown (1989). *Variation in drumlin orientation, form and stratigraphy relating to successive ice flows in southern and central Nova Scotia*. Sedimentary Geology 62: 223–240.

Sugiura, R., N. Noguchi and K. Ishii (2005). *Remote-sensing technology for vegetation monitoring using an unmanned helicopter.* Biosystems Engineering 90(4): 369-379.

Szeliski, K. and S.B. Kang (1994). *Recovering 3D shape and motion from image streams using nonlinear least squares*. Journal of Visual Communication and Image Representation 5(1): 10-28

Szeliski, R. (2010). *Computer Vision: Algorithms and Applications*. Springer, New York, 2010

Templeton, R.C., Vivone, E.R., Mendez-Barroso, L.A., Rango, A., Laliberte, A., Saripalli, S. (2010). *Emerging technologies for ecohydrological studies during the North American monsoon in a Chihuahuan desert watershed.* Poster H53B-1014. 2010 American Geophysical Conference annual conference, San Francisco, USA.

Tetracam (2011). Tetracam ADC lite. [online] Available at: <http://www.tetracam.com/adc_lite.html> Accessed 17.7.11.

Tokmakidis, K., E. Mamoto and F. Mori (1998). *Detail Surveys with Close-Range Photogrammetry in Archaeological Sites*. In: International Archives of the Photogrammetry, Remote Sensing and Spatial Information Sciences, Commission V Symposium Real-Time Imaging and Dynamic Analysis.

Tomasi, C. and T. Kanade (1992). *Shape and motion from image streams under orthography: a factorization method*. International Journal of Computer Vision 9(2): 137-154.

Tomlins, G. F. (1983). *Some considerations in the design of low-cost remotely-piloted aircraft for civil remote-sensing applications*. Canadian Surveyor-Geometre Canadien 37(3): 157-167.

Toutin, T. (2008). *ASTER DEMs for geomatic and geoscientific applications: a review*. International Journal of Remote Sensing 29(7): 1855-1875.

Trenhaile, A.S. (1975). *The morphology of a drumlin field*. Annals of the Association of American Geographers 65: 297–312.

Triggs, B., P. McLauchlan, R. Hartley and A. Fitzgibbon (1999). *Bundle Adjustment — A Modern Synthesis*. ICCV '99: Proceedings of the International Workshop on Vision Algorithms. Springer-Verlag. 298–372.

Trotter, F.M. (1929). *The Glaciation of East Edenside, the Alston Block and the Carlisle Plain*. Quarterly Journal of the Geological Society of London 85: 549–612.

Van Landeghem, K.J.J, A.J. Wheeler and N.C. Mitchell (2009). Seafloor evidence for palaeo-ice streaming and calving of the grounded Irish Sea Ice Stream: Implications for the interpretation of its final deglaciation phase. Boreas 38(1): 119-131.

Velic, J., I. Velic and D. Kljajo (2011). *Sedimentary bodies, forms and occurrences in the tudorevo and Mirovo glacial deposit of northern Velebit (Croatia)*. Geologia Croatica 64(1): 1-16.

Verhoeven, G. (2011). *Taking Computer Vision Aloft - Archaeological Three-dimensional Reconstructions from Aerial Photographs with PhotoScan*. Archaeological Prospection 18(1): 67-73.

Vierling, L. A., M. Fersdahl, X. X. Chen, Z. P. Li and P. Zimmerman (2006). *The Short Wave Aerostat-Mounted Imager (SWAMI): A novel platform for acquiring remotely sensed data from a tethered balloon*. Remote Sensing of Environment 103(3): 255-264.

Visnovcova J., Zhang L., Gruen A. (2010). *Generating a 3-D model of a Bayon tower using non-metric imagery*. Asian Journal of Geoinformatics 2(1): 11-18.
Visual Experiments (2010). PhotoSynth Toolkit. [online] Available at: < http://www.visual-experiments.com/demos/photosynthtoolkit/ > Accessed: 20.01.11.

Vozikis, E. (1983). *Analytical methods and instruments for mapping from balloon photography.* The Photogrammetric Record 11(61): 83-92.

Walker, J.W. and S.L. Devore (1995). *Low Altitude Large Scale Reconnaissance: A Method of Obtaining High Resolution Vertical Photographs for Small Areas.* rev. ed., Denver CO: U.S. National Park Service, Rocky Mountain Regional Office, Interagency Archaeological Services Division of Partnerships and Outreach.

Wellner, J. S., D.C. Heroy & J.B. Anderson (2006). *The death mask of the Antarctic ice sheet: Comparison of glacial geomorphic features across the continental shelf*. Geomorphology 75: 157–171.

Welty, E., W.T. Pfeffer and Y. Ahn (2010). *Something for everyone: quantifying evolving (glacial) landscapes with your camera.* [poster] IN33B-1314. 2010 American Geophysical Union annual conference, San Francisco, USA.

Wester-Ebbinghaus, W. (1980). *Aerial photography by radio controlled model helicopter.* The Photogrammetric Record 10(55): 85-92.

Westoby, M. (2011). *Constructing DTMs of breached moraine dam complexes (using 'Structure-from-Motion').* [Poster] British Society for Geomorphology Annual Conference 'Extreme Events – shaping the surface of the Earth' University of Liverpool: 28-30.07.11.

Wolf, P. R. and B. A. Dewitt (2000). *Elements of photogrammetry: with applications in GIS*, McGraw-Hill.

Wysota, W. (1994). *Morphology, internal composition and origin of drumlins in the southeastern part of the Chelmno-Dobrzy Lakeland, North Poland.* Sedimentary Geology 91: 345–364.

Zakrzewska Borowiecka, B. and R. H. Erickson (1985). *Wisconsin drumlin field and its origin*. Zeitschrift fur Geomorphologie 29 (4): 417–438.

Zaugg, E. C., D. L. Hudson, D. G. Long and Ieee (2006). *The BYU mu SAR: A Small, Student-Built SAR for UAV Operation*. New York, Ieee.

Zelcs, V. and A. Dreimanis (1997). *Morphology, internal structure and genesis of the Burtnieks drumlin field, northern Vidzeme, Latvia*. Sedimentary Geology 111(1-4): 73-90.

Zhou, G., C. Li and P. Cheng (2005). *Unmanned aerial vehicle (UAV) real-time video registration for forest fire monitoring*. In: IEEE International Geoscience and Remote Sensing Symposium, 1803-1806.

Zischinsky, T., L. Dorfner and F. Rottensteiner (2000). *Application of a new Model Helicopter System in Architectural Photogrammetry*. In: International Archives of Photogrammetry, Remote Sensing and Spatial Information Sciences, ISPRS Congress, Amsterdam, the Netherlands, XXXIII, B5/2, 959 - 965.

Appendices

DGPS data (UTM/WGS1984)

FID_	X	Y	Z

1	868895.1	6058989	327.9414
2	868895.5	6059022	323.7663
3	868912.7	6059056	323.0909
4	869082.9	6058795	320.6131
5	869040.4	6058661	321.8596
6	869031	6058661	321.9493
7	868868.4	6058746	331.0307
8	868865.3	6058644	334.2759
9	868826.1	6058615	338.2485
10	868779.6	6058617	341.3897
11	868738.6	6058596	340.6294
12	868727.8	6058607	338.8145
13	868534.7	6058692	337.3601
14	868550	6058710	337.9867
15	868606.9	6058763	336.1353
16	868661.9	6058795	334.0866
17	868757.5	6058947	327.0085
18	868807.9	6058990	326.2157
19	868623.8	6059067	327.2891
20	868550.3	6059073	328.4777
21	868480	6059091	328.2065
22	868424	6059097	326.7517
23	868424.9	6059089	328.1539
24	868393.6	6059022	328.8007